Investigation of Retrofit Techniques for Seismic Resistant Steel Moment Connections

by

Scott Adam Civjan, B.S. M.S.

Dissertation

Presented to the Faculty of the Graduate School of

The University of Texas at Austin

in Partial Fulfillment

of the Requirements

for the Degree of

Doctor of Philosophy

The University of Texas at Austin

August, 1998

Investigation of Retrofit Techniques for Seismic Resistant Steel Moment Connections

Approved by
Dissertation Committee:

Michael D. Engelhardt, Supervisor

James O. Jirsa

Joseph A. Yura

Jose M. Roesset

Eric B. Becker

Dedication

This dissertation is dedicated to the letter R and the number 3, and (reluctantly) to that darn 1072 that keeps burning in my brain. It also goes out to all of the canines of the world who so desperately wanted the dogbones to do better than they did, if only for the sake of personal pride.

Acknowledgements

A huge sloppy wet thank you to Sheryl, for her love, understanding, motivation and support. To Cacophony for checking up on me, Jane for reminding me that there are a multitude of ways to scratch an itch, and to Beau-Jangles for his youthful exuberance and daily walks. To my parents, grandparents, siblings and in-laws for their love and support. Gratitude is also extended to NIST, the THRUST 2000 and University Fellowships for the financial support without which none of this would have come about. Dr. Engelhardt was crucial with his guidance and knowledge which allowed me to continue. Thanks also to Dr. Jirsa, Dr. Tassoulas, and Dr. Paris for reminding me why I went through all of this in the first place. Wayne Fontenot came through as per usual with technical support, advice, and knowing winks. Blake Stasney and Mike Bell also went out of their way to make my ride smoother. And finally, my gratitude to Jeff Schmitz and the writings of Ken Kesey for screwing the bulb back in and reminding me to keep the lights on. May your glistening eyes see golden views...

Investigation of Retrofit Techniques for Seismic Resistant Steel Moment Connections

Publication No._____

Scott Adam Civjan, Ph.D.

The University of Texas at Austin, 1998

Supervisor: Michael D. Engelhardt

Typical steel moment resisting frame (SMRF) connections were shown to be vulnerable to brittle failures in the Northridge Earthquake. A study was undertaken to determine the effectiveness of two possible retrofit methods for typical pre-Northridge SMRF connections. The retrofit methods involved moving inelastic deformations away from the column face and consisted of either haunch or dogbone (reduced beam section) designs. Both methods were restricted to the bottom flange only. An experimental study was conducted in which six full scale interior beam-column subassemblages were tested. Alternating specimens included a composite concrete slab in order to study the effects of a composite slab on retrofit behavior. Specimen behavior was reported both in general terms as well as through a detailed series of analyses. The results were used to develop a methodology for the design of both haunch and dogbone retrofits. A complete design method was presented based on the findings of this study and previous

research. Design was based on limiting the applied stresses at the column face to critical weld stress values which vary depending on the degree of weld modifications. These methods could be applied towards new construction as well.

Table of Contents

List of Tables

List of Figures

Chapter 1: Introduction

Steel buildings are an essential part of the world's structures, utilized in everything from strip malls to skyscrapers. In order to provide lateral stability under gravity loads and withstand lateral loads such as wind or earthquake a steel building may be braced or equipped with rigid beam-to-column connections as a moment resisting frame (MRF). The lateral strength, stiffness, and ductility of MRF's are largely dependant on the integrity of the rigid connections. One of the most common rigid connections used for both seismic and non-seismic applications in the United States has been the welded flange-bolted web moment connection. As this connection became standardized throughout the industry the confidence in it resulted in its routine use in a wide range of applications. These applications ranged from small to jumbo sized beams and columns, and from highly redundant multiple frame structures to large buildings with only a minimum of MRF's.

This typical connection which was so widely used, this stalwart of modern steel construction, was suddenly revealed to be a misunderstood and fallible link in building behavior by the Northridge Earthquake of 1994. The history of modern steel construction will likely be measured in pre and post Northridge detailing as a determination of relative seismic performance.

A) Background of the Northridge Earthquake

On January 17,1994, residents of the Los Angeles area were awakened at

4:31 A.M. Pacific standard time by what would turn out to be the costliest earthquake in United States history. The earthquake had a magnitude of 6.7 (1). There were 57 deaths, relatively few due to the early morning time (1). The initially observed damage to structures was impressive, with some dramatic failures in wood apartment buildings, older non-ductile reinforced concrete buildings, pre-cast concrete parking garages, older concrete bridges, and other structures.

Initially, steel moment resisting frames appeared to have come through relatively unscathed. Few steel moment frame buildings showed any visible signs of damage.

It was about two weeks after the earthquake that the extent of problems began to manifest itself (1). It was noticed that some buildings that were currently under construction experienced some unexpected damage in the exposed steel connections (1). Structural damage was found in other occupied buildings by purely coincidental means. In most cases it was only during repairs of non-structural elements, or while attempting to correct the "plastic structure deformations" (permanent drifts) that the structural moment resisting connections were exposed (1). To the surprise of virtually all involved, the exposed connections often contained failures of a most brittle kind. Instead of the expected ductile yielding in the beams near the face of the columns, many joints contained fractures originating at the welds with no signs of plastic beam deformations. Most fractures appeared to originate in bottom welds near the backing bar (1,2,3,4). As a precautionary measure other joints were accessed throughout the damaged and apparently undamaged buildings. The precaution

was found to be warranted as many other similar failures were discovered. This was especially disconcerting as most of the buildings showed little if any permanent set or damage to non-structural elements. Within three months 50 steel frames were confirmed damaged, and after eight months over 100 steel frames were confirmed damaged (3). Reference 3 contains an estimate that approximately 1200 buildings in the Los Angeles area alone are of this type of construction, and about 40 percent of the 51 buildings surveyed had some cracking of the bottom flange welds.

B) Overview of a Typical Connection

The typical connection in use in California steel construction at the time of the Northridge earthquake can be seen in Fig. 1.1. A "pre-Northridge" connection is therefore represented by this welded flange-bolted web connection detail, and will be referred to as such throughout this report. A detail such as this was prescribed by the 1988 Uniform Building Code (UBC) and had been widely used since the early 1970's. This provision was superceded by a 1994 addendum to the UBC. Details of the bottom flange area which appeared to be the origin of most all brittle fractures in the Northridge Earthquake are shown in Fig. 1.2.

This connection utilized complete joint penetration (CJP) groove welds connecting the beam flanges to the column flange. The CJP welds were typically detailed as single bevel groove welds. To eliminate overhead welding, the root of the weld was typically placed at the bottom of each flange, and were often specified as a 3/8 in. root opening with a 30 degree bevel angle. These welds were most commonly made in the field, using the self shielded flux core arc

welding (FCAW) process.

The most commonly used electrode was the 0.120 in. diameter E70T-4 electrode. This electrode provides a specified minimum tensile strength of 70 ksi, but has no specification for minimum notch toughness. Pre-Northridge specifications did not typically require a certain notch toughness for weld metal or base metal, and so this electrode was primarily chosen for its very high weld metal deposition rates.

The beam flange groove welds were typically made using steel backup bars placed at the root of the weld, and steel weld tabs used to extend the groove geometry beyond the edges of the beam flange. Both the backup bar and weld tabs were normally left in place.

Depending on the vintage of the connection and member section properties, additional items such as continuity plates, doubler plates, and shear tab welds may have been provided. For example, doubler plates were fairly common before 1988, at which time column panel zone yielding was recognized by the UBC as a viable method for energy dissipation and the requirements for doubler plates were relaxed. Shear tab welds were also required in the 1988 UBC if the plastic moment capacity of the beam web exceeded thirty percent of the total beam plastic moment capacity. This provision was included in response to concerns that slip in the bolts could force almost all moment to be transferred by the CJP beam flange welds.

C) Connection Problems in Northridge

The connection failures found in the aftermath of the Northridge

earthquake were predominantly initiated by bottom weld failures, with fracture either in the weld itself or in the heat affected zone adjacent to the weld. These failures were often combined with top weld, shear, or column failures. Disturbingly, failures appeared to have occurred at relatively low rotations with little ductile behavior, significantly less than what was expected or assumed in design (1,2,3,4).

To be fair, a large proportion of weld failures reported were "incipient root cracks." These are by definition the precursor to a weld failure and can only be found by non-destructive testing (NDT) methods (3). It is not clear whether these blemishes were caused by the earthquake, or whether they existed previous to the event. Preexisting imperfections could have occurred due to the weld not being inspected during construction, due to the imperfection being a borderline case which was conservatively considered defective in the post earthquake evaluation, or due to significant differences between pre and post earthquake evaluations (5). Theories began to formulate among engineers defining the culprit to be poor workmanship, the influence of factors not accounted for in design, or a general flaw in the basic concept of the detail (2,6,7,8,9). A more complete description of concerns can be found in Chapter 2.

Despite the uncertainty of the total number of damaged connections, it can be stated conclusively that there were a significant number of serious and blatantly damaged connections which were reason for concern and raised serious doubts about the integrity of the standardized connection detail.

In a further blow to the understanding of the connection behavior, it was found that there was little or no statistical correlation of weld damage to any other

design variable (3).

D) Goals of Current Study

Damage was extensive in the Los Angeles area, and it was shown that the typical steel MRF connection detail used from the early 1970's until the Northridge Earthquake had inherent problems in its performance. The implications of this damage are far reaching, as the connection detail was utilized throughout California and other seismically active areas for over twenty years.

The correction of these problems involves several tasks. There is a need to understand the behavior of the failed connections in order to explain why these failures occurred. This knowledge can be used to design new connections that can preclude the problems, as well as retrofit methods to improve the existing connections. Along with these activities, there is a need for investigations to determine the existing buildings which are currently at risk and to decide the extent of improvements to existing structures that is practical.

Some owners have started their own voluntary inspection programs since the Northridge Earthquake, but many are waiting for government mandates to inspect, or specific retrofit guidelines. Solutions are therefore needed to improve the safety of existing buildings.

The goals of this project are as follows:

1) Review the possible causes of the connection failures.
2) Investigate effective, inexpensive and non-intrusive retrofit procedures, namely the dogbone and the haunch.
3) Investigate the influence of a building slab on the connection retrofit.

4) Develop design guideline recommendations for the retrofit of existing buildings.

E) Solution Schemes to be Investigated

Many concerns pertaining to the typical connection detail dealt with the problems in developing the full plastic moment of the beams at the face of the column. The retrofit procedures to be investigated are therefore based on the concept of forcing the beam plastic hinging away from the column face. This is accomplished by either weakening the beam at a certain distance from the column or by strengthening the beam at the column. Both procedures are based on previous testing which indicated some promise of their effectiveness (10,11,12,13,14,15,16,17,18,19).

1) Dogbone

In the dogbone approach, the beam flange is cut away at a given distance from the column face (Fig. 1.3), thereby weakening the beam sufficiently with the "dogbone" cutout to induce plastic hinging at this point. A full procedure for the design of these retrofits will be developed in Chapters 6 and 7.

2) Haunch

An alternative consists of strengthening the beam at the column face with a haunch (Fig. 1.4), thereby forcing hinging to occur beyond the haunch area and therefore away from the weld. Forces at the columns will be as large or larger than in the original detail, but a larger moment arm will be provided to reduce the weld forces. Chapters 6 and 7 will also develop a full design procedure for a haunch retrofit.

E) Organization of the Report

Chapter 2 will present a literature review on the topic from a historical perspective and present recent research. The test program conducted as part of this study is explained in Chapter 3, with the overall results presented in Chapter 4. A more detailed investigation of the test results is contained in Chapter 5. Chapter 6 develops the basis for designing a retrofit to an existing pre-Northridge connection, and then Chapter 7 develops specific design guidelines for both the dogbone and haunch procedures for cases both with and without a composite or partially composite slab. A summary is presented and conclusions are drawn in Chapter 8.

Chapter 2: Literature Review

Background on the welded flange-bolted web steel moment frame connections is described in this Chapter. First described is the early testing which was used as the basis for the typical pre-Northridge connection detail (defined in Section 1.B and Fig. 1.1). Next, early literature questioning the integrity of the connection and its wide use is discussed. in the post-Northridge literature, attempts to make sense of the Northridge failures and proposals for possible retrofit and new construction details are discussed. Finally, literature dealing with the two retrofit details to be studied (dogbone and haunch), as well as composite studies, are reviewed.

It will be seen from the early literature that there was a definite trend of the original detail towards inconsistent behavior. Unfortunately, drawing specific conclusions regarding the causes of failure, or even the prevalence of failures in the laboratory, is difficult. This difficulty arises due to test procedures, definition of failure and expectations of connections changing through the years and from researcher to researcher. For instance, there has not been a consistent loading history applied to tested specimens. Some testing was done solely with an incrementally increasing static load, others with cycles of increasing static load but differing numbers of cycles at each load level, and some were dynamically loaded. Some tests were stopped, or the load cycles decreased, when failure occurred while others continued. Some specimens were considered failed at the first onset of specimen buckling or fracture, others when the specimen lost the

ability to carry a certain percentage of its maximum load, while others were continued through many cycles of greatly deteriorated behavior. Some tests were terminated simply because the capacity of the test setup was reached. Specimens were considered successful in some cases if they were able to sustain the plastic capacity of the beams through several cycles. Later the concept of connection rotation was used as a performance criteria. Over the years, the accepted value for the maximum connection rotation in a seismic event was increased due to a better understanding of structure behavior. Earlier criteria were based on overall joint rotations, then plastic joint rotations were considered, and later studies concentrated on the beam plastic rotation capacities. The values cited for determining "acceptable" rotational capacities vary among researchers and through time. These criteria generally followed design trends, whereby the concepts of allowing the columns to yield, concentrating all plastic deformations in the beams, and allowing the panel zone area to absorb energy through distortions came in and out of favor.

A) Early Testing of Moment Connections

Testing of welded moment connections for steel frames began in earnest in the mid 1960's, as welding and high strength bolts began to replace the older riveted and ordinary bolted connections. At the 1965 annual meeting of the Structural Engineers' Association of California, Popov and Franklin presented tests of moment connections for 8WF20 beams to 8WF48 stub columns (20). The shapes used were considered "relatively large, in order to ensure similitude with full size structural connections." Four types of connection were tested, welded

flange welded web, a flange cover plate version of this connection, a bolted flange cover plate which was welded to the column, and a connection framing into the column weak axis.

The welded flange, welded web connection exhibited the best overall behavior of the tested specimens. The failure mode, however, was of a bottom weld fracture at the beam web which propagated across the bottom flange during the next cycle. This occurred at a "strain" (measured strain at the center of a beam flange at an "arbitrary distance from the column face") of two percent.

The final results of these studies were published in 1969 (21). The welded flange and welded web connection, described as "the simplest and perhaps most widely used flange connection," made up five of the twenty-four specimens. Failure was considered when "an increase in deflection was accompanied by a decrease in load within a current cycling amplitude." A general observation noted that "fracture was frequently in or near the welds, with several failures occurring in the groove welds of the flanges to the column face." Two of the five welded flange and welded web connections of A36 steel and two of two of grade A441 steel exhibited this failure mode. It was also mentioned that "sharp cornered web copes were a recurring source for initiation of web cracks."

The welded flange and welded web connections "show consistently high energy absorbing capabilities," and outperformed all of the other specimens. The authors also urged caution when extrapolating the results to other member sizes.

A follow up study with various sized sections of grade A36 steel concentrated on comparing the all-welded versus the less costly welded flange and bolted web specimens, and was reported in 1970 (22). Beam sizes were

W18X50 (five specimens) and W24X76 (three specimens) shapes attached to rigid stub columns. Column panel zone deformation effects were beginning to be understood at this time, and the use of doubler plates to prevent the action was utilized.

The all welded connections were shown to exhibit “excellent” ductility, while the bolted web connections had less ductility but were still presumed to be adequate. Of the five bolted web connections, four had a failure mode associated with a sudden fracture of a weld or heat affected zone. Both of the all welded connections exhibited excellent behavior, with the formation of plastic hinge in the beam and no failures before the end of testing. The results of the study indicated that the all welded connection performed best, but noted that all studied connections developed significant strength and ductility before failure. It was later noted that “For the rotation ductilities involved in these experiments, (beam) flange buckling was not a serious problem.” In addition, the web bolted connections never developed the “classic hinge” pattern in the beam web, presumably because of slip of the bolts. Interestingly, a specimen with no beam web attachment failed by a tearing from the bottom cope hole along the beam web just above the fillet area. An evaluation of these results with the previously tested W8X20 specimens was compared (23) and it was noted that there was good correlation of non-dimensionalized results between the different sizes of specimens.

In 1972, a study on the effects of panel zone deformations was initiated (24). Four interior connection specimens were tested, two with 10B15 beams framing intoW8X24 columns and the remaining two with 14B22 beams framing

into W8X67 columns. All steel was of A36 material. The first two specimens had weak panel zones which provided practically all plastic deformations prior to beam flange weld failures. Plastic hinges formed in the beams of the 14B22 specimens and they failed by lateral torsional buckling (LTB) of the beams. It was recommended that a balance be found between the rigid panel zones which provide large beam rotations and a very weak panel zone which absorbs little energy. Recommendations for panel zone design were presented in Ref. 25.

A review and analysis study of the previously mentioned tests was published in 1982 (26). It was noted that "In welded connections, deterioration is usually a consequence of crack initiation and propagation at points of stress concentration at welds. Unless failure is imminent, this deterioration takes place at a slow rate and will not affect the hysteresis loops to a significant degree." Also, "Failure in connections, which may be associated with considerable and rapid deterioration, is usually a consequence of critical crack growth at welds." The causes of premature fracture are then attributed to "undercutting of the welds, insufficient penetration, weld flaws, insufficient fusion, stress concentrations at the copes, and initial flaws and reduced fracture toughness in the through-thickness direction of the column flange material." The cause for any failures, therefore, was placed on poor workmanship or possibly the use of thick column flanges. The bolted web connection failures were attributed to bolt slippage. It was also pointed out that all weld fractures occurred after the formation of plastic hinges in the beam sections, and after considerable ductility and deformations. Review of studies in which panel zone yielding was designed to provide most of the energy dissipation mentioned that the beam-to-column welds could fracture

due to high stress concentrations caused by the kinking of the column flange just beyond the stiffer panel zone area. It was warned that the assumption of full penetration flange welds allowing the development of the plastic moment of the beam sections was only possible after significant strain hardening occurred in the flange material. This was felt to be questionable in the case of larger sections.

In the mid 1980's, several papers were published relating to the code requirements for column doubler plates and continuity plates (27,28). The shear strength requirements of panel zones were relaxed to allow for the shear contribution from the column flanges. Continuity plate requirements were strengthened to account for strain-hardening of the beam flanges. This was meant to reduce the possible stress concentrations at the weld area due to thin column flanges.

In Ref. 27 half scale interior connections were tested to assess the necessity of flange stiffeners and doubler plates. Beams were W18X40 sections of A36 steel, and the columns were 18 inch depth members of A572 Grade 50 steel. Specimens differed in their panel zone detailing. Six of eight specimens ultimately failed in the flange to column groove weld or heat affected area, with the remaining two (questionably) outside the heat affected zones. Tin the first six specimens yielding was confined to the panel zone, and they failed abruptly, while in the last two plasticity was forced to develop in the beams and they failed in a ductile manner. While only three specimens were considered to exhibit good behavior, most of the specimens were not designed conform to current codes and were used to develop code provisions on doubler and continuity plate requirements. These new provisions included the requirement of supplemental

web connection welds if 30 percent or more of the beam plastic moment was transmitted through the web, and continuity plates were required in more instances. In addition, panel zone deformations were specifically addressed.

In the mid to late 1980's accumulated test results were used to develop the concept of flexible connections in the inelastic range (29). In addition, much of the work relating to panel zone energy dissipation (27,30,31,32) was incorporated into codes to allow for the panel zone deformations in design (33). Much of the work in this area was based on analytical studies.

In 1986, Krawinkler reported the testing of twenty cantilever specimens subjected to constant deflection amplitude cycling (34). These were very small specimens, but the focus of the testing was on the development of mathematical models for connection deterioration. The first ten specimens of W4X13 beam sections contained flange groove weld failures, while the second ten of W6X9 beam sections failed by local buckling. The crack propagation at the groove welds was reported to begin with one or several cracks at the beam centerline at the weld toe, which joined and formed a single crack which then propagated through the heat affected zone until it reached approximately one half of the flange thickness at which point the flange abruptly fractured. The specimens held load until the final fracture. It was noted that "Inaccuracies in the analytical model... will be irrelevant compared to the uncertainties in life predictions caused by differences in initial crack size due to variations in workmanship or other parameters that affect the initial crack size." The testing and supporting calculations favored the gradual deterioration of the local buckling failure modes versus the sudden deterioration of flange groove weld failures, although the final

failure of local buckling modes was due to either fracture at the buckles or the beam flange groove weld. It was also noted that damage was accumulated through the total number of inelastic cycles seen by a connection throughout it's lifetime.

In the late 1980's and early 1990's research focused on quantifying the rotations corresponding to the ductility factors utilized in seismic design of steel frames. A study of 13 beam-to-column flange connections was reported in 1989 (35). The first set consisted of three W18X35 beams and three W21X44 beams. The two connections with welded flanges and ordinary bolts performed poorly, while the four with either twist off bolts or additional web welds performed better, although all four failed at moderate rotations. All tests ended with weld failures. Two specimens using twist off bolts and flux-cored arc welding performed extremely poorly, but this was attributed to inadequate welding. It was noted that the welding appeared sound, but no testing of the welds was performed. In addition, one beam of each size was tested with all welded connections and both showed excellent behavior, with no weld fractures occurring.

In 1991, a test was conducted to investigate the adequacy of post earthquake repair procedures (36). In the test, only two specimens consisted of connections to the strong axis of a W-shape column. The specimens before and after repair all provided rotation capacities in excess of the 0.02 radian that the study deemed critical in an earthquake, however all specimens, (including the box column and weak axis specimens), eventually failed due to cracks in the weld or heat affected zone. It is interesting to note that the typical connection detail was shown to have better behavior than many of the other connections studied.

In 1993, eight welded flange and bolted web connections were tested to investigate the need for supplemental web welding as recommended in previous studies (37). Beam sizes investigated were W24X55, W21X57, and W18X60, all of grade A36 steel and attached to a W12X136 section of A572 grade 50 steel. Two of the specimens included supplemental web welds and one was an all welded connection. All specimens failed in the beam flange groove weld or its heat affected zone. Seven of eight of these failures occurred in the bottom flange. Three of the specimens failed before any significant inelastic yielding had occurred. The three specimens with early failures were deemed to have failed due to welding defects at the beam cope area which was not detected by the ultrasonic testing. It was found that the extra web welding or fully welded connection details increased the ultimate capacity of the connection, but did not increase the plastic rotations at failure. A comparison of some previous testing against the newly accepted required plastic rotation capacities of 0.015 radian showed general trends to be marginally acceptable at best. This paper was the first to directly question the acceptability of the standard connections.

A further study of ten specimens was reported in 1994 (38). Beam sizes of W21X50, W21X62, W21X83, and W21X101 A36 steel were tested. Two specimens included slotted bolt holes and two others included supplemental web welding. Five of ten failed by fracture of the top flange groove weld, with the remaining five failing by fracture of the bottom flange groove weld. Plastic rotational capacities were found to be "erratic." Again, strengths of specimens were found to be improved with the supplemental web welds, although the plastic beam rotations were also improved in this study. Rotation capacities were found

to be “fair to satisfactory.” A new criteria for requiring supplemental web welds was presented in which the plastic capacity of the beam flanges at the ultimate moment must be greater than the section plastic capacity including strain hardening. It was mentioned that the beam rotation requirements were significantly reduced if panel zone deformations were allowed, and recommended this approach to design.

In addition, throughout this time period (1960’s to 1990’s) there were several studies on monotonically loading connections to failure (30,39,40,41,42). These studies concluded that all connections with differing web connection details reached the beam plastic moment before failure. Failure generally consisted of tearing in the weld material or heat affected zones. This occurred after substantial rotations were reached. An exception was found in the panel zone hinging study of Ref. 30, in that an early beam-to-column groove weld failure occurred. Unfortunately, it is difficult to compare the monotonic test results to cyclically loaded specimens.

B) Literature on the Questionable Integrity of the Typical Connection

Throughout the 1970’s and 1980’s the use of the typical moment frame connection detail was widespread. In addition, the increasing size of buildings and use of fewer moment resisting frames in a structure led to very large shapes for both the building beams and columns. The adoption of connection details which had undergone relatively few tests for situations which had not been studied at all began to trouble some engineers. In a paper deriving a crack propagation model for fracture of the flange groove welds Krawinkler reported

that “The inability to measure initial crack size together with the great variations in a_0 make the crack propagation and fracture problem a most difficult one and explain the many arguments about the reliability of welded connections.” (34).

In a review of design codes and research in 1988 (43), the following was noted by Popov:

“It must be emphasized that in the three series of experiments described above, the specimens were of modest size. Therefore, extrapolation to designs utilizing thick material and large welds must be done with great care. Experience has shown that in large, highly restrained joints, lamellar tearing may develop unless proper welding sequence and inspection procedures are strictly followed.”

In 1989, Popov and Tsai (35) reported the results of their newer study of moment connections with several reservations in the conclusions. It was reported that while all but two specimens achieved their expected strengths, five of the thirteen beam-to-column flange connections were of questionable ductility. The attained ductilities were not stated to be adequate, but only compared to previous test results. It was noted that “Variability in ductility of moment connections was observed in many instances.” It was warned that the initiation of cracks at the web copes and tack welds for back up bars were common, and steps should be taken to prevent these.

Engelhardt and Husain (37) reported some extensive problems with the flange groove welds in their test studies. It was noted that three specimens failed extremely early, which suggested poor workmanship. In addition, all specimens which performed adequately showed indications that the welds did not develop the full tensile strength of the beam flanges. The authors indicated that web

participation in moment transfer increased the strength of their specimens, but not the plastic rotation capacity. The supplemental web weld requirements were questioned as the "variability in the performance of the beam flanges appears to have had a much greater influence on plastic rotation capacity than Z_f/Z ratio or web-connection detail." The point was also made that the "results of the current test program in terms of the magnitude and variability of plastic rotations are similar to those of previous test programs." In summary the authors wrote "The results of this and previous test programs lead to concerns about the welded flange-bolted web detail for severe seismic applications." Seven of eight specimens failed to meet the acceptance criteria of 0.015 radian of beam plastic rotation, with specimen failures occurring in the weld or heat affected zone.

In 1994, Tsai, Wu and Popov (38) reported that the "plastic rotational capacities of these test specimens are erratic." They went on to indicate improvements in plastic beam rotations and strength when supplemental web welds were provided. A simple calculation showed the necessity of supplemental web welding in more cases than was currently required in order to preclude fracture of the beam flanges before hinging of the whole section. Higher strength steels where the ultimate strength to yield strength ratio is lower were shown to be especially critical. Finally, a warning was given that other connection details should be considered in applications where connection rotations are expected to exceed 0.015 radian.

C) Post Northridge Literature

Post Northridge literature can be broken up into three fairly distinct

groups, damage reports, explanations of damage, and connection designs to prevent similar failures.

1) Damage Reports

Immediately following the Northridge earthquake, preliminary field investigations consisting of quick visual inspections showed that steel moment frame structures performed as expected, with minimal damage (1,6,44). Over the following two weeks, however, severe connection failures were discovered. Damage was first discovered in buildings which were under construction. This led to the discovery of brittle connection failures in buildings which were under repair for what was expected to be minor yielding in the structural elements (1,6,44). The unexpected disclosure of failures instigated more rigorous inspections of other buildings, which also uncovered unexpected damage. Over 150 buildings were identified as containing connection failures by August of 1995 (75 percent of those investigated), and about 300 additional buildings were still to be investigated in the earthquake affected areas (1,6). Most of the buildings now identified as having failed connections showed no outward signs of being damaged (1,6,44). The damage was prevalent in buildings from one to 22 stories in height, and in buildings of all ages, with many of the damaged structures of post 1980 design, and the vast majority of fractures initiated in the bottom flange full penetrations weld area (1,44).

After the damage was discovered, the SAC joint venture was formed between the Structural Engineers Association of California (SEAOC), the Applied Technology Council (ATC), and the California Universities for Research in Earthquake Engineering (CUREe) (1).

An AISC Special task committee meeting on the Northridge earthquake was held on March 14-15, 1994 (2). It was noted that while ductile yielding was expected in the beams away from the column, “fracture in the region of this field welded connection, and some accompanying fractures of the column, occurred mostly in the vicinity of the beam bottom flange connection prior to overall beam yielding. Cracking was initiated in the region of the flange weld near the root at the backup bar and then propagated in to the adjacent supporting column or the beam flange weld. This primary bottom flange fracture was accompanied, in some cases due to the force redistribution, by secondary cracking of the beam web shear plate, fracture of the web plate bolts, and/or top beam flange damage” (2). It was also noted that there was no pattern to the failures and that they occurred in low to high rise buildings (2,44). A call was made to study “supplementary triangular flange reinforcing plates, either parallel or perpendicular to the beam flanges... also, the simple idea of removing a portion of the beam flange away from the connection to create a ductile “dogbone”” was presented (2).

In the same proceedings (2), Engelhardt reiterated his previously reported test results, explaining that a significant number of previously tested connections did not reach beam plastic rotations of 0.015 radian, and that much of the variability in response appeared to be related to the beam flange groove weld behavior overshadowing effects of Z_f/Z ratios and web connection details (2). A simplified analysis showing the significance of Z_f/Z ratios and the reduced ultimate to yield strength ratio of high strength steels was also presented, along with the increased stresses in flange groove welds when moment is not sufficiently transferred throughout the beam web connections (2).

A comprehensive report of steel moment frame damage and failures was presented in Ref. 3. Initial reports from Northridge revealed only minor non-structural damage. In repairing these isolated structures and inspecting some buildings under construction the weld failures were discovered. In opening up more connections and structures as a precautionary measure, much more damage was found. In three months after the earthquake, fifty steel frames were confirmed as damaged (3). Within eight months the number had grown to over one hundred steel frames. It is estimated that over 1200 buildings in the Los Angeles area alone could be affected (3). The most common damage was incipient root cracks, which can only be detected by NDT means, and could have been present before the earthquake (3). It was mentioned that many of these incipient root cracks were borderline cases possibly passing the original construction NDT testing, but failing in the more conservative hindsight evaluations of post Northridge inspections (3,6). Regardless, there were a significant number of connections which exhibited blatant failures, showing that there was a far reaching problem with the typical connection detail (3,6). The most significant aspect of this report was the determination that damage to steel moment frame connections had no significant correlation with any of the other factors studied, including building size, building age, nominal material strength, structural regularity, structural redundancy, number of bays per frame, frame dimensions, or member sizes (3).

2) “What Went Wrong” Literature

The AISC special task committee which met in March of 1994 had some preliminary comments on the causes of damage, citing stress concentrations in the

connection which “rendered the complete joint penetration flange welds to be more susceptible under cyclic load reversals to crack propagation originating from any initial notches, inadequate fusion/penetration, or other imperfections, including the naturally occurring notch-like condition that results from a properly fused but left-in-place steel backing bar” (2). Some interim recommendations for repairing damaged connections were included in the report, which consisted of removal of damaged areas and replacement with new material or weldments (2). In addition, backing bars were to be removed and finished with a reinforcing fillet weld, the beam web welded directly to the column flange, and steel flange plates added (2). The report also mentions other factors as possible causes of the failures, mainly inattention to detailing of the connection and workmanship in the welding process and inspection (2). It was hypothesized that the prevalence of failures in the bottom flange could be caused by the weld root being at the extreme fiber for this flange, the welding process being a start-stop operation to get around the beam web, and/or the restraint of the top flange weld by the floor slab or web connections (2). It was also noted that while materials met ASTM specifications, the beam material could have overstrengths as high as 1.75 and lower tensile ultimate strength to yield strength ratios (2).

Sabol reiterated the possible weld problems (2), and noted thin lines of slag present in bottom flange weld roots, which increased in thickness at the beam web. He noted that initial assumptions of poor weld quality were being supplanted by the realization that field weld failures were similar to previously reported failures in laboratory specimens, stating that “wide spread, faulty fabrication does not appear to be the primary cause of the weld failures” (2). The

possibility of improper weld interpass temperatures and uneven cooling were acknowledged as possible causes of incipient cracking which could lead to failures (2). In summary, "The tendency of the stress riser to initiate the propagation of a crack may be aggravated due to the presence of the included slag, weld execution problems caused by interference at the web, and the presence of built-in stresses due to the two step process used to weld the bottom flange" (2).

A report on failed connections from the Northridge Earthquake (4), found that the fractures in the root of the flange to column groove welds originated in the notch created by the weld backing bar and the associated incomplete fusion. The crack initiated at the mid-length of the weld at the beam web area. It was noted that while beam and column strength and toughness were adequate, the weld materials exhibited poor fracture toughness. It was concluded that the presence of initial defects would cause weld failures at loads associated with minimal beam yielding.

A review of the pre Northridge connections was presented in Ref. 45, in which several factors were presented as possible causes of the Northridge fractures. These causes include the restraint at the column face which gives rise to triaxial forces at the column face, the stress concentrations caused by the backing bar, and the material overstrength of the steel.

In October of 1995, Engelhardt and Sabol presented an overview of the steel moment frame damage in Northridge, along with a list of possible causes (45). Possible weld related contributors included the lack of fusion of the weld metal into the column face at the root of the flange groove welds near the cope

region, coupled with the difficulties of inspecting this area (due to the beam web and interference from the backup bar), and the use of high deposition electrodes. The “crack” at the backup bars and column interface was also cited as a problem due to associated stress concentrations. Discontinuities at the weld runoff tabs were also cited as areas of possible stress concentrations. Low weld toughness was the last weld related issue mentioned. In addition, the overall design concept of the connection detail was questioned. The transfer of most all of the moment through the beam flanges, coupled with material overstrengths, were shown to highly stress the beam flanges and full penetration welds. Assuming the flanges did not fracture, the high stresses in the welds would exacerbate the previously mentioned stress concentrations. The triaxial states of stress at the column face was also mentioned, as well as the fact that column flange bending can increase the stress at the beam flange centerline, even with the use of thick stiffener plates. This suggested that the recent design trend of fewer moment resisting frames in a structure which require much larger member shapes may contribute to greater triaxial forces and related brittleness. The issues of base metal toughness and through thickness properties of column steel were brought up as needing to be researched to fully understand their significance. A later list of factors by the same researchers (7) also included an increase in bottom flange stress and strain due to the existence of a composite floor slab and deformations of the panel zone.

Some researchers agreed with the basic premise that the flange groove welds were overstressed. Following up on previous reports that the beam web connection generally carries very little moment, a truss model was presented to provide a better calculation of actual stresses in the welds (46). This method

recommended the use of horizontal and vertical plates (cover and rib) to take the calculated forces into the column face. A single specimen was tested and it was found that the plastic hinge formed in the beam beyond the added plating. This paper attributed the prevalence of bottom weld failures to the fact that the slab would be able to resist the vertical component of truss force at the top flange.

The results of a series of interviews with engineers involved in Northridge was published in 1996 (6). A thorough list of possible contributions of failures were provided, with the engineers ranking their importance. This article gives insight into the thoughts of practicing engineers in the aftermath of the Northridge failures. The contributing factors included those of design practice (lack of redundancy, design force levels, joint design conception, triaxiality of stresses in joint, left in place back-up-bars, stress concentrations, increased stress due to panel zone shear deformations, existence of continuity plates, low cycle fatigue, and designer understanding of material sciences or weld procedures), connection testing not imitating real life situations and the over-optimism in implementing these details into design, construction materials (toughness of welds, strain rate and temperature effects on fracture resistance, use of high strength steel, ASTM standards for steel grades being too broad allowing for much higher strength and decreased ductility, and residual stresses in mill production), welding practice (non-conformance to existing AWS standards and practice, preheat and cooling, high deposition of welds, AWS definition of rejectable inclusions and weld flaws, welder and/or inspector qualification and certification, and inspection practices), and specific Northridge earthquake ground motion (ground motion values, vertical component, and rapid energy release). The most interesting finding of the

survey was the variation of responses, with respondents assigning a relative importance ranging from high to low for practically every variable. This indicated a belief that there were many factors involved in a highly inter-related fashion. Respondents generally seemed to feel that the connection design itself was flawed and had not been adequately tested in the laboratory. The various sources of stress concentrations, (back up bar, column web bending, and weld irregularities), were seen as sources for concern. In addition, the effect of load rate was a concern.

A paper published later in 1996 (8) also laid out several factors that were considered to have contributed to the failures such as the ground motions, design assumptions and details, material properties, workmanship, and inspection practices. Size effects between tested specimens and those used in recent design were pointed out to be significant, particularly relating to triaxial stresses. Stress concentrations and material overstrengths were mentioned. Emphasis was placed on the low weld metal notch toughness and degraded heat affected zone toughness due to welding procedures. High weld deposition rates, in addition to many factors of the bottom flange weld procedure were pointed out to cause weld quality problems in the vicinity of the beam web area. It was stressed that too much reliance had been placed on post-weld inspections instead of inspection of the welding process itself (in which many factors may contribute to the brittleness of the connection). It was noted that the maximum beam stresses should be moved away from the connection area stress risers and into an area of uniaxial stress by means of stiffening the connection (cover plate, rib, or haunch), or reducing the beam area (dogbone).

In an overview of the connection failures, Maranian (9) pointed out factors such as strain rates possibly exceeding the fracture tolerance level of connection materials, low toughness of older electrodes (although it was also pointed out that there was no correlation to damage and structure age), weld temperatures and cool down rates, poor workmanship and inspection procedures, residual stresses from welding, beam yield overstrengths, stress concentrations, and triaxial stresses.

An article was also published following the earthquake to further stipulate correct welding and inspection procedures to be followed (47).

3) Post Northridge Testing Programs

Shortly after the Northridge Earthquake, a series of sixteen full scale beam-column subassemblages were tested to investigate the standard connection as well as variations to improve its performance (48). Columns were of W14X455 or W14X426 shapes and A572 Grade 50 steel, while beams were W36X150 shapes and A36 steel. Pairs of similar connections were tested, each consisting of either the standard connection detail with improved welds, all welded connections, reinforced connections with either ribs or cover plates, or a "side strap" connection. A great deal of attention was paid to the welding and inspection processes to ensure that workmanship would not be a factor in the test results. The first four specimens, which included the standard connection with improved welds and the all welded connection, performed poorly. Brittle fractures in the beam flange groove welds occurred before significant plastic rotations were reached. Eight out of the ten cover plated or ribbed specimens performed very well. The side strap connection performed poorly. The results showed that improvements to welding alone did not appear to solve the

connection problems, nor did an all welded design. The addition of cover plates or ribs appeared to work well, although through thickness properties of the column were pointed out as the possible next weak link.

As reported in Ref. 45, three specimens of the standard connection were tested, all of which performed poorly. Fractures initiating at the bottom flange groove welds were the causes of failure. Calculations were developed to account for the stress concentration factors, and finite element modeling assuming initial cracking was performed which correlated quite well with the test data. In the conclusion it was stated that a "connection made by directly welding a compact beam flange to a column cannot attain the plastic moment of the beam." It was recommended that either non-compact beam sections be used to initiate earlier beam buckling, that the beam be weakened by drilling holes in the flanges, or that the beam be reinforced with flange cover plates. It was noted that concentration factors due to constraint were highest at the center of the welded flange and ranged from 1.2 to 1.46. A call was made by the authors for the regulation of steel grade minimum and maximum strengths. This would allow plastic hinging to occur when expected in design. Column web fractures were attributed to weak panel zones, which led to the recommendation that column webs should be strengthened when necessary by the use of doubler plates. It was finally noted that "Energy dissipation at a connection by the means of material yielding is notoriously unreliable. A small variation from the design value in beam or column strength will easily result in a totally different energy dissipating mechanism and failure mode."

A further overview of causes of failure for a single building was published

by Ojdorovic and Zarghamee in 1997 (49). The conclusions drawn were that failures occurred due to defects in the root pass of the welds, (slag inclusions and lack of fusion creating "initial cracks"), coupled with poor toughness properties of the weld material. It was determined that initial cracks in the connection were propagated by the high induced stresses during the earthquake combined with residual stresses from welding, stress concentrations from the connection geometry and left in place backing bars, and the composite slab which raises the neutral axis and increases stresses on the bottom flange. It was stated that it "appears that the material toughness of the weld was so low that even welds with acceptable flaw size and base metals with yield strength equal to the nominal value of 248 MPa (36 ksi) could not have prevented crack propagation in a strong earthquake shock."

In 1996, Roeder and Foutch revisited previous testing to check for trends in failures (50). There was considerable scatter in the data, confirming previous claims of erratic performance, but they expressed the opinion that there were trends relating to flexural ductility decreasing with increasing beam depth. Interrelated with this was the beam flange thickness which was determined to be a secondary factor relating to flexural ductility. As was found earlier, panel zone yielding seemed to reduce the beam ductility. It was postulated that a lower ratio of beam length to depth could increase the probability of an early connection failure. As mentioned, all data in this overview showed considerable scatter and many factors were not considered, such as the fact that most tests on larger specimens were more recent and may have therefore used different techniques or weld materials.

Reference 10 presented testing performed as part of the SAC initiative. Three specimens of pre-Northridge design consisted of W14X257 columns of A572 Gr. 50 material and W36X150 beams of A36 material. All three specimens performed poorly, with failure by fracture of the beam bottom flange groove weld at very small plastic rotations. Divot fractures of the column flange occurred, replicating a failure mode which was observed in Northridge but had not yet occurred in the laboratory. One specimen which was repaired to its original condition with higher toughness weld material at the bottom flange and improved with a welded web connection also performed poorly. It failed by fracture of the low toughness top flange groove weld with little plastic rotation. Fractures initiated at the center of the weld length due to incomplete fusion at the weld root, and then followed a path dependant on the stress field and relative toughness of the connection materials. One specimen was loaded dynamically but results were inconclusive as to the behavior comparison to those loaded quasi-statically. Through the loading of one specimen it was found that rejectable discontinuities had formed in the unsevered top weld, leading to the conclusion that some weld defects found in Northridge specimens which were originally attributed to poor workmanship may in fact have been caused by the earthquake. Additional tests are reported in Section 2.E.

In Ref. 11 the results are reported for another test performed as part of the SAC testing project. Three specimens of pre-Northridge design consisted of W14X176 columns of A572 Gr. 50 material and W30X99 beams of A36 material. All three specimens performed very poorly with two failing by brittle fracture in the top flange weld area and the other at the bottom flange groove weld. A large

variation in crack propagation was reported. The panel zones contributed significantly to the total plastic rotations. It was postulated that the prevalence of bottom flange fractures in Northridge was due to composite slab actions and bottom flange groove weld quality. The three specimens were then repaired and re-tested as reported in section 2.E.

Six specimens were tested dynamically to investigate weld metal toughness and load rate (12). Beams were W36X150 A36 material and columns were W14X311 shapes of A572 Grade 50 material. The first two specimens modeled a pre-Northridge connection and a similar connection with backup bars removed and the weld cleaned and reinforced with a fillet weld. Both specimens performed extremely poorly, failing to reach the yield capacity of the beams before brittle failures occurred in the weld material. The next two specimens were welded entirely with high toughness weld electrodes, backup bars were removed and the welds reinforced, and continuity plates were provided. These specimens were greatly improved, developing plastic hinges in the beams and beam plastic rotations of 0.0257 and 0.0374 radian. The fifth specimen included cover plates at the column and a dogbone cutout in addition to the improved weld materials and procedures. It showed excellent performance with a beam plastic rotation of 0.0510 radian. The final specimen consisted of a repair of the second specimen by replacing all welds with high toughness weld material using improved procedures and adding continuity plates. This specimen reached beam plastic rotations of 0.0379 radian. It failed by the gradual extension of cracks which initiated at access holes which were included for the repair.

In addition, several studies were conducted on new connection types.

Many of these were patented which led to relatively little reported information on their design and behavior. Some of these other methods were briefly explained in Refs. 9, 51, 52, and 53.

D) Dogbone Literature

The dogbone, or reduced beam section, design approach is fairly new. In 1990 Plumier (13) mentioned the use of straight dogbone cutouts as "prefabricated dissipative zones" to ensure the expected behavior of a structure in cases such as delivered steel with significant material overstrength. A brief mention of dogbone research by ARBED was included, with promising results. A U.S. patent (#5,148,642) was obtained for the procedure. In the wake of Northridge, the licensing fees and claims were waived on the patent (16)

After Northridge, some other researchers investigated the dogbone approach. Chen and Yeh (14) tested a series of 5 specimens investigating the approach of a dogbone tapered to match an assumed moment gradient. Beam sizes were H600X300X12X12 mm of A36 steel while columns were box shapes measuring 500X500X20X20 mm of ASTM a572 Grade 50 steel. Specimens reached plastic rotations of 0.0235 to 0.0484 radian. Excellent behavior was obtained when the dogbone section was designed to reach its plastic moment rather than yield moment, and some recommendations on design dimensions are given. Both the strength and stiffness of the reduced beam and connection were deemed adequate. A U.S. patent was also applied for based on this research (#5,595,040).

Six specimens of W27X178 beams and W14X455 columns were tested at

UC-San Diego (15). All steel was A572 Grade 50 material. The specimens consisted of a tapered dogbone in conjunction with strengthening ribs at the column face and all performed quite well.

Four specimens of a tapered dogbone design were tested at Smith Emery in late 1995 (16). Two specimens consisted of W30X99 beams and W14X176 columns, while the other two utilized W36X150 beams and W14X257 columns. All columns were of ASTM A572 Grade 50 material and beams of A36 material. Backup bars were removed at the bottom flange only. Plastic hinges formed in the dogbone area, and two of the tests had to be stopped due to the limits of the test setup. Another specimen provided excellent rotations before the top flange ruptured within the heat affected zone at a beam plastic rotation of 0.035 radian. The final specimen failed by a divot in the column in the heat affected zone at a beam plastic rotation of 0.025 radian.

Five tests of dogbone specimens were performed at the University of Texas at Austin (17) which were representative of a connection in a building under construction. Column sizes were W14X426 for five specimens and W14X257 for the final one, all of A572 Grade 50 material. Beam sizes ranged from W30X148 to W36X194 with measured strengths from 38.5 to 58 ksi. All welded connections were provided in addition to continuity plates and high quality welds. The top backing bars were left in place while the bottom plates were removed and the weld strengthened. The first dogbone was of a constant cut shape and failed at the flat portion of the cutout at a beam plastic rotation of 0.02 radian. Subsequent specimens utilized a radius cut dogbone and all four showed excellent behavior until testing was stopped due to the limitations of the test

setup. Some short guidelines for dogbone design were provided.

A much more extensive guideline for the design of dogbone flange reductions was given in Ref. 18. This included guidelines to account for gravity loads and the reduced connection stiffness as well as an application of this method to cover plated connections.

A dogbone connection with the addition of rib plates at the haunch was tested for three strong and three weak axis connections to columns (19). Results were quite good with the exception of the final weak axis connection which only achieved a beam plastic rotation of 0.02 radian.

As was mentioned previously, Ref. 12 included a dogbone specimen. This fifth specimen included cover plates at the column and a dogbone cutout in addition to the improved weld materials and procedures. It showed excellent performance with a beam plastic rotation of 0.0510 radian.

In addition, a study was conducted to determine the effects of load rate and isolated floor slabs on dogbone specimens (54). Push over, quasi-static incremental cyclic, and dynamic loadings were applied to W530X82 beams of CSA G40.21-350W steel and W360X179 columns of ASTM A572 Gr. 50 steel. Two of the six specimens included a composite slab which was isolated from the column. All specimens exhibited excellent performance, with all inelastic deformations occurring at the reduced section.

E) Haunch Literature

As mentioned previously, a haunch retrofit is a method of strengthening the connection at the joint in order to move the beam plastic hinging away from

the column face. An earlier mention of such a procedure consisted of adding cover plates to the beam flanges, while full haunch sections consist of a separation between the beam and haunch flanges with a web section. Literature for cover plated connections will be included along with literature concerning a standard "haunch" made from a section of W shape material.

Shortly after the Northridge Earthquake, one of a series of sixteen tested full scale subassemblages included both cover plates and vertical ribs (48). The addition of cover plates or ribs appeared to work well, although through thickness properties of the column were pointed out as the possible next weak link.

In Ref. 10, testing performed as part of the SAC initiative was presented. Cover plated and/or haunch repairs were made to previously failed connections of W14X257 columns of A572 Gr. 50 material and W36X150 beams of Gr. A36 material. One specimen was repaired with a triangular bottom haunch of W18X143 grade A36 steel, one with top and bottom haunches, and another with a similar bottom haunch and top cover plate. The bottom haunch only repair performed fairly well, reaching 0.02 radian of plastic rotation, however it's failure consisted of a brittle fracture of the top flange groove weld. The addition of the top haunch or the top cover plate resulted in very good performance with no connection failures. When haunches were provided the plastic rotation contributed by the panel zones was greatly decreased. When only a bottom haunch was provided an unsymmetric contribution of the panel zone was noticed, with virtually no contribution when the haunch was in tension but about 20 percent of the total plastic rotation occurring in the panel zone when the haunch was in compression. For the bottom haunch only repair, very low strains were

measured on the beam bottom flange, which was in line with a simplified analysis calculation of the neutral axis location. The bottom haunch flange strains, however, were similar to the beam top flange strains which was not in line with a simplified stress analysis. Shear strains measured in the beam panel zones were much higher than those found in the haunch panel zones. It was noted that the repairs which did not improve the top flange beyond removal of the backup bar and repair of weld defects fractured at this weld. It was recommended that improvements to the top flange connection be provided, although the presence of a floor slab was mentioned as a factor which may help the top weld and a subject in need of further study. The dual haunch specimen's previous bottom beam flange weld fracture was not reattached and this led to significant twisting of the beam section. It was recommended that the severed weld be repaired to prevent this twisting. A final new construction cover plated connection was tested and provided excellent performance. Significant amounts of plastic rotation were provided by the panel zone in this specimen.

A second SAC project was reported in Ref. 11. Cover plated and/or haunch repairs were made to previously failed W14X176 columns of A572 Gr. 50 material and W30X99 beams of A36 material. One specimen had only a straight replacement of damaged areas with thicker plates and weld improvements. This specimen failed prematurely, although this was due to the detailing of a web cope hole at the end of the added section. The other two specimens were repaired with a bottom haunch cut from a W21X93 section of A36 steel. In the first haunch repair the bottom flange had severed in the original connection and was not reattached to the column. In the second repair a section of the top flange was

replaced with a thicker plate section in addition to the addition of a haunch at the bottom of the beam. The cope detail for the added plate was also improved. The triangular haunches greatly improved the behavior of the specimens. It was recommended that the bottom weld fractures be repaired to prevent the strength degradation which was experienced by the specimen without any bottom beam flange connection to the column. Plastic deformation in the panel zone areas was reduced, with most inelastic deformations occurring in the beam section beyond the haunch. A final new construction specimen with a rectangular haunch was tested and it was found that stress concentrations at the end of the haunch led to the separation of the haunch from the beam bottom flange. It was recommended that the detail be fitted with end stiffeners and re-tested.

A specimen was tested which included both cover plates and a dogbone cutout (12). It showed excellent performance with a beam plastic rotation of 0.0510 radian.

Additional testing was performed on relatively small specimens, with columns of W12X106 and beams of W21X68 sections both of A36 material (55). Continuity and doubler plates were included on the three specimens. Three retrofit schemes were tried using cover plates, specifically standard cover plates attached to the top and bottom flanges, shortened versions of the cover plates, and a cover plate applied to the bottom flange only. Results have not been published to date.

Lee and Uang (56) built on the panel zone recommendations of Krawinkler (31) to propose a simplified method of modeling a haunch panel zone. It was noted from finite element modeling that the haunch slope did not vary the

panel zone stress within a practical range of haunch dimensions, and that an assumed bilinear variation of stress with depth was reasonable for an exterior connection or interior connection with haunches on each side of the column. The neutral axis of the beam was found to remain essentially at the mid-depth of the beam although this was not in line with the results of Ref. 10. It was found that most deformation was concentrated in the upper panel zone (beam area). The analytical model was compared to a previously tested specimen and showed good correlation.

An analytical study of the implications of strengthening with haunches was investigated for a single building by Hart et al (57). A building frame was modeled with the original connection, and then with six, twenty, or all 24 moment connections strengthened with haunches. It was concluded that the response varied significantly for the different amounts of strengthening and therefore a full dynamic analysis would be required to complement any strengthened building design.

F) Composite Literature

With the prevalence of bottom flange groove weld failures in the Northridge Earthquake, much discussion has postulated that the composite slab reinforces the top groove weld area while increasing the section capacity and shifting the neutral axis upward to overstress the bottom flange groove weld. While many studies have been done to investigate composite effects on gravity loaded beams, very few have studied the composite action in these laterally loaded structures. The composite action is very different between gravity and

lateral load cases. Typically only lateral load would result in significant positive moments at the column face, (which would place the slab in compression). This literature review compiles studies applicable to lateral loading.

Early testing of composite, interior subassemblages was carried out, both with monotonic (58) and cyclic (similar sign of moment on each beam) (59) loadings. Several specimen details were not representative of a typical connection, however. For instance, the panel zone areas were highly reinforced, thereby losing many of the stress concentrations which may occur at the weld locations. It was recommended that the capacity of the slab area in contact with the column be used in calculations of positive moment, while the full slab width longitudinal reinforcement be assumed active in tension for an interior column (58).

Most composite testing has been geared towards determining effective slab widths in gravity loading situations (58,59), or determining the effectiveness of shear studs (60). There were only a few tests prior to the Northridge Earthquake which studied the composite response to a true lateral loading. An early study (61) consisted of sixteen composite beam-to-column connections which were cyclically loaded in positive moment only. Beams were W12X27 or W16X40 shapes and these were connected to a thick plate which was attached to a test frame. The slab was therefore not integral with the "column," and was either allowed to deflect, or supported by hangers to prevent vertical motion at the "column." Specimens were fully composite, although the distribution of shear studs differed between specimens. An assumption of $1.3F'_c$ times the slab area acting on the column face was assumed as a lower bound on compressive forces

in the slab. This value was based on confinement of $0.4F'_c$, which was felt to be provided by the slab continuity and shear studs. In general, specimen experimental ultimate strengths slightly exceeded the "lower bound" predicted by analysis, (based on $1.3F'_c$ concrete compressive stress). Effects of several variables were studied, such as the effects of a shrinkage gap at the column face, shear stud connector density at the column face, concrete compressive strength, beam depth, formed metal decking versus full depth slab, lateral beam support, and repeated loads.

Two studies were carried out in Japan (62,63). The first of these (62) attempted to determine the compressive concrete force at the column face when the section was subjected to positive bending moment at this location. Values averaged $2.49F'_c$ for the first three pullout specimens, but dropped to $1.74F'_c$ for the fourth specimen which had larger dimensions (although similar sizing ratios). The peak load for all four specimens was very similar. Next, seven composite joint specimens were loaded in a quasi-static manner. Specimens varied in slab thickness, column width, and continuity of the slab at the column location. The beam specimens were small (H300X150X4.5X6), and the neutral axes were expected to be located within the slab. It was found that yield and ultimate moments increased with increasing slab depth as well as with increasing column width. The continuity of the slab appeared to have little significance.

A second study in Japan (63) tested a section of a building consisting of a bay of two W16X57 columns connected by a grid of W14X30 longitudinal and W14X26 transverse beams. A composite slab was provided which had a total depth of 165 mm. A progressive quasi-static cyclic load pattern was applied and

the resulting hysteretic loop was compared to one calculated based on a concrete compressive force of $1.8F'_c$ acting over the width of the column face in positive moment, and one assuming the reinforcing steel within a full slab effective width (based on gravity load provisions) was effective in resisting negative moment. Attained moments at the connection were based determined by calculating the moment diagram based on strain gage data at elastic portions of the specimen. Results were fairly consistent between the specimen and the analytical model.

Another test program of three specimens was also reported in 1989 (64). The three specimens modeled a typical interior and typical exterior moment connection, as well as an exterior moment connection attaching to the column web. Beams were W18X35 shapes and column sizes varied. Panel zone deformations were expected to dominate in the interior connection, while the exterior connection was expected to have some panel zone action component, and the web connection was expected to be dominated by beam deformations. A composite slab of 1.2 m width was provided. The interior and exterior joint connections were dominated by panel zone deformations and ultimately fractured due to cracking near the cope holes. The web connection was dominated by the beam deformations due to the flexibility of the connection. An analytical model was then compared to the test results. The model was based on a concrete compressive force of $1.3F'_c$ at the column face during positive moment and no tensile strength of the concrete (based on Ref. 61). For the typical moment connection tests, the analytical model did not predict the positive moment behavior very well. For the specimen framing into the column flange which was not dominated by panel zone deformations (EJ-FC), the experimental capacity

was well below the predicted positive moment ultimate capacity. This could indicate that the assumed compressive force of $1.3F'_c$ was not attained. It was found that the presence of the composite slab increased the stiffness and strength of the beams in positive moment bending, as well as the stiffness and strength of the panel zones. The increase in panel zone strength and stiffness was found to correlate to a composite panel zone depth extending from the mid-point of the bottom flange to the mid-depth of the slab. Cope hole detailing was felt to have contributed to the ultimate failure of the typical moment connection specimens, and the bolted web connection's inability to transfer shear was felt to limit the increase in positive moment capacity due to the composite slab. Finally, it was found that only a slight increase in energy dissipation was associated with composite action.

After the Northridge Earthquake an attempt was made to study slab effects on steel framing (65). In this study, three composite subassemblages were tested, one bare steel of pre-Northridge design, and two similar frames with composite slabs of differing shear stud arrangements. In the bare steel specimen the bottom weld of one beam failed before any significant rotations were reached. The other beam which had its bottom flange backup bar removed achieved greater rotations. It was noted that the bottom flange had significantly larger tensile strains than compressive strains, and that the neutral axis shifted towards the top flange due to the shear tab being placed closer to the top flange. The first composite specimen failed both beams before acceptable rotations were reached, with fractures occurring in the bottom flange groove welds and heat affected zones. Strain gages indicated that the slab did not participate in moment resistance when

placed in tension, but the neutral axis moved towards the top beam flange when the slab was placed in compression. The top beam flange remained mostly elastic throughout the test, while the bottom beam flange showed early yielding. In the second, partially composite specimen, backup bars were removed. It achieved better performance, failing by low cycle fatigue of the bottom flange at the access hole. Due to the partially composite action, top flange strains were higher than those in the fully composite specimen. A computer model was also developed. The analytical model of composite sections showed that there were significantly higher strains at the bottom beam flanges than at the top beam flanges. Therefore, retrofit of the top beam flange area may be unnecessary when a composite slab is present.

Another study included composite slabs on two of the six dogbone specimens which were tested (54). The slabs were isolated from the column and were shown to exhibit behavior similar to the bare steel counterparts.

G) Literature Trends and Impact on Current Study

The literature to date can be divided into several areas. Early studies provided the basis for the pre-Northridge connection. Subsequent to the Northridge Earthquake research focused on reporting damage, causes of failure, and testing of details to prevent these failures.

Testing in the late 1960's resulted in the development of the typical connection detail. Early research examined the influence of supplemental web welds on moment transfer at the column face, as well as the effects on connection behavior due to panel zone deformations and continuity plates. These findings

were integrated into building codes. Testing just prior to the Northridge earthquake indicated significant deficiencies in connection performance, and pointed out that connections had displayed a tendency towards erratic behavior in previous testing.

After Northridge, damage reports indicated the prevalence of bottom flange weld fractures in the absence of inelastic beam deformations. Observed damage did not correlate with any factors which were studied in Ref. 3.

Post-Northridge testing of pre-Northridge connection details corroborated the damage observed in the Northridge earthquake. Successful solutions for new construction design were tested, including flange cover plates, ribbed connections, haunch, and dogbone designs. All of these utilized higher toughness electrodes as well as other weld improvements. Weld improvements alone, or in conjunction with all welded connections, did not result in acceptable connection behavior.

A number of articles and experimental studies attempted to determine the causes of the Northridge failures. The major factors identified include the low toughness of pre-Northridge connection welds, the stress concentrations and general flange overstress present in the typical connection, the influence of leaving steel backing bars in place (leading to stress concentrations, possible weld inclusions, and added difficulty in inspecting the welds), the stop and start bottom flange weld procedure, and the presence of a composite slab.

In post-Northridge construction many of these possible factors are minimized through the use of moderate toughness weld materials and the removal and cleanup of backing bars and runoff tabs. It is also typical to use methods which force the plastic beam hinging away from the column face.

In the case of a retrofit design, it is desirable to minimize these factors as well, but there are often restrictions imposed by the existing structure. Stress concentrations and weld vulnerability can be incorporated into a design method which introduces a "fuse" away from the column face which can thereby limit the stresses applied at the flange groove welds. From this perspective, different levels of improvement to existing welds would require varying levels of fuse capacity. Specific design methods are developed according to this philosophy in Chapter 7.

Relatively little testing has been done to study the effects of a composite slab on connection behavior. Almost all testing to date has included a fully composite slab with significant amounts of slab reinforcement. When subjected to cyclic loads, the slab contribution is determined as a compression zone emanating from the face of the column flange. The compressive stress acting at this location was reported as $1.3F'_c$ in Ref. 61, although a true cyclically loaded specimen did not reach the estimated moment capacity based on this assumption (64). Another test correlated with data based on a compressive stress at the column face of $1.8F'_c$ (63), although this consisted of testing a full frame. The attained beam plastic moment in this test was determined from an analysis of the moment diagram, based on strain gages which were still in the elastic range as the beam reached its plastic moment. Both previously tested specimens were fully composite with respect to gravity load conditions. It is unclear which value is applicable for concrete compressive force in an actual building, although it appears that our specimens would have less confinement than those in Ref. 64, and as such, a value of $1.3F'_c$ would appear to be an upper bound for the specimens of this study.

It is the goal of this project to advance the understanding of the effects of specific retrofits on connection performance. Previous testing has concentrated on Pre-Northridge connections, new construction designs, and repair methods. A preventive retrofit program has not been investigated. In addition, the presence and influence of a concrete slab is still not fully understood for the case of a laterally loaded structure.

Chapter 3: Test Setup and Specimens

A) Objectives of Experiments

The goal of this project is to experimentally evaluate methods of retrofitting existing steel moment connections and to derive guideline recommendations for the retrofit of connections. To this end, a series of six models of an interior building connection were tested. The specimens incorporated either a dogbone or a haunch retrofit. In addition, alternate specimens included a composite slab. Through the observations and data obtained in these tests the effectiveness of the retrofit procedures and influence of a composite slab were evaluated. The development of guideline recommendations and evaluation of existing retrofit recommendations is presented in Chapter 6.

B) Acceptance Criteria

It must be acknowledged that estimating required demands on a connection within a building is difficult at best. In addition, the specimens tested in this study were approximations of the response of a connection in a real structure. However, these idealized test subassemblages require some basis for evaluating the observed behavior. The strength of a structure must be sufficient, but the connection ductility is even more critical in a seismic MRF. There are many possible ways to measure ductility of the system, such as the plastic rotations of the connection (either overall, or beam, column, panel zone, etc.),

cumulative plastic rotations, or total energy dissipated.

For the purposes of this study, the overall design criteria was referenced to total plastic rotations, as will be defined in Chapter 4. While it was felt that a beam weld fracture would be closely tied to beam rotations, it was noted in Chapter 2 that panel zone rotations can influence the stress concentrations at the welds. It may therefore be prudent to include their effects in the acceptance criteria. In any case, beam deformations were expected to dominate the tested specimens, and therefore beam plastic rotations should be comparable to the total plastic rotations. In Chapter 5, relative deformations of the column, panel zone, and beams will be reported. In addition, the cumulative energy dissipations will be discussed.

Plastic rotational demands on individual connections were evaluated and reported in previous research for ten buildings ranging from two to seventeen stories in height subjected to the Northridge Earthquake (66) and maximum values were found to be approximately 0.010 to 0.015 radian. The same study found that maximum total plastic rotations in the range of 0.015 to 0.025 radian were possible in these buildings when subjected to more severe ground motions on the order of a 10 percent probability of being exceeded in 50 years. It is possible that other building configurations could impose values higher than these, but over the range of typical building construction these values appear to be reasonable. In line with these findings, the FEMA 1995 Interim Guidelines and Advisory No. 1 (67,68) recommended that the new construction standard for connections should be 0.030 radian of plastic rotation without failure.

It should be noted that there is an inherent factor of safety in these

recommendations for plastic rotation as they exceed the expected values from research. This high standard for new construction is not necessarily appropriate for a retrofit design. In fact, most retrofit design guidelines provide factors of safety at levels below new design standards, as evidenced by the reduced seismic design coefficient C_s for existing buildings in Ref. 69 as compared that for new construction in Ref. 70. The reasoning behind this is that it is very expensive to retrofit an existing building, and the cost can quickly become extreme as the required performance level is increased. Providing a cost effective solution which would allow a much wider base of structures to be upgraded while still providing for life safety is felt to be a more attainable goal. Such structures would provide a significant improvement in performance as compared to existing pre-Northridge connections. In line with this reasoning, the acceptance criteria of 0.020 radian total plastic rotation is used in this report for retrofitted connections.

While 0.020 radian plastic rotation has been selected as an acceptance criteria for connection retrofit, site specific studies for particular buildings may show that either higher or lower levels of plastic rotation may be appropriate to achieve building performance goals. In such cases it is anticipated that the experiments described herein should still provide valuable data on the range of plastic rotation capacities supplied by the haunch and dogbone retrofit techniques.

C) Description of the Test Frame

Tests were performed on full sized interior joint subassemblages. Points of inflection were assumed at column story mid-heights and at beam mid-spans. A typical story height of twelve feet and beam spans of twenty-four feet were

assumed. The overall test frame schematics can be seen in Figs. 3.1 and 3.2.

The specimens were loaded at the column tip by means of a 300 kip capacity ram. A clevise was placed at the end of this ram, as well as at the bottom of the column, and rigid links were provided at the tip of each beam. The column and beams of the specimens were extended to pass through Teflon coated lateral restraints which provided lateral bracing of the elements, while allowing motion in the plane of testing.

D) Design and Details of Test Specimens

The test specimens were chosen to be representative of typical building construction details in common use prior to the Northridge Earthquake, and also to not duplicate sizes investigated elsewhere. The beams were chosen as W30X99 sections of Grade 36 steel, typical for a large building. The columns were chosen as W12X279 sections of Grade 50 steel to provide strong column, weak beam action and to provide for a strong panel zone. Three pairs of specimens were tested. Each pair consisted of a bare steel specimen and a similar specimen with a composite slab attached. In the first pair the dogbone retrofit was investigated. In the second and third sets a haunch retrofit with slightly differing weld procedures was investigated. In keeping with the actual construction order the specimens were all assembled as an “original connection”, and then retrofitted. This choice of specimen size was also beneficial in that similar sized specimens of pre-Northridge design were tested previously as part of the SAC program (71). These previous results can be referenced as a benchmark for the performance of the retrofit specimens.

Beam and column sections were fabricated by a large commercial structural steel fabricator in California. Bolting and welding of the beam-to-column connections was not, however, performed by the fabricator due to the completed specimens being too large to ship. The fabricator prepared the beam ends, including preparation of bolt holes, weld access holes, and beam flange bevels. The fabricator also welded the shear tabs to the columns. The column and beam sections were then shipped to the University of Texas Ferguson Structural Engineering Laboratory for final construction and testing.

Overall specimen details are compiled in Table 3.1.

1) Original Connection

The "original" connection was designed, detailed, and constructed in a manner assumed to be typical of mid 1970's pre-Northridge building construction. Past editions of the Uniform Building Code (UBC), structural engineers, fabricators and erectors were consulted regarding past design and construction practices. Details of the connection are shown in Fig. 3.3. As was common practice prior to the Northridge Earthquake, the beam flange groove welds were made by the self shielded flux cored arc welding process with an E70T-4 electrode. The welds were made using backing bars and weld tabs. These were left in place, as was also common practice prior to the Northridge Earthquake. As described in Chapter 2, the low fracture toughness of the E70T-4 electrode has been identified as a major contributing factor to the poor performance of welded moment frame connections in the Northridge Earthquake. Similarly, the practice of leaving backing bars and weld tabs in place has been conjectured as a contributor to the failures. The welding procedure used to make

the beam flange groove welds is presented in App. A.

Construction consisted of first installing the web bolts which were then fully tensioned using the turn of the nut method. This was followed by the welding of the complete joint penetration (CJP) beam flange groove welds.

Design calculations for the original connection can be found in App. B. All design calculations utilized minimum specified yield stress values. The W12X279 column section was chosen to provide a strong panel zone. The test specimens are therefore not representative of cases with weak column panel zones as were permitted by the 1988 UBC code. Detailing provisions of the 1988 UBC code would require supplemental web welds for the test specimens. These welds were not provided, however. It was believed that a larger number of existing moment frame buildings were designed prior to the 1988 UBC and therefore would not likely have included these additional welds.

2) Dogbone Retrofit

There were some special considerations in the case of the dogbone retrofit. First, discussions with fabricators indicated that in order to cut out a top flange dogbone, the floor slab would most likely need to be removed around the beam. This was felt to be a costly procedure. The decision was therefore made to only reduce the cross section of the bottom flange.

The second criteria imposed limited the flange area reduction to a maximum of 50 percent of the total flange area due to concerns over the stability of the beam should larger flange reductions be provided. To date, there have been no dogbone designs tested with flange cutouts greater than 55 percent of the flange area. Calculations for the dogbone retrofit can be found in App. C. As can

be seen there, the use of a dogbone cutout in the bottom flange only combined with only a 50 percent flange reduction did not permit a substantial reduction in moment at the face of the column. The calculations show that the attained moment at the column face is expected to be approximately the plastic moment of the beam.

After fabrication of the "original" connection per section 3.C.1 the dogbone specimens were completed by using a torch to cut the dogbone contours out of the beam bottom flanges. The contour was then ground smooth in a direction parallel to the flange to avoid the formation of notches across the flange which could act as stress risers. For the bare steel dogbone specimen (DB1), the backing bar and weld tabs were removed at the bottom flange welds, and a 5/16 in. reinforcing fillet weld was provided at the base of the groove weld using an E71T-8 electrode in an attempt to avoid the bottom weld fractures which were prevalent in the failed Northridge connections. No modifications were made to the top flange groove welds as the top welds were felt to be less susceptible to fracture, especially with the presence of a composite slab.

Due to the poor performance of the bottom weld on the bare steel specimen, the entire top and bottom flange groove welds were removed and replaced with the E71T-8 electrode for the composite specimen DB2. The E71T-8 electrode provides a minimum specified Charpy V-notch value of 20 ft-lbs at -20^{o}F. This electrode has been frequently used since the Northridge Earthquake where welds of improved fracture toughness are desired, and was provided in an attempt to avoid the fractures which occurred in specimen DB1. It was felt that the presence of the composite slab in DB2 would increase the bottom weld

stresses and therefore most likely result in earlier bottom weld fractures in the absence of additional weld modifications. The dogbone details can be seen in Fig. 3.4.

3) Haunch

The haunch retrofit consisted of welding a section of W21X93 Grade 50 steel into the area of intersection of the bottom beam flange and column flange. A pair of stiffeners are also placed at the end of the haunch to distribute the vertical forces into the beam web. All retrofit welding was performed using the E71T-8 electrode. Details of the retrofit can be seen in Fig. 3.5.

The retrofit is dependant on the beam developing a plastic hinge in the main span beyond the haunch. This results in a moment at the face of the column which is larger than the plastic moment of the beam itself. The original connection welds were not altered, however, since the increased depth of the overall section at the column reduces the weld forces from the values which would be seen in the original connection. Top flange welds in specimens HCH3 and HCH4 were repaired until they were free of rejectable flaws in order to assess the necessity of repairing top flange welds in the retrofit procedure. Sizing of the haunch was chosen to replicate details tested with moderate success in Ref. 11.

E) Slab Details

An 8 foot wide composite slab was included on one of the two "matched" specimens in each set of specimens. Detailing was felt to be representative of typical construction practice and was recommended in discussions with practicing engineers. From previous studies (10,11) it was found that when the bottom of a

pre-Northridge connection was reinforced, weld fractures often occurred in the top flange groove welds. In addition, it was mentioned in Chapter 2 that there was a prevalence of bottom weld fractures in the Northridge Earthquake, and it was postulated that the presence of floor slabs could be in part responsible for this trend. It was therefore of interest to study the ability of a composite slab to prevent top flange weld failures. It was not the purpose of this study to find a level of slab reinforcing which would prevent top weld fractures, but merely to provide a "minimal" slab and see if any benefit was incurred from its presence. Detailing was in accordance with this goal.

Metal decking was oriented across the beam (flutes running perpendicular to the beams). Lightweight concrete was used and the composite action achieved through the use of 3/4 in. diameter by 5-1/2 in. long shear studs welded at twelve inches on center (one stud per metal floor deck rib). These shear studs do not provide fully composite action as defined by the AISC LRFD code. They are designed to provide the capacity of the expected maximum compressive force in the concrete slab, which was determined to be $1.3F'_c$ times the effective slab area in contact with the column flange as recommended in Ref. 61. These studs were hand welded to the beam flange using shielded metal arc welding with E7018 electrodes. Stud welding was not used for the specimens because the cost was prohibitive for the low number of studs used. The welds were then tested by bending the shear studs over thirty degrees by use of the pipe method, in accordance with the AWS code (72). Number three reinforcing bars were placed perpendicular to the beams to prevent longitudinal temperature and shrinkage cracking and a 6X6 welded wire mesh was provided. This wire mesh provided

the only longitudinal reinforcement in the slab, with the exception of two number three bars running along the perimeter of the slab. These number three bars were provided in response to concerns expressed by other researchers that extremely wide cracks were found to occur at the slab edge in previous testing of slabs. This was felt to be an unrealistic result, as the continuity of the slab in a building would prevent these cracks. The number three bars were therefore added to provide a more realistic boundary condition at the slab edges. Details of the slab are shown in Fig. 3.6 and 3.7.

F) Weld Procedures and Inspection Processes

As described earlier, all welds in the "original" connection were made using the SS-FCAW process with a 0.120 in. diameter E70T-4 electrode. Beam flange to column flange welds were detailed as single bevel complete joint penetration (CJP) groove welds with a 30 degree bevel and a 3/8 in. root opening. Backing bars and weld tabs were left in place for the "original" connection. All "retrofit" welds were made using self-shielded FCAW with a 0.072 in. E71T-8 higher toughness electrode. Properties of these electrodes may be seen in Table 3.2. In comparison, E70T-4 has a much higher deposition rate and lower toughness. The welder employed commented on its being rather hard to control due to the high deposition rate.

A single welder from a local steel erection firm who was both experienced and qualified in self shielded FCAW was brought in to perform all connection welding for the project. Welding variables (voltage, wire feed speed, electrical stickout, etc.) were chosen to be approximately in the middle of the electrode

manufacturer's recommended range. All welding was specified to be in accordance with AWS D.1.1-94. The welding procedure specification was enforced during welding and included checks on tolerance of joint fit-up, application of pre-heat, and use of specified welding variables.

All welds were ultrasonically tested by a commercial weld inspection firm. Reports were provided on each weld. "Original connection" welds were left "as is" with reports provided (App. D) documenting their condition. The exception to this was the final set of haunches (specimens HCH3 and HCH4) in which "original connection" top flange welds were repaired until they passed inspection. Specimen HCH3 was repaired using the E70T-4 electrode while HCH4 was repaired with the E71T-8 electrode. "Retrofit" welds were tested when they were critical and reports are provided (App. D). This would include the replaced flange groove welds of DB2, any repaired welds, and the haunch welds of specimens HCH1 and HCH2. The replacement E71T-8 flange groove welds in specimen DB2 were repaired until they were determined to be sound.

Specimen DB1 contained no rejectable flaws as per the AWS Structural Welding Code (72). Specimen DB2 contained no flaws in the top flange welds, however, rejectable flaws were found in both the bottom flange groove welds. The weld material at the flaw locations was replaced and re-tested until no rejectable flaws were revealed.

Specimen HCH1 was determined to have 5 rejectable flaws in the north beam bottom flange groove weld. Four rejectable flaws were reported in the bottom flange of the south beam, as well as two rejectable flaws in the south beam top flange. These defects were left in place as it was felt that removal of the weld

material could significantly alter the material properties at the weld location. In addition, it was felt that the bottom flange defects would not be critical as the stresses at the bottom flange were anticipated to be greatly reduced in the haunch retrofit. The top flange flaws would also be very difficult to repair in the presence of a composite slab. Specimen HCH1 was also found to have weld flaws in the haunch flange welds, and these were also left in place as the "flaws" were actually a result of the 5/16 in. fillet welds which were placed behind the groove weld which was not intended to provide material continuity with the groove weld.

Specimen HCH2 was similarly shown to contain rejectable flaws in several locations. One defect was found in each of the beam bottom flange groove welds as well as in the south beam top flange groove weld. These were all left in place, as the presence of the slab and haunch were expected to reduce the stresses on the top and bottom flange welds respectively. The haunch flange welds were also found to have rejectable defects which were left in place similarly to those in HCH1.

In specimen HCH3 rejectable defects were indicated in all four beam flange groove welds, while in HCH4 only the south beam bottom flange weld revealed no rejectable flaws. All top flange welds were repaired and re-tested until acceptable weld quality was achieved. Bottom flange defects were left in place based on the behavior of the bottom flange groove welds in specimens HCH1 and HCH2 which also contained defects. Haunch welds were not inspected as the presence of "flaws" in specimens HCH1 and HCH2 appeared to be in line with the welding procedures.

Shear studs were hand welded and then a sample was bent to thirty

degrees to inspect the welds in accordance with the AWS Structural Welding Code (72). After most of the shear studs were failed during the testing of specimen HCH2, every shear stud weld was tested in the remaining two slab specimens (HCH4 and DB2).

G) Load History

The specimens were loaded under quasi-static cyclic loading as per ATC-24 guidelines and detailed in Table 3.3. It can be seen that the load history is based on δ_y, the yield displacement of the specimen. In order to be able to directly compare all of the results, load histories are based on the δ_y of the "original" connection, which corresponded to a column tip displacement of 1.2 inches.

H) Instrumentation

1) Overall Test Setup Instrumentation

Instrumentation of the overall test specimen is shown in Fig. 3.8. Load cells were provided at the loading ram, as well as in line with the rigid links which provided beam support reactions. Horizontal displacements of the column were measured with 25 inch linear transducers (Rayelco P-25A) at the point of loading on the column (Fig. 3.9). Horizontal displacements were also measured at the mid-height of the beam using 15 inch transducers (Rayelco P-15A). The displacement transducers were mounted on isolated stub columns and were used to measure the displacement of the column south flange and the beam stiffener above the rigid links. All displacement transducers were placed in pairs,

equidistant to the east and west of the specimen centerline. Readings at each location were averaged to minimize effects of twist of the members. Beam mid-height displacements were measured at two points (column and stiffener) in order to quantify the beam shortening due to plastic deformations throughout the tests. In an actual building this shortening would be restrained by the other columns along the building column line as well as by the building slab. When the values of beam shortening become large, the direct relevance of the results to an actual building may become suspect.

2) Instrumentation for Dogbone Specimens

The dogbone specimens were equipped with four types of gauges. Strain gauges with a gage length of 0.125 in. (Micromeasurements gage EA-06-125AD-120) were used to measure longitudinal strains on the beam web and flanges. Strain rosettes with gage length of 0.125 in. (Micromeasurements gage EA-06-125RA-120) were used to measure panel zone strains. All strain gages were attached using M-bond 200 adhesive and assorted protective coverings were provided. Two inch displacement transducers (Patriot/Magnatech MP-2A) were used to measure the panel zone deformations. Panel zone strains were measured independently for the beam panel zone and slab area panel zone, and overall panel zone deformations were measured at the beam panel zone. Inclinometers (Lucas AccuStar) were used to measure the angle of inclination at the four beam flange to column flange intersections. These inclinometers are reported by the manufacturer to have a resolution of 0.001 degrees and a linearity of $\pm$ 0.1 degrees from zero to ten degrees. Inclinometers were attached to the east and west column flanges at each location. Locations of these gauges can be seen in Figs.

3.10 and 3.11, and are detailed in Fig. 3.12.

3) Instrumentation for Haunch Specimens

The haunch specimens were equipped with four types of gauges. Strain gauges with a gage length of 0.125 in. (Micromeasurements gage EA-06-125AD-120) were used to measure longitudinal strains on the beam web and flanges as well as on the haunch flanges. Strain rosettes with gage length of 0.125 in. (Micromeasurements gage EA-06-125RA-120) were used to measure panel zone strains. All strain gages were attached using M-bond 200 adhesive and assorted protective coverings were provided. Two inch displacement transducers (Patriot/Magnatech MP-2A) were used to measure the panel zone deformations. Panel zone strains were measured independently for the beam panel zone, haunch panel zone, and slab area panel zone. Overall panel zone deformations were measured for the beam and haunch panel zones. Inclinometers (Lucas AccuStar) were used to measure the angle of inclination at the four beam flange to column flange intersections as well as at the north haunch flange to column flange intersection. These inclinometers are reported by the manufacturer to have a resolution of 0.001 degrees and a linearity of $\pm$ 0.1 degrees from zero to ten degrees. Inclinometers were attached to the east and west column flanges at each location. Locations of these gauges can be seen in Figs. 3.13 and 3.14, and are detailed in Fig. 3.15.

4) Slab Instrumentation

The slabs were instrumented with two types of gauges. Displacement transducers were provided at three locations along the length of the north beam to measure slip of the slab with respect to the beam top flange. These were located

at the north end of the slab, and at the first and second metal decking flutes from the column face (Figs. 3.16 and 3.17). In addition, points were epoxied to the slab surface at two inch gage lengths, and deflections were measured between these points with a mechanical clip gage (DMEC) at peak column tip displacements. The locations of these manual strain gauges can be seen in Fig. 3.18. Additional points were placed on specimen HCH4 in order to get a better representation of the compression strains at the column face (Fig. 3.19). In addition, masking tape was placed at each flute of the decking to allow a visual inspection of the slip of the slab relative to the top beam flange (Fig. 3.20).

I) Limitations of Experiments

The test specimens and setup are intended to provide a reasonable approximation of a steel moment connection in a building during an earthquake. This setup was similar to those used in other tests to allow for the direct comparison of results. However, it must be noted that there were several limitations to the test setup which must be considered when interpreting the test results, including the following.

Axial forces in the column were not considered. Gravity loads, overturning moments, and vertical seismic accelerations can contribute to significant axial loadings in compression or tension.

The columns were specifically chosen to provide minimal column bending and panel zone contributions to the total plastic rotations. Where significant yielding of the panel zone is expected the demands on the connection may be less than those studied, however previous research has indicated that the beam

capacities may be reduced (24,26).

Actual strain rates were not simulated. Specimen loadings were in accordance with ATC-24 and consisted of slowly applied cyclic loads. Strain rate effects which may be encountered in an actual earthquake were not modeled . These effects may include altered steel mechanical properties in addition to differing initiation and propagation characteristics of fractures.

Similarly, the actual time history of an earthquake was not modeled. The earthquake loading experienced by a connection is highly dependant on the individual characteristics of the earthquake in question, the connection location in the building, and the buildings design. A meaningful single time history is not possible. Instead, the test loading follows an accepted standard to provide an envelope to expected time history results, and allow comparative evaluations with other studies.

The beam shortening experienced in the testing of several of these connections became large. This occurred subsequent to weld fractures or in the later stages of loading. In an actual building other columns along the span line will restrain this shortening. This was not modeled in the test setup.

The composite slabs, when included, were oriented with their flutes spanning perpendicular to the beams. This orientation was chosen to model a minimal slab contribution. When the decking is oriented parallel to the beam the slab contribution will be increased. Additionally, only one depth of slab and type of decking was included in the study.

Chapter 4: Description of Overall Test Performance

In this chapter, the overall experimental performance for each of the six test specimens is described. For each specimen, a description is provided of significant events that occurred during the test, including the initiation and progression of yielding, buckling, and fracture at various locations within the specimen. Photographs are provided to highlight specimen performance at selected points throughout each test. In addition, three plots of experimentally measured response are provided for each specimen. The first plot shows load versus displacement (δ_{ctot}) at the column tip. Negative values of load and displacement correspond to the column tip being pushed to the north (see Fig. 3.1). On this same plot, in addition to column tip displacement, drift ratio (percent drift relative to story height) is also reported. Drift ratios were computed by dividing the column tip displacement by 144 inches (the height of the column between clevise pins) and then multiplying by 100.

The remaining two plots provided for each specimen show bending moment versus total plastic rotation referenced to the north and south beam of each specimen. For each beam, the moment was computed by multiplying the measured beam end reaction by the distance to the face of the column (136 in.). Positive moment in these plots correspond to tension in the bottom flange of the beam. Total plastic rotation (θ_{totp}) was computed as follows. First, the total rotation (elastic plus plastic, θ_{tot}) was computed by taking the column tip displacement (δ_{ctot}) and dividing by 144 inches. Note that total rotation is identical to drift ratio, except that it is not multiplied by 100. The elastic portion of the total rotation was then computed by taking the beam bending moment and dividing by the initial elastic slope of the individual moment versus total rotation plot. Finally, the total plastic rotation was computed by subtracting the elastic

rotation from the total rotation. The plastic rotation computed in this manner is equivalent to the rotation of a theoretical plastic hinge located at the intersection of the beam and column centerlines. Further details of rotation calculations are described in Appendix E.

For each plot of moment versus total plastic rotation, the total plastic rotation includes all sources of inelastic deformation, including those within the beam, the column panel zone, and the column regions outside of the panel zone. Observations and measurements made during the tests, as described in the following sections and in Chapter 5, indicate that the majority of total plastic rotation occurred within the beam. Only slight yielding was observed in the column panel zones, and no yielding was observed in the columns regions outside of the panel zone.

The remainder of this chapter summarizes the experimental performance of each specimen, as described above. Further detailed analysis of experimental data will be provided in Chapter 5.

A) Specimen DB1

Specimen DB1 was a bare steel specimen. As described in Chapter 3, the connections of Specimen DB1 were retrofitted by the addition of bottom flange dogbone cuts. No modifications were made to the existing low toughness E70T-4 beam flange groove welds, except that the backing bar and weld tabs were removed from the bottom flange groove welds, and a small reinforcing fillet weld was added (see Fig. 3.4). As discussed in Chapter 3, this specimen was intended to represent a low cost connection retrofit strategy.

1) Experimental Observations

Significant yielding of specimen DB1 was first observed during the

loading cycles of 2.40 in. Yielding was concentrated in the dogbone area in the bottom flanges, and near the column face in the top flanges (Figs. 4.1 and 4.2). In addition there was a significant amount of yielding at the web-flange junction at the bottom of the beam, running from the dogbone area to the bottom web cope cutout (Fig. 4.3). Some panel zone yielding was observed on the east side of the column.

The beam bottom flange groove welds both fractured during the first cycle at 3.60 in (Fig. 4.4). In each case, the fracture appeared to be within the weld metal, near the weld-beam interface. The fracture appeared to initiate at the center of the flange, near the beam web cope. Subsequent to the weld failures the web bolts progressively sheared. This continued until the 8.40 in. displacement cycles. By the end of the test all of the north beam bolts and all except the top bolt in the south beam had sheared. In addition, the north beam top flange groove weld appeared to have the initiation of a crack at the end of the test (Fig. 4.5).

The load deflection plot of the column tip applied load and deflection became increasingly pinched at cycles beyond the weld failures. Significant strength degradation was seen in the second cycle of all loading cycles beyond 3.60 in.

The test was terminated after the completion of two loading cycles at 8.40 in. Figure 4.6 shows the specimen at the end of testing.

2) Overall Hysteretic Response

The load versus column tip deflection (δ_{ctot}) as well as story drift is plotted in Fig. 4.7. The moment versus total plastic rotation is referenced to each beam (θ_{totpn} and θ_{totps}) and plotted in Figs. 4.8 and 4.9. It can be seen that the north and

south beams developed 0.009 and 0.006 radian of plastic rotation respectively prior to failure of the bottom flange connection. Thereafter, the flexural capacity of each beam under positive moment (bottom flange in tension) deteriorated quite severely.

3) General Observations

The specimen performed poorly. Failure of the bottom flange welds occurred at total plastic rotations of approximately 0.006 to 0.009 radian. Since the failure occurred in the bottom flange connections it is doubtful that a composite floor slab would improve the performance.

B) Specimen DB 2

In the initial experimental plan, Specimen DB2 was intended to be identical to Specimen DB1, with the exception that Specimen DB2 was to be provided with a composite slab. This was intended to directly study the influence of the slab on connection performance and to determine if the presence of the slab might delay failure of the top flange welds. However, since the performance of the bare steel DB1 was very poor, with failure occurring at the bottom flange welds, it appeared that addition of the slab would likely further worsen the already poor performance of this retrofit technique. Consequently, it was decided that for Specimen DB2, in addition to providing a composite slab, the retrofit procedure would be modified from that provided for Specimen DB1. As described in Chapter 3, the bottom flange dogbone cuts for Specimens DB1 and DB2 were identical. However, for Specimen DB2, the existing low toughness E70T-4 weld metal was removed at both the top and bottom flange groove welds. The beam

flange groove welds were then re-welded using the higher toughness E71T-8 electrode. Backing bars and weld tabs were removed at the bottom flange welds. At the top flange welds, weld tabs were removed and the backing bar was welded to the face of the column. Consequently, the top and bottom beam flange groove welds of Specimen DB2 were similar to current standards for construction of new steel moment frame connections.

1) Experimental Observations

The first concrete crack appeared at the face of the column on the tension side at approximately 0.25 in. of column tip displacement. Significant yielding occurred during the 2.40 in. loading cycles. Yielding occurred at the bottom flange in the dogbone area, along the bottom web-flange junction at the bottom of the beam from the dogbone area to the bottom cope cutout, and in the top flange at the column face (Figs. 4.10 to 4.12). Note that the dogbone yielding is not centered on the cutout and does not appear to distribute evenly to the column face. Some panel zone yielding was noticed on the west column face.

During the 4.80 in. load cycles, fractures initiated at the bottom cope holes and propagated along the bottom edge of the beam web with each cycle (Fig. 4.13). This was followed on the next cycle at 4.80 in. by the fracture of the bottom flange groove weld in both beams (Fig. 4.14). These welds fractured across the full flange width in the first cycle at 6.00 in. (Fig. 4.14). The fractures initiated at the center of the beam flanges, near the beam web cope. Inspection of the weld fracture surfaces revealed some rather large slag inclusions which were not detected by ultrasonic testing (Fig. 4.15). These inclusions may have contributed to the failure of these welds. Behavior in subsequent cycles was

similar, and consisted of the bottom flange closing up against the column face, buckling of the dogbone area, followed by the cope crack extending. On the opposite beam some slight top flange buckling occurred beyond the first shear stud.

Slip of the slab with respect to the beam flange was first noticeable during the 2.40 in. cycles. Slip was only observed for directions of loading that placed the slab in compression. Measured slip was approximately 1/8 in. at the end of the slab, constant over about the last three feet of slab, and then tapered gradually to zero at the column face. During the 4.80 in. load cycles the slip had grown to about 1/2 in. at the final two feet of the slab, and tapering to 1/16 in. at the column face. By the end of the 4.80 in. load cycles the slab had shifted about 1/4 in. to the east at the south end of the beam and the slab had a definite tilt, increasing in elevation from the east to the west. This suggested that the slab was shifting due to the failure of some shear studs.

The test was terminated after the completion of two loading cycles at 8.40 in. Figure 4.1 shows the specimen at the end of testing.

2) Overall Hysteretic Response

The load versus column tip deflection (δ_{ctot}) as well as story drift ratio is plotted in Fig. 4.17. The moment versus total plastic rotation is referenced to each beam (θ_{totpn} and θ_{totps}) and plotted in Figs. 4.18 and 4.19. It can be seen that the north and south beams each developed ± 0.020 radian of plastic rotation prior to failure of the bottom flange connection. Thereafter, the flexural capacity of each beam under positive moment (bottom flange in tension) deteriorated quite severely.

3) General Observations

The specimen performed significantly better than the previous specimen DB1. Failure of the bottom flange welds occurred at total plastic rotations of approximately ±0.020 radian. Once the bottom flange welds failed, however, the behavior was extremely poor and degraded substantially during the second cycle at the later load cycles. It was noted that the fracture surfaces in the bottom flange welds contained some rather large slag inclusions which were not detected by ultrasonic testing and which may have contributed to the failure of these welds. Very little inelastic deformation occurred in the beam webs prior to the weld fractures. Although the specimen obtained beam plastic rotations meeting or exceeding the 0.020 radian of plastic rotation acceptance criteria, the weld fractures occurred at levels very close to this acceptance criteria. Variations in slab details, such as stronger concrete, more reinforcing steel, or steel decking oriented in the other direction, may cause an earlier fracture. Therefore, the connection detail tested must be viewed with caution. Further discussion will be provided in Chapters 5 and 7.

C) Specimen HCH 1

Specimen HCH1 was a bare steel specimen. As described in Chapter 3, the connections of Specimen HCH1 were retrofitted by the addition of a welded haunch at the beam bottom flange. No modifications were made to the existing low toughness E70T-4 beam flange groove welds (see Fig. 3.5).

1) Experimental Observations

Significant yielding of specimen HCH1 was first observed during the

loading cycles of 2.40 in. The yielding pattern included yielding at the bottom flange just beyond the haunch and on the top flange near the column face (Fig. 4.20). In subsequent cycles, the yielding spread into the beam web in the region near the end of the haunch. The yield lines indicated a flow of forces both into the stiffener from the bottom flange and curved towards it from the top flange (Fig. 4.21). The yield lines in the beam web extended beyond the stiffener on the column side by approximately one to two inches. Some panel zone yielding was observed on the east side of the column.

During the first cycle of 3.60 in. the north beam top weld fractured over approximately one half of its length (Fig. 4.22). The fracture appeared to initiate at the west edge of the beam and progress toward the east. By the end of the 3.60 in. cycles the fracture had propagated over the full width of the flange (Fig. 4.22). Little deterioration in the overall strength of the specimen was observed until the fracture propagated across the full flange width. Significant local buckling and lateral torsional buckling of the beams as well as some twisting of the column was observed in the latter cycles of the test.

Web bolts on the north beam progressively sheared off as the loading cycles progressed, with none remaining at the completion of testing. A crack was detected on the south beam top flange weld on the 6.00 in. cycles. The fracture was observed at the weld-beam interface, near the edge of the beam flange (Fig. 4.23). The fracture did not propagate across the beam flange. During the 7.20 in. cycles a fracture developed in the north beam, extending from the bottom cope hole to the stiffener just above the bottom flange (Fig. 4.24).

The test was terminated after the completion of two loading cycles at 7.20

in. Figure 4.24 shows the specimen at the end of testing.

2) Overall Hysteretic Response

The load versus column tip deflection (δ_{ctot}) as well as story drift ratio is plotted in Fig. 4.25. The moment versus total plastic rotation is referenced to each beam (θ_{totpn} and θ_{totps}) and plotted in Figs. 4.26 and 4.27. It can be seen that the north beam developed approximately 0.012 radian of plastic rotation prior to failure of the top flange connection. At the first loading cycle at this rotation the beam sustained approximately 80 percent of the peak attained moment. The south beam developed approximately ±0.044 radian of plastic rotation throughout the test, although only about 50 percent of the peak attained moment was sustained at this rotation. Over 80 percent of the peak attained moment was sustained at the acceptance criteria of 0.020 radian of total plastic rotation.

3) General Observations

Specimen HCH1 showed significantly better performance than Specimen DB1. For each of these specimens, the existing low toughness groove welds were left in place. These results suggest that if existing welds are not replaced with higher toughness weld metal as part of a connection retrofit, then the haunch may provide a greater improvement in connection performance as compared with the bottom flange dogbone. Further, after weld fracture, the haunch specimen (HCH1) showed a significantly higher residual strength than the dogbone specimen (DB1).

The south beam connection of Specimen HCH1 did not fail in the course of the test, developing a total plastic rotation of 0.040 radian. Although the load carrying capacity was substantially reduced at this level of rotation, the

connection was able to sustain 0.020 radian of total plastic rotation with only a slight decrease in moment capacity. Small fractures were observed at the top flange groove weld of the south connection, but these did not propagate across the full flange width. The north beam connection fractured at the top flange weld at a total plastic rotation of 0.012 radian, and therefore did not meet the acceptance criteria of 0.020 radian

. It is clear from this test that the haunch retrofit is vulnerable to fracture at the existing low toughness top flange weld. Further improvement in performance would therefore be possible by replacing the existing low toughness top flange weld with a higher toughness weld, and/or modifying the top flange connection with cover plates, a top flange haunch, or other reinforcement. However, there is also the possibility that the presence of a composite slab may help delay fracture of the top flange weld. This possibility was examined in specimen HCH2. In addition, it may be possible to size the haunch in order to restrict the stresses on the existing welds to levels low enough to prevent fracture.

D) Specimen HCH2

Specimen HCH2 was identical to Specimen HCH1, except that Specimen HCH2 was provided with a composite slab. The purpose of this specimen was to evaluate the influence of the slab on connection performance, and to determine if the presence of the slab would help delay fracture at the existing low toughness top flange weld.

1) Experimental Observations

The first concrete crack appeared at the face of the column on the tension side at about 0.20 in. of column tip displacement. Significant yielding occurred

during the 2.40 in. loading cycles. The yielding pattern included yielding at the bottom flange just beyond the haunch and on the top flange near the column face (Figs. 4.28 and 4.29). Yielding patterns in subsequent cycles were quite similar to those observed in specimen HCH1 (Fig. 4.21). Some panel zone yielding was observed on the east side of the column (Fig. 4.30).

Starting with the 2.40 in. cycles loud bangs were heard during loading with no apparent damage to the connection. It appeared that this sound was due to the fracture of welds connecting the shear studs to the beam. By the 6.00 in. cycles it appeared that all shear stud welds had failed.

Slip of the slab with respect to the beam flange was first noticeable during the 2.40 in. cycles. Slip only occurred in the compressive side of the slab. By the end of the 6.00 in. load cycles a twisting motion had shifted the slab in a direction transverse to the beam approximately 3 in. at the beam ends. This indicated that all of the shear studs had had failed.

The test was terminated after the completion of two loading cycles at 6.00 in. The test was terminated due to safety concerns with respect to the concrete slab stability. Figure 4.31 shows the specimen at the end of testing. No fractures were observed at the beam-to-column connections.

2) Overall Hysteretic Response

The load versus column tip deflection (δ_{ctot}) as well as story drift ratio is plotted in Fig. 4.32. The moment versus total plastic rotation is referenced to each beam (θ_{totpn} and θ_{totps}) and plotted in Figs. 4.33 and 4.34. It can be seen that the beams each developed in excess of ±0.028 radian of plastic rotation at the completion of the test, although the moment capacity at these rotations was

reduced to as little as 53 percent of the peak attained moment. Sustained moments were in excess of 80 percent of the peak attained moment at the acceptance criteria of 0.02 radian of total plastic rotation.

3) General Observations

The composite haunch retrofit was very successful, exhibiting excellent overall performance. The beams developed in excess of 0.028 radian of beam plastic rotation prior to termination of the test due to safety concerns. Although the load carrying capacity was substantially reduced at this level of rotation, the connection was able to sustain 0.020 radian of total plastic rotation with only a slight decrease in moment capacity. No connection failures were experienced. Beam flexural capacity deteriorated gradually due to local and lateral buckling of the beams. The results of this test suggest that the presence of the slab was beneficial to the performance of the top flange weld.

E) Specimen HCH 3

Specimen HCH3 was a bare steel specimen, and was a nominal replicate of specimen HCH1 (see Chapter 3 for details).

1) Experimental Observations

The progression of yielding in specimen HCH3 was very similar to specimen HCH1. Significant yielding of specimen HCH3 was first observed during the loading cycles of 2.40 in. The yielding pattern included yielding at the bottom flange just beyond the haunch and on the top flange near the column face (Figs. 4.35 and 4.36). In subsequent cycles the yielding spread into the beam web in the region near the end of the haunch. The yield lines indicated a flow of

forces both into the stiffener from the bottom flange and curved towards it from the top flange. Some slight panel zone yielding was observed on the west and very faintly on the east sides of the column.

During the first cycle of 4.80 in. the south beam top flange groove weld fractured over its entire length. This fracture occurred in two stages, first over approximately two thirds of the flange width and then over the entire flange width (Fig. 4.37). This fracture appeared to initiate at the edge of the beam flange. Significant local buckling and lateral torsional buckling of the beams as well as twisting of the column were observed.

During the final cycle of 4.80 in. the north beam top weld fractured over its entire length. This also occurred in two stages, first over all but one inch of the weld, with significant load loss, and then completely severing the flange (Fig. 4.37).

Web bolts on the north and south beams progressively sheared as the loading cycles progressed. During the 7.20 in. cycles a crack developed on the south beam from the bottom cope hole to the stiffener just above the bottom flange (Fig. 4.38). The stiffness of the haunch section and the flexibility of the unattached beam section, (once the bolts were sheared), resulted in stress concentrations at their interface and caused the crack propagation.

The test was terminated after the completion of two loading cycles at 7.20 in. Figure 4.39 shows the specimen at the end of testing.

2) Overall Hysteretic Response

The load versus column tip deflection (δ_{ctot}) as well as story drift ratio is plotted in Fig. 4.40. The moment versus total plastic rotation is referenced to

each beam (θ_{totpn} and θ_{totps}) and plotted in Figs. 4.41 and 4.42. It can be seen that the north and south beams developed approximately 0.023 and 0.013 radian of total plastic rotation respectively prior to failure of the bottom flange connection, although the load carrying capacity was diminished by as much as 35 percent in attaining the larger rotation. Thereafter, the flexural capacity of each beam under positive moment (bottom flange in tension) deteriorated quite severely.

3) General Observations

Overall, the performance of Specimen HCH3 was quite similar to the replicate specimen HCH1, except that both connections fractured in HCH3 whereas only one connection fractured in HCH1. The north beam connection fractured at the top flange weld at a total plastic rotation of 0.023 radian, although this was associated with a decrease in load carrying capacity of approximately 35 percent. The south beam connection fractured at the top flange weld at a total plastic rotation of 0.013 radian and therefore did not meet the acceptance criteria of 0.020 radian. Specimen HCH3 confirms that that the haunch retrofit is vulnerable to fracture at the existing low toughness top flange weld, even when precautions are taken to ensure that the existing weld contains no rejectable defects.

F) Specimen HCH 4

Specimen HCH4 was a composite specimen and was a replicate of specimen HCH2. Note that the weld tabs of the top flange groove welds of HCH4 were inadvertently removed. The weld tabs were left in place in all other haunch specimens.

1) Experimental Observations

The performance of specimen HCH4 was quite similar to HCH2. The first concrete crack in HCH4 appeared at the face of the column on the tension side at about 0.20 in. of column tip displacement. Significant yielding occurred during the 2.40 in. loading cycles. The yielding pattern included yielding at the bottom flange just beyond the haunch with a line of yielding continuing on the bottom side of the flange directly under the beam web, and some slight yielding on the top flange near the column face and above the haunch (Figs. 4.43 and 4.44). Yielding patterns in subsequent cycles were quite similar to those observed in previous haunch specimens (Fig. 4.35). Some panel zone yielding was observed on the west side of the column.

During the first cycle of 3.60 in. the north beam top flange weld appeared to develop a hairline crack while loading to the south. While some other possible hairline cracks were noticed, they never extended into a distinct crack. There was no loss of load carrying capacity associated with these possible cracks. This possible top flange weld crack can be seen in Fig. 4.46 at the completion of testing.

Starting with the 2.40 in. cycles loud bangs were heard during loading with no apparent damage to the connections. As with specimen HCH2, it appeared that this sound was due to the fracture of welds connecting the shear studs to the beams. By the 6.00 in. cycles it appeared that all shear studs had failed.

Slip of the slab with respect to the beam flange was first noticeable during the 2.40 in. Slip only occurred in the compressive side of the slab. The slip was

approximately 3/16 in. at the end of the slab tapering gradually to zero at the column face. During the 3.60 in. load cycles the slip on the north beam had grown to about 3/8 in. and remained constant until approximately 3 feet from the column face at which point it tapered to zero. The south beam showed 1/2 in. of slip at the end tapering to 3/16 in. at the 3rd flute from the column face, and zero over the first two flutes at the column. Slip increased over subsequent loading cycles until reaching about 1.75 in. during the 6.00 in. cycles. There was also as much as 3 in. of offset to the slab in a direction transverse to the beam (Fig. 4.47). This indicates that the slab was shifting due to the failure of shear studs.

The test was terminated after the completion of two loading cycles at 8.40 in. Figure 4.48 shows the specimen at the end of testing. No failures occurred at the beam-to-column connections.

2) Overall Hysteretic Response

The load versus column tip deflection (δ_{ctot}) as well as story drift ratio is plotted in Fig. 4.49. The moment versus total plastic rotation is referenced to each beam (θ_{totpn} and θ_{totps}) and plotted in Figs. 4.50 and 4.51. It can be seen that the beams each developed in excess of 0.050 radian of plastic rotation prior to completion of the test due to reaching the limitations of the test setup, although the sustained moment capacity was as low as 30 percent of the peak attained moment at these rotations. Over 80 percent of the peak moment capacity was sustained at the acceptance criteria of 0.020 radian of total plastic rotation.

3) General Observations

The composite haunch retrofit resulted in excellent performance of the connection. The beams developed in excess of 0.050 radian of beam plastic

rotation prior to completion of the test. Although the load carrying capacity was substantially reduced at this level of rotation, the connection was able to sustain 0.020 radian of total plastic rotation with only a slight decrease in moment capacity. No connection failures were experienced. Beam flexural capacity deteriorated gradually due to local and lateral buckling of the beams. This test provides further evidence that the slab provided a beneficial effect for the top flange welds.

G) General Observations on Experimental Results

An summary of the test results is presented in Table 4.1. These results can be compared to previous testing of W30X99 beams of pre-Northridge connection details which was performed as part of the SAC initiative and compiled in Ref. 71. In these previous tests the low toughness electrodes were utilized. There were several differences from the specimens in this project. First, supplemental shear tab welds and continuity plates were used (each of which may improve connection performance, see Chapter 2). Also, columns were of W14X176 shapes. The connections tested were only one sided, yet this smaller column shape allowed for panel zone deformations which provided plastic rotations on the order of the beam plastic rotations. As will be discussed in Chapter 5, the specimens tested as part of this project were dominated by beam plastic deformations. Panel zone deformations have been shown to increase total plastic rotations (see Chapter 2). Each of the six similar specimens in Ref. 71 resulted in fractures of the beam flange weld or heat affected zone. These fractures occurred at total plastic rotations of 0.008 to 0.021 radian. Approximately half of these

rotation values were associated with beam deformations.

The bare steel bottom flange dogbone (specimen DB1) exhibited the poorest performance of all specimens tested. Both bottom flange groove welds failed at low levels of plastic rotation (0.006 and 0.009 radian). This specimen did not provide any increase in performance over a non-retrofitted connection.

The composite bottom flange dogbone (specimen DB2) exhibited a marked improvement over specimen DB1, achieving beam plastic rotations on the order of 0.020 radian. Both connections, however, still failed by fracture of the bottom flange groove welds, despite the fact that a higher toughness weld metal was provided for specimen DB2. Due to differences in the weld material provided in the composite specimen (see Chapter3, section C2), differences in performance between DB1 and DB2 reflect both the effects of the composite slab and the differences in weld metal toughness. Nevertheless, specimen DB2 sustained much higher levels of plastic rotation than DB1, likely due to a substantial benefit from the higher toughness weld metal. Specimen DB2 provided total plastic rotations on the order of the maximum values achieved in Ref. 71. However, it is difficult to compare the performance between specimens due to differences in connection detailing and weld materials.

Three of the four bare steel bottom haunch connections (specimens HCH1 and HCH3) failed by fracture of the existing E70T-4 top flange welds at total plastic rotations in the range of 0.012 to 0.023 radian. The fourth connection (south beam of HCH 1) did not fail by fracture, but simply deteriorated gradually due to local and lateral buckling. These specimens performed better than DB1 although a bottom haunch retrofit may still be vulnerable to fracture at the

existing low toughness top flange welds. These specimens achieved rotations are similar to the non-retrofitted connections of Ref. 71. Detailing and panel zone contributions of the previous tests would be expected to result in higher performance than the "original" connection of this study. Therefore, these similar rotations may indicate an improvement in specimen performance. It was hoped that the top weld fractures of HCH1 and HCH3 would be prevented by the provision of a composite floor slab.

With the addition of a composite floor slab (specimens HCH2 and HCH4) the connection behavior was excellent. None of the four connections failed by fracture, but simply deteriorated gradually due to local and lateral buckling of the beams. The top weld fractures of specimens HCH1 and HCH3 were prevented by the inclusion of a composite slab. Testing of both specimens was stopped due to testing limitations and total plastic rotations were in the range of 0.028 to 0.055 radians when testing was stopped.

Peak rotations were often associated with substantial loss of load carrying capacity. All connections, (with the exception of the north beam of HCH3), which achieved 0.020 radian of total plastic rotation sustained in excess of 80 percent of the peak attained moment when reaching this critical level of rotation.

In general, specimens with a composite slab achieved peak forces that were approximately 15 percent higher than the companion specimen without a slab.

Specimens with bottom haunch performed much better than specimens with a bottom flange dogbone. The bottom haunch specimens performed quite well, with excellent performance when the composite slab was included.

Further discussion of specimen performance is provided in Chapter 5.

Chapter 5: Further Analysis of Experimental Data

In this Chapter, the experimental performance of each of the six test specimens is described in greater detail than was covered in Chapter 4. First, a description of specimen materials data is presented. From this data a comparison between expected and attained section strengths is developed. Detailed descriptions of deformations and energy dissipation for each specimen are then presented. The slab effects are then analyzed, initially through the instrumentation specific to the composite specimens (mechanical strain gages, slip measurements), and then through a comparison to the corresponding bare steel specimens. Finally, relevant strain gage readings which were not included elsewhere are reported. Calculations for data reduction can be found in App. E.

A) Materials Data

1) Mill Certificate Data

Mill certificate data is listed in Table 5.1 for the beam and column sections for all specimens. It should be noted that although the columns were specified as A572 Gr. 50 steel and the beams A36 steel, reported yield strengths were in the range of 50 to 55 ksi for all delivered steel. In fact, column yield strengths reported on the mill certificates were lower than for the beams.

2) Tensile Coupon Test Results

Material for 0.5 inch diameter tensile coupons with a two inch gage length was taken from four locations of each column specimen as shown in Fig. 5.1.

Similarly, four standard plate type tension coupons with an eight inch gage length were taken from one beam of each specimen as shown in Fig. 5.1. Haunch material coupons were obtained from locations similar to beam coupons. Coupon materials were obtained from the non-yielded column tip and beam end sections of specimens. All testing was done in accordance with ASTM procedures at Ferguson Laboratory. The results of tensile coupon data can be seen in Table 5.2.

Several interesting factors were found while testing the coupon specimens. The column web quarter point specimens consistently exhibited higher yield and ultimate strengths, no yield plateau, and lower ultimate elongation when compared to coupons from other column locations. This may be related to the shape production process, namely the act of straightening the jumbo column shapes, which may lead to yielding and hardening of the section web in the area approaching the web-flange intersection (73,74). Also, the beam flange material coupons did not exhibit a well defined yield point or upper yield point, but still possessed a distinct yield plateau.

3) Other Materials Data for Steel and Weld Materials

Weld material from specimen HCH1 was sent to a certified testing laboratory for weld toughness property testing. Charpy V-Notch tests were conducted in accordance with ASTM E23. Half of the specimens were tested at +70 degrees Fahrenheit, the other half at -20 degrees Fahrenheit. Material was acquired from two welds, the bottom beam flange to column flange weld (E70T-4 electrode, “original” weld), and the haunch flange to column flange weld (E71T-8, retrofit weld). Material from six locations in each weld was tested. Results are tabulated in Table 5.3.

As would be expected, the weld toughness was seen to decrease as the temperature decreased. For post-Northridge construction, it has become typical to specify a weld toughness minimum of 20 ft-lb at -20 degrees Fahrenheit. It can be seen that toughness results of the E71T-8 weld material exceeded the 20 ft-lb minimum specification of the material for both temperatures tested. The E70T-4 material, however, did not attain 20 ft-lb for any of the specimens. The brittle behavior of the E70T-4 specimens was also indicated by the low lateral expansion measurements as well as the very low percentage of sheared fracture surface. Overall, the toughness properties of the E71T-8 material far exceeded those of the E70T-4 material.

It should be noted that while the weld toughness of the E70T-4 material was found to be very low, other studies have reported the in place toughness of this electrode to be less than 10ft-lbs at 70^{o} F (12). Therefore, the toughness of the weld material used in this study may actually be higher than typical for E70T-4 material, and results should be evaluated accordingly.

4) Concrete Compressive Strengths

A standard 3000 psi lightweight concrete was ordered for all composite specimens. The mix was recommended by the supplier to obtain an actual 28 day strength approaching 4000 psi. Delivered material was very dry and water was added to arrive at the recommended standard slump of five to six inches. In addition, concrete for specimen HCH4 had additional water added at delivery to achieve a slump of approximately nine inches in order to provide a concrete strength differing significantly from specimen HCH2. This strength difference was desired in order to investigate the influence of the differing concrete strengths

on composite performance. Six inch diameter by twelve inch long test cylinders were cast from concrete extracted midway through the placement of material for each slab. Three to four concrete cylinders were tested at an age of 28 days, in addition to ages corresponding to the test days of the specimens. Results of these compression tests are listed in Table 5.4. Actual delivered material for all specimens far exceeded the 3000 psi specified strength. Only the mix for HCH4 (which had a significant amount of water added at delivery) approached the nominal strength.

5) Observations from Materials Data

Column material properties found from coupon tests were quite similar to values reported from the mill certificates, while beam material property test results were lower than the mill certificate data. While the A572 Gr. 50 column steel had a yield value of approximately 50 ksi, the A36 beam steel consistently had yield strengths of approximately 50 ksi. Concrete compressive strengths were also generally much higher than specified, even with the addition of water at delivery. Weld material toughness values were substantially higher for the E71T-8 as compared to the E70T-4 electrodes.

B) Analysis of Test Specimen Forces and Strength

1) Section Properties

The nominal section properties and general properties are listed in Table 5.5. Actual measured dimensions and corresponding properties are listed in Table 5.6. It can be seen that, in general, the delivered beam sections were slightly deeper and the flanges were thinner and slightly wider than the nominal section.

Values of the plastic section modulus (Z) were correspondingly about five percent lower than nominal values. Column sections delivered were had slightly smaller dimensions than their nominal values and a slightly lower Z value.

2) Analysis of Beam and Column Moments

A comparison of nominal and estimated plastic moment capacities of the bare steel W30X99 beam sections is shown in Table 5.7. Nominal capacities (M_{pn}) are based on the nominal section dimensions of Table 5.5 and the minimum specified F_y (36 ksi for the beam sections, 50 ksi for the column sections). Estimated capacities (M_{pe}) are based on the measured section dimensions of Table 5.6 and the dynamic tensile coupon data of Table 5.2. Material yield strengths used in the calculations were separated into those of the web (F_{yw}) and of the flanges (F_{yf}). Strain hardening is neglected in these calculations (as well as others throughout this Chapter). It can be seen that the beam sections had plastic moment capacities far exceeding their nominal values, due to the overstrength of the delivered material.

Nominal and estimated moment capacities of the bare steel dogbone section (at center of reduced flange area, M_{nRBS} and M_{pRBS}) and haunch section (at column face, M_{nHCH} and M_{pHCH}) are listed in Tables 5.8 and 5.9 respectively. Nominal capacities (M_{nRBS} and M_{nHCH}) are based on the nominal section dimensions of Table 5.5, dogbone flange reduction and haunch addition as shown in Figs. 3.4 and 3.5, and the minimum specified F_y (36 ksi for the beam sections). Both estimated capacities are based on the measured section dimensions and measured dynamic yield strengths. There is some question as to the thickness of the haunch flange to be used in the calculation of M_{nHCH} and M_{pHCH}. The actual

projected flange section on the column face is equal to the thickness of the flange divided by the cosine of the haunch angle, a value in excess of the flange thickness. However, the maximum stress possible in the flange would be limited by the capacity of the flange in its longitudinal direction, which would correspond to the thickness of the flange. Finally, it could be argued that the maximum stress perpendicular to the column face is therefore limited by the flange thickness times the cosine of the haunch angle. To simplify the calculation procedure, the nominal flange thickness was used. It will be seen that the section at this location has considerable overstrength, and this simplification is reasonable.

A comparison of nominal and estimated plastic moment capacities of the composite W30X99 beam sections is shown in Table 5.10. Nominal capacities (M_{pCn}) are based on the nominal section dimensions of Table 5.5, the minimum specified F_y (36 ksi for the beam sections, 50 ksi for the column sections), and nominal F'_c (4000 psi). Nominal capacities at the center of dogbone (M_{pCnRBS}) and haunch at column face (M_{pCnHCH}) are calculated similarly, with dimensions modified as in Figs. 3.4 and 3.5. Estimated capacities are based on the measured section dimensions of Table 5.6, dynamic tensile coupon data of Table 5.2, and actual concrete strengths on the days tested as reported in Table 5.4. Estimated capacities are reported for two locations for each specimen, at the column face (M_{pCe} for dogbone, M_{pCHCH} for haunch), and at the critical section (M_{pCRBS} for center of dogbone, M_{pCe} for end of haunch). Material yield strengths used in these calculations were separated into those of the web (F_{yw}) and of the flanges (F_{yf}). Assumptions of concrete effective width equal to the column flange width (nominal width in M_{pn}, measured width in M_{pe}) and maximum compressive

strengths of $1.3F'_c$ were used (as recommended by Ref. 61 and 64). Only the concrete above the metal decking flutes was considered effective and the minimal longitudinal reinforcement was neglected in calculations. Slab contributions were neglected when the slab was placed in tension.

It can be seen from Tables 5.7 to 5.10 that the beam sections had plastic moment capacities far exceeding their nominal values, due to the overstrength of the delivered materials.

Attained values for all tested specimens are reported in Tables 5.11 through 5.14. These are reported as both maximum moments attained at the face of the column or the critical section (center of dogbone cutout, end of haunch), as well as in terms of percentage of estimated plastic moment capacities (from Tables 5.7 through 5.10). The attained moment is calculated as the support reaction multiplied by the distance to the column face (136 in.), or distance to the critical section (121 in. for center of dogbone, 118 in. for end of haunch). All specimens attained in excess of the nominal plastic capacity of the sections (from Tables 5.7 through 5.10), except for the haunch specimens at the column face locations. This is due to the "fuse" in the haunch specimens being much more effective at limiting the stresses at the column face, although it raises additional concerns regarding the fracture of the bare steel specimen top flange welds. It can be seen that the achieved to estimated ratios are lowest at the face of the column for all specimens, as would be expected from the design philosophy of the retrofits (forcing inelastic deformations to the center of dogbone or end of haunch). The ratio reduction at the column face is much greater for the haunch

specimens, indicating a larger factor of safety and greater reduction of weld stresses inherent in the specimen's design.

Dogbone specimens did not reach the estimated plastic capacities at the column face in any specimen, (indicated by ratios in Tables 5.11 and 5.12 of less than one). At the critical sections both the bare steel and composite specimen only achieved the estimated plastic capacity in negative bending of one beam. This was indicated in Chapter 4 by the lack of inelastic deformations in the beam sections prior to the early bottom weld fractures.

Of the bare steel haunch specimens of Table 5.13, the lower attained moments in the south beam of HCH1 could explain the fact that of all four bare steel haunch connections, only this one remained intact throughout testing. Bare steel attained to estimated moment capacities at the critical section (end of haunch) exceeded values of one, indicating some strain hardening of the sections. This was indicated in Chapter 4 by beam yielding and slight buckling of the sections prior to weld fractures.

The composite haunch specimens (Table 5.14) attained capacities exceeded estimated values for the negative moment at the end of haunch location. These ratios are generally larger than the bare steel ratios, indicating that there was some tensile capacity being contributed by the slab even at extreme stresses. This occurred despite the fact that a large crack had opened across the entire slab at the column face. Composite haunch attained capacities were generally lower than calculated values for the positive moment. This could either indicate that the assumption of $1.3F'_c$ was an overly optimistic assumption for the compressive slab stresses, or that the shear stud failures occurred before the maximum

moments could be attained, and therefore the slab contributions were limited at later stages of loading by the lack of shear connection. Although the shear studs only provided a partially composite section according to the gravity load specifications in the AISC LRFD code provisions, the design capacity of the shear studs exceeded the maximum concrete compressive force assumed in the design of positive moment capacity at the column face. It is possible that the shear stud failures were caused by twisting action of the specimen and related torsional forces and not due to ordinary shear action, although failures could also be due to poor shear stud welds. Therefore, no conclusions can be drawn with regard to the adequacy of the AISC shear stud strength provisions, although it is tentatively recommended that the nominal capacity of shear studs for cyclic design may need to be lowered until further research is done. More information on shear stud failures is included in section 5.E.1.

An additional comparison of estimated composite haunch plastic moment capacities is listed in Table 5.15. Here, an assumption of $0.85F'_c$ is used for the maximum compression in the concrete (rather than the $1.3F'_c$ of Table 5.14). It can be seen that this assumption provides a lower bound of the compressive strengths (all positive moment ratios approach one). Assumptions of concrete effective width was still assumed equal to the column flange width (measured width in $M_{pCHCH}(.85)$). The attained positive moments for specimen HCH2 and HCH4 were matched rather well when an assumption of $0.85F'_c$ rather than $1.3F'_c$ compressive stress was used, and this value may therefore be more applicable to strength calculations. In the case of a retrofit design, the larger value of $1.3F'_c$ should give a safe bound on the results. A reduction of nominal shear stud

capacity on the order of 0.85/1.3= 0.65 may be applicable for cyclic design of shear studs, although the early shear stud failures in this study may have been due to other factors as discussed earlier.

In the bare steel haunch specimens it was observed that attained moments did not reach yield moment capacities of the section at the column face (M_{yHCH} of Table 5.9). Therefore, maximum stresses on the extreme weld locations were below the base material yield stress at the point of any weld fractures. However, the attained moments are on the order of 94 to 99 percent of the estimated yield moment capacity. This would correspond to a stress on the extreme weld locations exceeding 45 ksi (the percent of yield times the measured dynamic yield stress). Due to the uncertainty of the actual compressive forces attained in the composite slabs it was difficult to determine stresses on the welds for these specimens, although yield lines on the specimens indicated that top flange weld stresses were close to the base material yield stress.

Maximum column moment applied to the specimens was calculated as the maximum applied load times the distance to the top of the beam flange, (57.175 in.). For the dogbone specimens this moment would theoretically be reached in the column both above and below the beams, while the haunch specimens would have a reduced moment in the lower column portion due to the column having a lower panel zone in the haunch region. Attained column moments and their ratio to the moment capacity are listed in Table 5.16. The maximum column moment occurred in specimen HCH3 and had a value of 17700 kip-in. The column sections were expected to exhibit elastic response throughout the tests, as the yield capacity of the columns was calculated as 23300 kip-in (from Table 5.7).

3) Analysis of Panel Zone Shear Forces

Panel zone shear capacities are tabulated in Table 5.17. Code capacities are based on $V_n=0.55F_{ycw}d_ct_{cw}[1+3b_ct_{cf}^2/d_bd_ct_{cw}]$

where:

V_n = Panel zone strength based on Equation 11-1, Section 2211.7.2.1 of the 1997 UBC

F_{ycw} = Yield stress of the column web

d_c = Depth of column

t_{cw} = Column web thickness

b_c = Width of column flange

t_{cf} = Thickness of column flange

d_b = Depth of panel zone

This UBC code equation is based on work by Krawinkler and is intended to include the contribution of column flanges towards panel zone shear strength. It should be mentioned that the beam depth at the column face was not clearly defined in specimens other than DB1. Composite specimen calculations assumed the value of d_b to extend to mid-height of the entire slab thickness, or 3.12" above the top beam flange, as recommended by Ref. 64. Haunch specimens were assumed to extend to the bottom of the haunch.

In addition, a simplified value of panel zone shear strength which neglects the contribution of the column flanges is shown. Restricting panel zone shears to values lower than these should limit panel zone behavior to the elastic range. Here $V_p=0.55F_{ycw}d_ct_{cw}$

where:

V_p = Plastic shear capacity of the column web

F_{ycw} = Yield stress of the column web

d_c = Depth of column

t_{cw} = Column web thickness

Values are shown for each equation at nominal yield strengths of 50 ksi and dynamic yield values of 56.6 ksi.

Maximum panel zone shears attained in the course of testing were calculated as follows $V_{max} = \frac{|M_{nb}| + |M_{sb}|}{.95d_b} - |V_{col}|$

where

V_{max} = Maximum shear force developed in the column panel zone

M_{nb} = Maximum beam moment developed at the face of the column in north beam

M_{sb} = Maximum beam moment developed at the face of the column in south beam

d_b = Depth of beam

V_{col} = Column shear force (outside of panel zone) when M_{nb} and M_{sb} are reached (applied column tip load)

It should be mentioned that the beam depth at the column face was not clearly defined in specimens other than DB1. Composite specimen calculations assumed the value of d_b to extend to mid-height of the entire slab thickness, or

3.12” above the top beam flange, as recommended in Ref. 64. Haunch specimens were assumed to extend to the bottom of the haunch.

Values of V_{max} were included in Table 5.17. It can be seen that all specimens were expected to yield ($V_{max}>V_p$) when compared to the nominal column strengths, although only DB1 would be when the actual measured dimensions and dynamic yield strengths were used. All maximum shear values were well below the ultimate capacity of the panel zones when column flange contributions were accounted for (V_n).

4) Observations from Strength Analysis

Beam yielding and hinge formation as determined by flaking of whitewash during testing was extensive for both composite haunch specimens, the south beam of HCH1 and the north beam of specimen HCH3. The remaining two bare steel haunch connections showed moderate yielding. The majority of yielding in specimen DB2 was concentrated in the lower beam web. The bare steel dogbone showed only minor beam yielding prior to failure. These observations were in agreement with the results tabulated in Tables 5.11 through 5.14, where all haunch specimens approached or exceeded the calculated plastic capacities of the end of haunch cross sections (attained to estimated values of 1.04 or higher for bare steel, 0.94 or higher for composite positive moment, 1.07 or higher for composite negative moment), while the bare steel dogbone failed to reach the limiting plastic moment capacity at the center of dogbone reduction for three of four cases, (attained to estimated values of 0.90 to 1.02). The composite dogbone also failed to reach the plastic positive moment capacities calculated in three of four cases, (attained to estimated values of 0.93 for composite positive moment,

0.97 to 1.03 for negative moment). Composite specimen results indicated that negative moment capacities were underestimated when no composite contributions were assumed, and positive moment capacities were overestimated when a concrete compressive force of $1.3F'_c$ acting over the column width was assumed. Composite specimen positive moments were better estimated when $0.85F'_c$ was assumed for the compression stress, although shear stud failures may have impacted this lower strength. It should be noted, however, that the $1.3F'_c$ value of Ref. 61 was based on a slab with a greater amount of reinforcement and associated confinement of the compression zone than these specimens. In addition, the test of Ref. 64 which was subjected to a cyclic loading into both positive and negative moments also achieved lower positive moments than predicted assuming a value of 1.3. Attained to estimated ratios were much higher at the column face for the dogbone specimens than for the haunch specimens, indicating a greater factor of safety against weld fractures in the haunch specimens..

No whitewash flaking was observed for the columns outside of the panel zone for any test. This observation was in line with calculations.

Minor panel zone yielding was observed in all specimens, and was most pronounced in specimens DB2 and HCH4. It appeared as though the haunch specimens experienced more inelastic panel zone action than calculations based on the full haunch and beam cross sections would indicate.

The yielded locations of panel zones, however, indicated that the assumed panel zone depths were reasonable. Specimen DB1's panel zone yielding appeared to be centered on the beam section, while DB2's seemed to be offset

towards the top of the beam section. Likewise, the composite haunch panel zone yielding extended closer to the top beam flange than the bare steel specimens, which had yielding starting approximately equidistant from the top beam and haunch flanges.

C) Analysis of Test Specimen Deformations

This section provides an analysis of deformations measured in the test specimens. Displacements measured at the tip of the column (δ_{ctot}) are decomposed into components attributable to deformations in the beams, in the column panel zone, and in the column segments outside of the panel zone (δ_{cb}, δ_{cpz}, and δ_{cc}). This analysis is conducted both for total displacements (elastic plus plastic) as well as for the plastic portion of the displacements alone. Definitions of symbols used and calculations methods for isolating individual components are included in the glossary and App. E. Plastic connection rotations (θ_{con}) are similarly decomposed into contributions from the beams and column panel zone (θ_b, θ_{pz}). Note that the column deformations do not contribute to defined connection rotations (see App. E). These analyses are intended to identify the portions of the test specimens that contributed to the overall deformation and ductility developed by each specimen.

Calculations for data reduction are presented in App. E. In general, panel zone deformations (including panel zone rotations and column tip displacement due to the panel zone deformations) were computed from the displacement transducers which measured displacements along the two diagonals of the panel zones (Figs. 3.11 and 3.14). Beam rotations were computed by taking the total

rotations at the beam-column interface, as reported by inclinometers, and subtracting out the panel zone rotations. Beam contributions to column tip displacement were found by multiplying the beam rotations by the column height. Panel zone contributions to column tip displacement were found by multiplying the panel zone shear deformations (γ) by the panel zone height and then subtracting the specimen rotation required to meet the beam end constraints multiplied times the column height. Finally, column deformation contributions to the column tip deformations were found by subtracting the beam and panel zone contributions from the total measured column tip deflections. Plastic components for components were found by subtracting out the elastic portions of each individual plot.

As larger inelastic deformations occurred in the specimens the measured rotations varied among the inclinometers. An average value was used in the calculations. The cause of the difference among inclinometer readings was not determined. However, it is speculated that it was caused by a combination of several factors, including column twist, the placement of the gages at an area of high differential panel zone rotations (panel zone rotations should be somewhat constant through the area of the panel zone, but not at the panel zone/column interface), and gage error.

1) Column Tip Displacement

Column tip displacements (δ_{ctot}) were broken into those attributed to column, panel zone, and beam deformations (δ_{cc}, δ_{cpz}, and δ_{cb}, respectively, in App. E). Total displacements due to each of these components for each specimen can be seen in Fig. 5.2. The plastic components of these deflections are plotted in

Fig. 5.3. For all plots, column contributions are represented by the gray line, panel zone contributions by the area between the gray and thin black lines, and beam contributions by the area between the thin and thick black lines. For both bare steel haunch specimens there was virtually no plastic component of the column or panel zone contributions. In these specimens practically all plastic column tip displacements are attributed to the plastic beam deformations. The composite haunch specimens showed increases in column as well as panel zone plastic contributions as compared to the bare steel specimens. It was felt that much of the increase in column plastic deformation may have actually been concentrated in the portion of the column bounded by the slab depth which was not instrumented as a panel zone. This would correspond to the composite specimen panel zone yield patterns as well as previously reported findings (Ref 64) which indicate an effective panel zone which extends into the slab area. There was no observed indication of yielding in the columns. Some specimens appeared to show some negative contributions of the column in later cycles of loading. This occurred subsequent to the dogbone bottom flange fractures (DB1 and DB2) or after extreme beam local buckling (HCH4), where the gage readings may become suspect.

2) Rotation

Connection rotations (θ_{con}) were broken into those attributable to the beam and panel zone, (θ_b and θ_{pz} respectively, as defined in App. E), and are plotted in Fig. 5.4 for the total rotations and Fig. 5.5 for the plastic rotations for the specimens. It was noted that most total rotations were provided by the beams, of which the north and south beams provided identical total rotations, as the total

rotation was identical for both sides of the connection. The north and south beams provided relatively similar peak plastic rotations as well, even in the case of HCH1 where one connection flange weld severed and the other remained intact. This just indicates that the north beam was well beyond elastic behavior when the fracture occurred, as was indicated by comparing $M\text{-}_{max}$ of Table 5.13 with M_{ye} of Table 5.7. It was also seen in Fig. 5.5 that panel zone plastic rotations were negligible in later cycles after the largest reaction forces (and moments) were realized. Beam plastic rotations dominated the inelastic response in later cycles.

3) Observations from Deformation Analysis

Individual component contributions to total column tip deformation and total rotations were shown in Figs 5.2 to 5.5. It can be seen that the panel zone was generally effective early in the loading series, but it's contribution peaked once the maximum applied moments were reached, after which the beam response dominated the data. This was likely due to the full capacity of the panel zone never being reached, and therefore as the applied loads decreased with the decreased capacity of the beam sections (brought on by local instabilities or weld fractures), the essentially elastic panel zone contributions were also reduced. This would be most apparent in the plastic components. The column response was predominantly elastic, although data was erratic. The erratic nature of the column response was likely due to the accuracy of the instrumentation used as well as the fact that, especially at later loading stages, the extreme deformations and buckling of the beams in the haunch specimens provided non-uniform rotations at the locations measured.

D) Analysis of Test Specimen Energy Dissipation

The ability of a structure to withstand and absorb the cumulative energy applied by a seismic event is critical. For this reason, earthquake design is often thought of in terms of energy dissipation. This energy absorption, or dissipation, is manifested as inelastic deformations of the components (beams, columns, and panel zones), and is related to the structure ductility. The cumulative energy dissipated is therefore another important basis for comparing test specimens.

Total energy dissipation was measured as the area enclosed by the column tip load versus column tip deflection plots (Figs. 4.7, 4.17, 4.25, 4.32, 4.40, and 4.49). Energy dissipation taking place in each of the connection components, (beams, panel zone, and column), was then calculated as the area enclosed by plots of column tip load versus individual contributions to column tip deflection (δ_{cb}, δ_{cpz}, δ_{cc}).

1) Total Energy Dissipation

Total cumulative energy dissipated by the specimens is plotted in Fig. 5.6. It can be seen that both dogbone specimens dissipated relatively little energy in the later cycles of loading, shown by a flattening of the plot. In fact, 65 and 75 percent of the total dissipated energy for specimens DB1 and DB2 respectively occurred through the load cycles at which the bottom flange welds fractured (3.6 inch and 4.8 inch respectively). The bare steel haunch specimens (HCH1 and HCH3) are initially quite similar to the composite dogbone specimen with regard to energy dissipation, but are still dissipating energy at the later cycles of loading. This energy dissipation occurred even after the top flange welds fractured. In

contrast to the dogbone specimens, only 35 and 69 percent of the total dissipated energy for specimens HCH1 and HCH3 respectively occurred through the load cycles at which the top flange welds fractured (3.6 inch and 4.8 inch respectively). The HCH3 specimen would likely have dissipated more energy had it been subjected to an additional load cycle as were the dogbone specimens. The difference between the two bare steel haunch plots could be attributed to only one weld fracturing in HCH1 and both welds fracturing in HCH3. It is interesting to note that the plots for the bare steel haunch specimens are similar at the 3.6 and 4.8 inch load cycles, indicating that energy dissipation of the beams was comparable until both connections fractured. The composite haunch specimens (HCH2 and HCH4) were nearly identical in energy dissipation and were still dissipating large increments of energy when the tests were terminated. The slab increased the total energy dissipation of the dogbone specimen by 130 percent. The composite haunch specimens HCH2 and HCH4 showed the composite specimen increased the total energy dissipation by 80 percent over specimen HCH3 through the 7.2 inch load cycle. A comparison to HCH1 (where one flange weld was still intact) showed an increase of 55 percent.

2) Beam, Column, and Panel Zone Energy Dissipation

Energy dissipated by the beam, column, and panel zone is broken out in Fig. 5.7. For all of the bare steel specimens (DB1, HCH1, HCH3) the energy dissipated by the column was negligible and that dissipated by the panel zones was quite small compared to the total values. Specimen DB2 also showed very little energy dissipated by the column although three times as much energy was dissipated by the panel zone as compared to DB1. The composite haunch

specimens (HCH2 and HCH4) showed significant increases in both panel zone and column energy dissipations. As there was no yielding observed in the column outside of the panel zone areas, it is conjectured that the increase in energy dissipated by the column was almost entirely due to energy dissipated in the additional "panel zone" bounded by the slab depth. Deformations in this area were not included in the panel zone results.

Finally, it is noted that calculated energy dissipated by the column had a consistent anomaly associated with it. In all cases, cumulative energy dissipated by the column decreased over the final load cycles, which would not be possible. As was seen in Fig. 5.7 the column portion of total energy was generally small and this error could be neglected. The column deflections which were used to calculate energy dissipation were based on the full measured column tip deflection minus the beam and panel zone components. These values would therefore have had the largest possible error of all measurements.

3) Observations from Energy Analysis

An overview of the cumulative energy dissipated by the specimens was shown in Fig. 5.6. The composite specimens showed a much greater capacity to dissipate energy than the corresponding bare steel specimens. At the end of the tests, all haunch specimens were still actively dissipating energy, while the dogbone specimens dissipated relatively little energy in later load cycles. Similar haunch specimens dissipated very similar amounts of energy at each load cycle, although the bare steel specimens diverged beyond the 4.8 inch load cycles at which point specimen HCH1 had only one fractured weld while HCH3 had fractured welds in both beams.

E) Analysis of Slab Effects

Specimens which included a composite slab allowed a direct comparison between bare steel and composite specimen behavior. Insight into the distribution of forces in the slabs was also of interest.

1) Shear Stud Failures

During the testing of the composite specimens, failure of the shear studs at the welds often occurred. Locations of failed shear studs were determined through visual inspection following removal of the concrete slab after each specimen was tested. With the exception of the end shear studs which spalled the end of the slab in all cases, all shear studs eventually failed in specimen HCH4, while in HCH2 only the 2nd shear stud from the column face on the north beam was intact at the end of testing. Specimen DB2 did not reach the higher loads of the haunch specimens, and the shear studs were left mostly intact. The location of failed shear stud welds on this specimen is shown in Fig. 5.8. The failed shear studs in DB2 were still attached to the beam flange after demolition of the concrete slab, but were easily removed from the flange by impacting the stud with a sledgehammer. Typically, shear stud welds severed (Fig. 5.9), although at least one shear stud sheared completely through the stud itself (Fig. 5.10).

Shear stud failures similar to these were not mentioned in previous testing of composite sections (58,59,62,63,64,65), although many of these included fully composite slabs per gravity load requirements. Reference 65 included two specimens which were partially composite, (only a percentage of shear studs required per the fully composite gravity load requirements of the AISC LRFD

code were provided). These specimens were 55 percent (specimen 2) and 35 percent (specimen 3) composite. Specimens for this study were approximately 25 to 40 percent fully composite, (with respect to gravity load criteria), when actual material strengths were used. It would therefore appear that the shear stud failures should have been reproduced in specimen 3 of Ref. 65, although there are some significant differences between the specimen in Ref. 65 and specimens tested here. Specimen 3 of Ref. 65 was a typical pre-Northridge connection, whereas specimens HCH2 and HCH4 were strengthened. They would therefore achieve a higher moment at the column face (compared to M_p of the section), and could result in higher shear stresses. Although the specimens provided only partially composite action when gravity loading was considered, the specimens were provided with shear stud capacity to withstand a maximum concrete compressive force equal to $1.3F'_c$ times the effective concrete area for lateral loads (width of column flange times slab thickness above the steel decking). This slab compressive force was not generally attained prior to the shear stud failures.

Failures of shear studs appeared to initiate in the 2.4 inch load cycles, and continue through the 6.0 inch cycles. Failure of the shear studs was indicated by a loud bang at stages of loading for which no visible deterioration of the specimen was noted. Initially these occurred sporadically, and then in quick succession at later loadings. At the end of testing the number of such aural indicators appeared to match the number of failed shear studs. These failures may be due to inadequate shear stud to beam flange weld quality, shear stud capacities less than design values, or other forces on the studs. Transverse shear forces may have been present on the shear studs. A noticeable twist of the column was noted

during the later load cycles. Column twist was restrained by the lateral support at the column tip, but only after an initial twist occurred to close the gap between the column flanges and lateral support beam. The initial gap between these elements was approximately 1/16 to 1/4 inch. In an unrestrained specimen, this small twist at the column would cause lateral displacements at the ends of the beams on the order of 1 to 4 inches. This twist was restrained in the steel beams by the lateral bracing at the supports. The slab, however, would only be restrained against this twist by the beams through the shear studs, which could result in large transverse stresses on the shear stud at the ends of the slab. It was therefore speculated that the shear studs may have fractured at the ends of the slab first, and the fractures then progressed towards the column. This was consistent with observations on the slip of the slab (section 5.E.4). Indications of slab slip became noticeable at the 2.4 inch load cycles and appeared to be constant at the end of the slab over the last few feet of HCH2 and HCH4. This length of constant peak slip progressed towards the column with subsequent loadings. These possible transverse shear forces would not be a realistic behavior in buildings, as the slab rotation would be resisted by the entire story's columns due to continuity of the slab. Therefore, even though there may be some question of the acceptability regarding hand welded versus stud welded shear studs, the failures of the shear studs in this study do not necessarily indicate that such failures would be likely in a building, or that the shear capacity would be inadequate. These failures did show that the shear stud/weld interface (which coincides with the point of slip of the slab with respect to the beam) was the weakest link during cyclic behavior. It was not possible to conclusively identify the cause of shear stud failures in the specimens. Due to

this uncertainty it is tentatively recommended that shear stud design capacities under cyclic load be reduced by the ratio of attained shear in our specimens to expected shear stud capacity. This would correspond to 0.65, (the lower bound concrete compression factor of 0.85 (section 5.B.2) to the assumed value of 1.3).

This loss of composite connection through the testing of the specimens made the slab influence at later cycles of loading much more difficult to evaluate. It is unclear whether the shear stud failures in specimens DB2, HCH2, and HCH4 indicate an inadequacy in the shear stud strength provisions of the AISC code, high transverse shear forces from specimen twisting, or poor weld quality in our specimens.

2) Overall Slab Effects

The total plastic rotation versus moment at the column face plots of Chapter 4 are superimposed for bare steel and composite specimens in Fig. 5.11. From these plots it can be seen that the composite slab provides a slight increase in initial elastic stiffness, and increased positive moment capacity on the order of ten to twenty percent. Negative moment capacities are sometimes slightly increased by the composite slab (DB1 and DB2 south beams, HCH1 and HCH2 south beams, HCH3 and HCH4 north beams), but this effect is not apparent in the other specimens.

3) Slab Data

a) Crack Patterns

A series of photos showing the crack progression in HCH4 is presented in Figs. 5.12 to 5.16. HCH2 and DB2 showed similar results. The following description is applicable to all three composite specimens.

The first crack in the slab occurred at the column face and extended mostly across the entire slab by the 0.4 inch load cycle (Fig 5.12). During the 0.8 inch cycle cracks appeared at approximately 4 feet from the original cracks (Fig. 5.13). In the 1.2 inch load cycle cracks appeared about midway between the existing cracks, at approximately a two foot spacing. Cracks generally formed at the minimum depth areas of the slab. In addition, a crack developed along the beam centerline, from the column face and running approximately half the length of the slab. Cracks also began to appear at the edge of the slab at about one foot spacing (Fig. 5.14). The 2.4 inch load cycle extended several cracks, especially the one foot interval edge cracks which generally joined the existing cracks about two feet from the slab edge (Fig. 5.15). In addition, the end of the slab began to spall at the beam centerline (Fig. 5.17). The 3.6 inch load cycle initiated some slight crushing at the column flange faces. This crushing became more substantial at the 4.8 inch load cycles (Fig. 5.18). The 4.8 inch load cycle also extended many of the one foot spaced cracks into neighboring cracks and extended the longitudinal crack over the beam centerline to nearly the length of the slab. The cracking to the east and west of the column between the initial cracks became substantial, and the main cracks at the column face developed a vertical offset of up to 0.5inches, indicating that the wire fabric had likely severed (Fig. 5.19). This crack was usually controlled at the edge of the slab by the longitudinal reinforcing. Subsequent load cycles saw little crack development, but a continuation of the crushing at the column flange faces and some web cracking at the edge of the slab. An overall post test photo is shown in Fig. 5.16, and a view of the column flange faces is shown in Fig. 5.20. A compression zone

is indicated by the predominantly longitudinal cracking which extends from the corners of the column and gradually bounds a wider swath of the slab. It is felt that this type of crack pattern was somewhat restrained by the transverse steel which was provided for shrinkage and temperature control.

Some diagonal cracks propagating from both the column flange face as well as from the inside edges of the far column flange were seen. It may therefore be speculated that maximum concrete compressive forces may not only be increased beyond F'_c, but that the effective width of the compression zone at the column face is wider than the column flange face. This increase in effective width of the compression zone would be related to the stress distribution of the compression zone which initiates at the inside of the opposite flange face. Maximum compressive forces would not only be a factor of column flange width, but of depth as well. The compression zone distributed at approximately 15 to 30 degrees, as estimated from crack patterns in the specimens.

b) Mechanical Concrete Strain Measurement Results

A mechanical clip gage (DMEC) was used to measure concrete strains between points set at two inch gage lengths. Measurements were taken at peak column tip displacements at locations on the slab surface as detailed in Chapter 3. Results are referenced to DMEC rows and spacings as indicated in Fig. 3.18.

Early cracking of the concrete preempted the reading of in the initial uncracked slab, and results from DMEC readings were often dominated by localized strains. Strain readings throughout the slab were complicated by the fact that at the edge of any crack, concrete strains were generally compressive. As the reinforcement bond forces developed between cracks, strains became

tensile. In addition, cracks eventually formed between several gage points, after which readings at these locations measured crack widths and not concrete strains.

Nevertheless, some overall observations were found, and the extra gage points added at the face of the column of HCH4 provided insight into the compression zone at the column face. It was noticed that the concrete often reached strains well above the ACI assumed rupture strains, (as based on the modulus of rupture divided by the modulus of elasticity, see Table 5.4), before a crack was noticed at the location. Compressive strain peak values at the column face reached for each cycle are found in Table 5.18.

The strain peaks at the face of the column quickly dropped off away from the column face due to the distribution of the compressive zone across the slab. There were signs of degradation of the slab upon reloading in the later load cycles. Details for each specimen follow.

i) DB2

The progression of strains in DMEC row number 3, (along the column centerline, see Fig. 3.18), at load cycles from 0.4 inches to 2.4 inches is shown in Fig. 5.21. The first and third cycles had quite reproducible results through the 0.8 inch cycles, while the later cycles showed a loss in recorded compressive strains for the third cycle. The maximum strain recorded in compression was approximately -0.0024 for the 1st cycle at 4.8 inches.

Peak values for the DMEC rows 2 and 4 were about half those of the center row (Row 3) through the 1.2 inch cycles at which point row 2 had values approaching those of row 3 while row 4 continued to have values about half of

those on row 3, presumably due to the twisting of the specimen in later load cycles.

Rows 1 and 5 tended to have strains below 0.0002 in/in but with values which depended more on the local crack configuration than on the overall flow of forces.

Typical compressive strain values for spans NB1 and SB1, (across the slab, see Fig. 3.18), are presented in Fig 5.22 and 5.23. There was a general increase in the strains with increasing load cycles, although there was a loss in peak strain beyond the 1.2 inch load cycles for the later cycle at similar displacements. This occurred even though the load held was fairly constant except in the 4.8 inch load cycles in which the north beam weld fractured in the 2nd cycle. Values at NB2 and SB2 followed a similar trend with the peak values being on the order of 1/3 to 1/5 those at the 1st rows. The peak compressive strain observed at the column face was -0.0024 in/in.

ii) HCH2

The progression of strains in DMEC row number 3, (along the column centerline, see Fig. 3.18), at load cycles from 0.4 inches to 2.4 inches is shown in Fig. 5.24. The first and third cycles had quite reproducible results through the 0.8 inch cycles, while the later cycles showed a loss in recorded compressive strains for the third cycle (a crack was apparent in the 4th cycle at 1.2 inches in the south direction at the south column face). The maximum strain recorded in compression is approximately -0.0017 for the 1st cycle at 3.6 inches.

Peak values for the DMEC rows 2 and 4 were about half those of the center row (Row 3) through the 1.2 inch cycles at which point rows 2 and 4 had

values approaching or exceeding those of row 3 in the north side of the column, while cracking made it difficult to ascertain the trends on the south side.

Rows 1 and 5 tended to have strains below 0.0003 in/in but with values which depended more on the local crack configuration than on the overall flow of forces. There was a prevalence of cracking through the gage points which made readings sporadic.

Typical values for spans NB1 and SB1, (across the slab, see Fig. 3.18), can be seen in Fig 5.25 And 5.26. Although there is some trouble with cracking in the area of gage points, it can be seen that there is a general increase in the strains with increasing load cycles, although there is a loss in peak strain beyond the 1.2 inch load cycles for the later cycle at similar displacements. Values at NB2 and SB2 followed a similar trend with the peak values being on the order of 1/2 to 1/4 those at the 1st rows. Once again, the peak compressive strain observed at the column face was -0.0020 in/in.

iii) HCH4

The progression of strains in DMEC row number 3, (along the column centerline, see Fig. 3.18), at load cycles from 0.4 inches to 2.4 inches is shown in Fig. 5.27. The first and last cycles had quite reproducible results through the 0.8 inch cycles, while the later cycles showed a loss in recorded compressive strains for the last cycle. The maximum strain recorded in compression is approximately -0.0030 for the 1st cycle at 4.8 inches.

Peak values for the DMEC rows 2 and 4 were about half those of the center row (Row 3) throughout the load cycles.

Rows 1 and 5 tended to have strains below 0.0003 in/in but with values which depended more on the local crack configuration than on the overall flow of forces.

Typical values for spans NB1 and SB1, (across the slab, see Fig. 3.18), can be seen in Fig 5.28 and 5.29. Increased instrumentation allowed for the detailing of strains across the column face. Peak strains which would typically correlate to approximately 85 percent of full compression stress (about -0.0010 in/in) were attained for the 0.8 inch load cycles, while at the 2.4 inch load cycles this value was exceeded across the entire two feet of gage readings (exceeding the column face width of 13.14 inches). Values at NB2 and SB2 followed a similar trend with the center values being on the order of 1/3 of those at the 1st rows. Once again, the peak compressive strain observed at the column face was -0.0030 in/in.

c) Compressive Force at Column Face

As was found in the HCH4 DMEC readings at the column face, by the time that the 2.4 inch load cycles were achieved, the compressive force at the top surface of the concrete should have been close to F'_c over the center 24 inches of the slab. This width exceeds the column flange width of 13 inches, indicating the initiation of the compression zone at the far column flange as was discussed in section 5.E.3.a. At the 2.4 inch load cycles the achieved reactions were approximately 90 to 95 percent of the total achieved in the test. Unfortunately, strain gage data was not able to locate the neutral axis in the beam at the column face as will be discussed in section 5.E.5. Therefore it was impossible to determine the actual compressive force of the slabs or estimate a strain

distribution through the slab thickness. A comparison of achieved moments as compared to the predicted moments based on a concrete compressive force of $1.3F'_c$ acting over the column flange width was reported in Tables 5.12 and 5.14. This showed the achieved moments of HCH2 and HCH4, (the two composite specimens which did not fail prematurely), to be only 94 to 108 percent of the estimated plastic moments based on tested dynamic yield stresses and measured section properties. The bare steel haunch specimens HCH1 and HCH3 achieved 104 to 110 percent of the estimated plastic moments. It can therefore be presumed that the assumption of a concrete compressive force of $1.3F'_c$ acting over the column face is too large for a lower bound value. In order to obtain a safe design boundary on the haunch test results, (all attained moments safely approximated by the estimated values), a concrete compressive force of $0.85F'_c$ over the compressive face of the column flange should have been used in calculations. Table 5.15 showed this assumption to result in achieved moments of 102 to 115 percent of estimated values. A lower value would be required by the dogbone specimen, but the flange weld fractures appeared to occur while the beam capacities were still increasing. It should be noted that due to the failure of the shear studs it is felt that this compressive strength of the slab is a minimum value that could be attained in an actual building as the column and slab twisting which may have been responsible for the shearing of the specimen shear studs (see section 5.E.1) would be somewhat restrained, and indeed the 1.3 multiplier may in fact be attainable. Should the shear stud failures be due to inadequate welding, or the percentage of fully composite action provided, the 0.85 multiplier may be most appropriate for similarly detailed structures.

4) Slip of Composite Slab

Slip of the Composite Slab was measured by two means. First, three linear potentiometers were attached to the beam flange and measured displacement with respect to a piece of rebar which was epoxied into the slab (Fig. 3.17). These gages were placed to measure slip at the first and second flute of metal decking from the north column face, at distances of approximately 1'-6" and 2'-6" from the column centerline. The final gage was placed at the north end of the slab (Fig. 3.16). In addition, a visual measure of the slip in the slab was taken by placing pieces of marked masking tape at each decking flute (Fig. 3.20).

a) Visual Record

Observations regarding the visual inspection of slab slip was reported for the individual specimens in Chapter 4. Slip of the slab with respect to the beam flange was first noticeable during the 2.40 in. cycles for all specimens. These were also the load cycles at which it was believed that the shear studs began to fail. The failure of shear studs appeared to initiate at the ends of the slab and then shear off subsequent studs towards the column as was discussed in section 5.E.1. Practically all shear studs were failed by the 6.0 inch load cycles, with the exception of DB2 which lost much of its load capacity after the 4.8 inch load cycles and only failed a portion of its shear studs (Fig. 5.8). At the conclusion of the tests, the end shear studs were intact, but bent over and had spalled the concrete at the ends of the slab (Fig. 5.17). For specimens HCH2 and HCH4, practically all other shear studs had their welds severed (Fig. 5.9), although at least one shear stud sheared completely through the stud itself (Fig. 5.10).

Slip only occurred at points where the specimen was subjected to positive moment (slab in compression). Observed slip returned to zero when the load was reversed. For the 2.4 inch load cycle the slip was approximately 1/8 in. over a short section of constant slip at the end of the slab and tapered gradually to zero at the column face. Observed slip increased over subsequent load cycles, with a maximum value of approximately 1.75 inches at the end of HCH4 testing. In later load cycles of HCH2 and HCH4 the length of constant slip at the ends of the slab increased substantially over that observed at the 2.4 inch load cycle.

In addition, once all the shear studs failed the slabs began to rotate about the column centerline, presumably following the twist of the column. The slab offset with respect to the beam flanges at the ends of the slab were as much as 3 inches at the conclusion of testing. It was felt that the shear stud failures may have been due to the forces generated by the slab attempting to twist while the lateral braces resisted such rotation of the beams, as discussed in section 5.E.1.

b) Linear Potentiometer Slip Data

It can be seen from Fig. 5.30, which plots slip through the 3.6 inch load cycles, that most slip occurred at the ends of the slab. At the start of the 2.4 inch cycles, the concrete at the end of the slab began to spall as indicated by the fact that the slip did not return to zero when the load was reversed. The fact that the shear studs at the column face were intact for specimens DB2 and HCH2 but not HCH4 is shown by the minimal slip at the first flute for the first two specimens, while HCH4 exhibits values similar to those at the 2nd flute. The 2nd flute slip readings for DB2 and HCH2 appear to be erroneous as they did not show a zero slip when the load was reversed as the visual inspections showed. This could

have been due to instrumentation error, perhaps a slight buckling of the top flange affecting the instrument placement. Gage trends were similar through the completion of testing, with maximum second flute values reaching approximately 0.85 inches for the 6.0 inch load cycles in specimens HCH2 and HCH4.

5) Location of Neutral Axis

The neutral axis of bending in the beams was estimated from the strain gage readings taken at the center of the dogbone or end of the haunch. Strain gage locations are indicated in Figs. 3.10, 3.11, 3.13, and 3.14. Individual strain gage histories were examined to determine the location of delaminated or erratic gages, while data for all gages at the cross section were referenced to evaluate the linearity of the strain gradient. For all specimens, it was not possible to determine the neutral axis location beyond the 2.4 in. load cycles as the data exhibited a wide scatter even among the gages which appeared to be functioning correctly. This was to be expected as this was typically the point at which visual records showed there to be a large amount of local and lateral torsional buckling.

a) Neutral Axis in Beam at Center of Dogbone and End of Haunch

Strain gage locations are indicated in Figs. 3.10, 3.11, 3.13, and 3.14. Peak strain gage readings for each cycle of the 0.4 inch load cycles are plotted for gages at the center of dogbone or end of haunch locations of the bare steel specimens (DB1, HCH1, and HCH3) in Fig. 5.31. The specimen should be in the elastic range during this load cycle. Data is included for loadings in the north and south loading directions. The data was linear, with the exception of the values at the lower flange which were of a greater absolute value than would be extrapolated from the other data (as indicated by the straight lines on the plots).

For DB1, the values are elevated equally at the top and bottom faces of the bottom flange. This variation from a linear strain distribution is most probably related to the discontinuity of the cross section at the dogbone location. The concentrated "bottlenecking" of forces at the reduced flange section, where the bottom flange capacity is reduced by the flange reduction, would likely affect the bottom flange strain readings as the changing cross section may not allow the flow of forces into the beam web. This was also indicated by the neutral axis for positive and negative moments at approximately the mid-depth of the section instead of offset towards the top flange as would be calculated from the dogbone cross section. Yielding patterns indicated that the redistribution of forces at the dogbone bottom flanges were not ideal. For instance, there was early yielding of the web at the k-region above the bottom flange (Fig. 4.3) which may have been an indication of shear flow into the web. Also, at the column face the bottom flange yielding was concentrated at the center of the flange (over about the width of the dogbone reduction) instead of over the full flange width (Fig. 4.2). In addition, the initial yielding of the specimen as well as yield patterns at the end of testing (Figs. 4.2 and 4.6), showed bottom flange yielding at the dogbone location, but top flange yielding was concentrated at a location much closer to the column face. This indicates an active cross section for moment resistance which is not oriented with the beam y axis. These were indications of non-idealized behavior at the dogbone location which could explain the increased strains in the bottom flange. Increasing in the length of the dogbone reduced section and the distance to the beginning of the reduced flange section from the column face may

provide for a more uniform distribution of forces in the section, and reduce non-linearity of the strain distribution.

The bottom flange readings on the bare steel haunch sections were also highly elevated, although only at the bottom extreme fibers. This variation from a linear strain distribution is likely related to the discontinuity of the cross section at the end of haunch location and the high shear concentration in the lower flange caused by the vertical component of the haunch flange axial force.

Calculations of the neutral axis for the bare steel specimens versus those obtained from strain gage data are tabulated in Table 5.19. Bottom flange strains were not included in the calculations for neutral axis location, as these values appeared to be elevated.

It was found that the DB1 measured neutral axis position differed for positive and negative moments, with the values in the positive direction better matched to the calculated values. At earlier cycles the neutral axis was below the elastic calculated axis of 16.74 in., and the positive moment values (dogbone in tension) then increased in elevation until they exceeded the plastic calculated neutral axis value of 17.83 in. in the 2.4 inch load cycle. The negative moment values (dogbone in compression) decreased with each load cycle until they were located below the centerline of the beam. This seemed to indicate that the top flange was never fully effective in tension. This could perhaps be improved by providing a reduced flange section of a greater length which would allow a fuller redistribution of forces from the bottom flange into the full cross section.

Bare steel haunch neutral axis measured locations were fairly similar in the positive and negative directions and were less than calculated values, likely

due to the presence of the adjacent haunch influencing the behavior and drawing the neutral axis toward the bottom of the section. The movement of the neutral axis towards the center of the beam in the 2.4 in. load cycle corresponded with the onset of significant yielding at the section and indicates that the full yielding of the bottom flange reduced the influence of the haunch.

The addition of the composite slab to the section results can be seen in Fig. 5.32 and Table 5.19. Bottom flange strain readings varied from a linear strain distribution similarly to the bare steel sections. It can be seen that, as expected, the neutral axis location for positive moment was located nearer the top of the sections as compared to the bare steel sections, and that there was a disparity between the positive and negative moment neutral axis locations due to the slab being much more effective in compression than in tension. The negative moment neutral axis locations (slab in tension) approached those of the bare steel sections, despite the fact that attained moments were reported to exceed that of the bare steel specimens in section 5.B.2. At later cycles of loading the positive moment measured neutral axis locations tended to decrease as the specimen reached its plastic moment capacity. All composite measured neutral axis locations were well below the calculated plastic neutral axis values, indicating that the full plastic capacity of the slab and beam, (assuming $1.3F'_c$ acting over the column face), was not reached in the specimens through the range of reliable strain gage readings. Yielding patterns observed during testing (Figs. 4.16, 4.31, 4.48) indicate yielding which is closer to the column face at the top flange than at the bottom flange. It is possible that this indication of an active cross section for moment resistance which is not oriented with the beam y axis would cause a

measured neutral axis from our strain gages (oriented at the beam y axis) to be closer to the bottom flange than expected.

b) Neutral Axis in Beam at the Column Face

Strain gage locations are indicated in Figs. 3.10 and 3.13. Strain gage readings at the column face were much more difficult to interpret, partly due to the location of the gages chosen (none on the beam web), but mostly due to the non-uniform distribution of forces, non-uniform web cross section (due to shear connection), and restraint of the section (by welding to the thick column flanges) at this location. Typical data is shown in Fig. 5.33. For the dogbone sections the scatter of data points was particularly large. Haunch data was somewhat less scattered although the top flange data was widely scattered. Estimates of the neutral axis depth neglecting the top flange data would be based on only data from the bottom beam flange extreme lower fiber and the bottom face of haunch flange. Estimates based on these two points proved to be much different than calculated values. This was felt to be due to the shears introduced at the haunch flange due to the vertical component of the flange axial force in addition to the relatively low number of readings used for the neutral axis estimate.

6) Flange Strains

Strain gage locations are indicated in Figs. 3.10, 3.11, 3.13, and 3.14. The maximum average flange strains for each load cycle are plotted through the 1.2 in. load cycles of the specimens in Fig. 5.34 to 5.37. Beyond this load cycle, local post yielding strains could vary substantially and data was erratic.

Figure 5.34 shows the dogbone specimen data at the center of dogbone section. It can be seen that the addition of a composite slab significantly reduced

the top flange strains. At the bottom flange the peak strain values were slightly reduced by the slab in the 1.2 in. load cycle. Overall, it was seen that the moment capacity was expected to increase on the order of 30 percent (see Tables 5.8 and 5.10), while the increase in effective depth was approximately from 29.1 in. to 34.0 in., or about 20 percent. The increased moment is therefore greatly offset by the increase in moment arm length between tensile and compressive forces, so the effect on the bottom flange strains was not expected to be substantial. Similar results were seen at the column face locations (Fig. 5.35). Therefore, while several researchers have speculated that the presence of a composite slab will overstress the bottom flange welds, changes in weld stress will depend on the beam and slab cross sections used.

It was noted that yielding occurred at rather low strains at the column face in tension, whereas data at the dogbone centerline was mostly elastic. This may be due to the presence of residual stresses at the column face, presumably due to the cooling of the welds.

Figure 5.36 shows the average flange strains for the haunch specimens at the end of the haunch location. The top flange strains were reduced when the composite slab was included, more so in specimen HCH2 which had a higher concrete compressive strength. Peak positive values were similar for all specimens, indicating that the slab had little influence when in tension. Once again, strains at the bottom flange were not significantly affected.

Figure 5.37 contains similar haunch data taken at the column face. Top flange strains showed the composite specimens to have slightly reduced differential strains, although peak values between specimens were inconclusive.

Composite haunch flange strains were slightly increased in the negative moment direction indicating the increased measured negative moment capacity over the bare steel specimens (Tables 5.13 and 5.14). Bottom flange strains were much lower than the top flange strains for all haunch specimens, showing the downward shift of the neutral axis due to the presence of the haunch.

7) Slab Effects on Beam Shortening and Instability

Beam shortening was measured as the change in distance between the south column flange and beam stiffener above the south beam reaction. Both measurements were taken at the beam centerline (Fig. 3.8). Values of beam shortening throughout the testing of each specimen is shown in Fig. 5.38. The actual beam shortening reported consisted of average values from gages placed equidistant to the east and west of the beam web, as this reduced the effects of beam distortions. Through the 3.6 inch load cycles (at which point most inelastic behaviors had initiated), bare steel specimens had shortening below 0.2 inch, with the exception of DB1 which had an elongation of up to 0.4 in. in the 3.6 in. load cycle which was due to the "opening up" of the bottom flange away from the column face due to the bottom flange weld being fractured. Composite specimens had shortening well below 0.1 inch, with the exception of DB2 which had an elongation of almost 0.2 in. due to the "opening up" of the bottom flange away from the column flange due to the bottom weld being fractured. In later cycles the dogbone shortening and elongation increased in magnitude, reaching values of about 1.0 inch at the final loading cycles.

In an actual building, shortening of the beams would be restrained by the slab continuity and other beams and columns in the structure. Therefore, there is

some question as to the validity of specimen test results where beam shortening is significant, as these restraining forces have the potential to significantly alter the behavior. Care must therefore be taken in interpreting test results at these later stages of loading. Connection rotations which are attained in conjunction with large values of beam shortening would quite possibly not be realized in a structure. The lower values of beam shortening in composite specimens could indicate these specimens to be more representative of behavior of connections in a structure.

For the most part, visual assessments as to the effects of the slab on structure instabilities (local and lateral buckling) was hampered by the weld fractures in the bare steel specimens, beyond which extreme cases of local buckling and lateral torsional buckling were observed. The dogbone specimens both contained weld fractures, however instabilities were not present prior to the extremely early occurrence of such fractures in DB1.

A comparative measure of instability between bare steel and composite specimens could, however, be inferred from the beam shortening plots of Fig. 5.39. In comparing the beam shortening effects through the 3.6 inch load cycles it was seen that all of the bare steel specimens had divergent values for the east and west sides of the beam. These differences in values from the east to west sides of the beam indicated that there was significant twist and distortions of the beam. Such behavior was still evident, but at a much smaller scale in the composite specimens. This disparity became even more extreme at later loading cycles.

Another significant effect on local instabilities can be seen in Fig 5.40. The local buckling of the top flanges for specimens HCH3 and HCH4 are

compared at the 4.80 inch load cycle (subsequent to the flange weld failure load cycle in HCH3). It appeared that the top flange buckling was controlled by the slab, and was an explanation for the failures of welds in the bare steel haunch specimens but not in the composite specimens. Note how the flange was held level at the weld location by the slab, and was cycled through large magnitude distortions at the flange edges in the case without the slab (Fig. 5.40). Prior to the weld fractures top flange buckling was of a much lower magnitude, but still apparent at the weld locations. The weld failures in both HCH1 and HCH3 appeared to initiate at the edge of the beam flange in contrast to the dogbone weld fractures which appeared to initiate at the center of the welds. It was therefore concluded that beyond the brittle fractures which occurred in Northridge and our specimen DB1, the next weak weld link may be due to low cycle fatigue from high amplitude distortions. The presence of a slab appeared to control this behavior very well at the top flange. It is felt that a composite slab with metal decking placed longitudinally to the beam, (or the case of a full depth slab with no metal decking), would also provide restraint to local flange buckling.

It follows that a retrofit which reduces the stresses on the bottom beam welds, such as the haunch, benefits from the slab's presence at the top flange, while a retrofit which still has high stresses on the bottom flange (dogbone) may still fracture the bottom weld even when weld improvements are made. In other words, once the applied stresses at the welds are reduced to prevent initial weld fractures (which was not accomplished in our dogbone specimens), later low cycle fatigue fractures may be prevented by the presence of restraint to lateral

torsional and local buckling. The presence of a slab appeared to provide this restraint at the top flange welds.

8) Observations from Slab Analysis

The compressive zone at the top of the slab was found to extend over at least the middle 24 inches of the slab at the column face once the slab was actively participating in the composite section, a ratio of 1.8 times the column flange width, and the shape of the strain distribution could be estimated as triangular. Unfortunately, the neutral axis at the column face could not be reliably evaluated during testing, so a direct calculation of slab compressive forces was not possible at the column face. It was found that a minimum compressive stress value of $0.85F'_c$ over the width of the column flange was appropriate for calculations with AISC defined partially composite connections, and that the nominal shear stud capacity may need to be reduced by a factor of 0.65 when designing for cyclic loads.

Flange strains were decreased at the top flange when a composite slab was added, although strains at the bottom flange remained similar. Neutral axis locations were raised towards the slab, and haunch neutral axis locations were lowered towards the haunch material.

Overall, a major contribution of the slab appeared to be related to specimen stability. It appeared that the composite haunch specimen's excellent performance was attributable in part to the slab's restraint of lateral torsional and local buckling at the top flange. Thus, once stresses on existing welds were reduced, the slab restrained the top flange strains at the weld area. In the dogbone specimens, however, the stresses were not reduced sufficiently to prevent the

bottom flange weld fractures, even when the welds were improved. In order to provide dogbone designs where stresses are sufficiently reduced, the bottom flange, (which is not directly restrained by the slab), would require greater stress reductions, (or more weld improvements), than the top flange.

F) Additional Strain Gage Data

1) Uniaxial Strain Gage Data

For DB1, all strain gage data for the beam area at the center of the dogbone cutout was quite uniform across the top flange width (Fig. 5.41). Strain readings at the center of the dogbone bottom flange were also very consistent, although the west side yielded earlier than the rest of the flange. After the fracture of the bottom flange welds there was no tensile capacity to relieve the compressive strains in the bottom flange when the load cycles were reversed, and the bottom flange remained in compression. There was some slight cycling, however, indicating an elastic rebound of the bottom beam flange as it stopped compressing against the column flange (Fig. 5.42). After the bottom flange fractures the top flange cycled from minimal strain in compression into tension and back indicating that there was some moment capacity as the bottom flange went into compression against the column flange (Fig. 5.43). As the shear bolts fractured the minimal compressive top flange strains become zero.

At the column face DB1 top and bottom flange strains were lowest at the ends of the flange throughout the gage data (Fig. 5.44), and readings were symmetric about the beam web for the top flange. It was also quite apparent that residual stresses were quite high at the column face, as is indicated by the

divergence of plots from being symmetric about the horizontal axis in Fig. 5.45 at a much lower strain value for the gages at the column face. Yielding occurred at values well below the assumed yield strain of 54/29000=0.00186 in./in., even as low as 0.0009 in./in at the top flange and 0.0006 in/in at the bottom flange, compared with a minimum value in excess of 0.0013 in./in. at the beam section (15 in. from the column face). These values of first yield are taken as the last peak strain value for which strains remained similar at similar absolute moment values in the positive and negative bending modes. The lowest value of all strain gages at a given location, (at column face or center of dogbone), was specified. This early yielding at the column face was presumed to be due to the residual stresses introduced during the connection welding process which placed this area of the flange in a residual tensile state.

For DB2, all strain gage data for the beam area at the center of the dogbone cutout was quite uniform across the top flange width until the 3.6 in. load cycle during which the west end of the flange yielded while the east end remained elastic. Strain readings at the center of the dogbone bottom flange were also uniform, although the east side yielded earlier than the rest of the flange, in the 1.2 in. rather than 2.4 in. load cycles. After the bottom flange fractures the top flange cycles from minimal strain in compression into tension and back indicating that there was some moment capacity as the bottom flange went into compression against the column flange. As the shear bolts fractured the minimal compressive top flange strains become zero.

At the column face DB2 top and bottom flange strains were lowest at the ends of the flange throughout the gage data, and readings were symmetric about

the beam web for the top flange. It was also quite apparent that residual stresses were quite high at the column face, as yielding occurred at values well below the assumed yield strain of 54/29000=0.00186 in./in., as low as 0.0010 in./in at the top flange compared with a minimum value in excess of 0.0013 in./in. at the beam section (15 in. from the column face). This was presumed to be due to the residual stresses introduced during the connection welding process placing this area of the flange in a residual tensile state.

For HCH1 and HCH3, all strain gage data for the beam area at the end of the haunch was quite uniform across the top flange width until yielding occurred in the 2.4 in. load cycle in which the center of the flange yielded while the ends remained mostly elastic (except for the west end of HCH3 which also yielded). Strain readings at the bottom flange at the end of the haunch showed fairly early yielding in the 0.8 in. cycles for HCH1 while HCH3 saw the entire flange yielded in the 2.4 in. load cycles. Subsequent to fracture the west side (HCH1) or center (HCH3) of the fracture closed first and took most of the compressive strains. After the fracture of the top flange welds there was no tensile capacity to relieve the compressive strains in the top flange when the load cycles were reversed, and the top flange remained in compression. There was some slight cycling, however, indicating some elastic rebound of the top beam flange as it stopped compressing against the column flange. This cycling in the east side of HCH3 was significant, indicating that there must also have been some tensile redistribution into the top flange from the beam web at the end of the haunch. Post fracture the west side (HCH1 and HCH3) of the beam top flange at the end of the haunch began to cycle in progressively larger strain cycles (Fig. 5.46) indicating that the haunch section

itself was developing moment capacity. This haunch moment capacity would be provided by a section bounded by the bottom beam and haunch flanges at the column face. At the end of the haunch, the compressive or tensile force in the haunch flange would be distributed into the beam bottom flange and this coupled with a stress distribution reaching to the top beam flange.

This moment capacity of the haunch section subsequent to the top weld fractures could also be seen in the data for HCH1 at the column face. In Fig. 5.47 it can be seen that the average strains at the bottom of the haunch flange followed an opposite path to the strains at the west side of the bottom of the beam flange (the east side data was no longer available) after the fracture of the top flange. Data from HCH3 only showed a smaller cycling at the bottom of the haunch flange. At the column face the top flange strains of HCH1 and HCH3 were much less uniform than in the dogbone specimens, with widely scattered peak values, but differential strains were generally highest at the center of flange and lowest at the ends. It was also quite apparent that residual stresses were quite high at the column face, as yielding occurred at values well below the assumed yield strain of 54/29000=0.00186 in./in., even as low as 0.0006 in./in at the top and bottom beam flanges compared with a minimum value in excess of 0.0015 in./in. at the beam section (19 in. from the column face). This was presumed to be due to the residual stresses introduced during the connection welding process placing this area of the flange in a residual tensile state.

For HCH2 and HCH4 all strain gage data for the beam area at the end of the haunch was quite uniform across the top flange width until yielding occurred in the 2.4 in. load cycle. Strain readings at the bottom flange at the end of the

haunch show a fairly even onset of yield in the 1.2 in. cycles for HCH4 while HCH2 had compression yielding of the flange tips in the 0.8 in. cycles.

At the column face the top flange strains were much less uniform than in the dogbone specimens, with widely scattered peak values, but differential strains were highest at the center of flange and lowest at the ends. Haunch flange strains were uniform across the flange width.

2) Strain Rosette Data

Strain rosette locations corresponded to the mid-depth of slab, mid-depth of beam section, and mid-depth of haunch (Figs. 3.11, 3.14). Data was then reduced to report the principal strains as well as the principal axis of strain. This principal axis of strain gives an indication of the angle of compression strut provided in the panel zone and all angles are reported with respect to the column longitudinal axis.

From the strain rosette data it was found that all shearing strains in the column at the center of the slab area were elastic, (although the HCH2 gages were not functioning at this location), (Fig. 5.48). This was expected in the bare steel specimens as the column shear capacity was greater than the applied shear. In the composite sections it was noted in the deformation analysis section (5.C) that there was some plastic column behavior that was assumed to take place in the slab area. This would correspond with Ref. 64 which depicted the panel zone extending to the mid depth of the slab. The portion of panel zone actions between the measured beam section panel zones and rosette locations were not measured. It is speculated that the small unmeasured portion of panel zone deformations as

well as errors due to the accuracy of the instrumentation could account for the apparent column inelastic actions.

While the HCH1 and HCH3 data at the slab location increased in magnitude with each cycle until failure of the specimens the HCH4 data remained fairly low until the 6.0 in. load cycles, at which point the values pick up significantly even as the load capacity of the specimen decreased. This could possibly indicate that the shear studs were completely severed and the slab rotations introduced additional shears into the column section.

The dogbone beam panel zone shearing strains were quite similar between the bare steel and composite specimens through the failure of the welds in specimen DB1 (Fig. 5.49). The panel zone yielded in shear during the 2.4 in. load cycle for both specimens and the principal axis for both specimens was oriented at approximately 45 degrees, although specimen DB2 had a significant decrease in the angle (principal angle of 25 to 35 degrees) after the weld fractures. The principal axis orientation is larger than would be expected (bare steel dogbone specimen $Tan^{-1}(15.85/29.65)=28$ degrees, composite dogbone specimen $Tan^{-1}(15.85/32.78)=26$ degrees), although the similarity of orientation between bare steel and composite sections is not surprising given the accuracy of our instrumentation. The change in angle once the welds fractured would be expected as the positive moment side of the connection would have a very small effective depth and the panel zone would become skewed, which would significantly alter the panel zone stress distribution. Specimen DB2 showed significantly more yielding in load cycles 3.6 in. and 4.8 in. which was in line with the panel zone deformations reported previously.

The haunch specimen beam panel zone shearing strains also yielded at the 2.4 in. load cycles (Fig. 5.49), and had principal axis of stress at approximately 45 degrees. These principal axis orientations were expected to be less than the dogbone panel zone values due to the increased effective panel zone depth, however the fact that they were no longer placed at the center of the effective panel zone depth may have influenced the strain orientation. Values of maximum shearing strains were very similar between the bare steel and composite specimens until yielding in the 2.4 in. load cycles at which point the composite strains were higher. After the fracturing of the top flange welds the angle of principal axis of strain was seen to increase for the bare steel specimens. The change in angle once the welds fractured would be expected as the negative moment side of the connection would have a reduced effective depth, (equal to the haunch depth), and the panel zone would become skewed which would significantly alter the panel zone stress distribution. The composite specimens had widely ranging values for the principal axis angle in later load cycles.

Haunch panel zone shearing strains were almost exactly half of the values obtained at the beam panel zone locations (Fig. 5.50), indicating that the entire effective panel zone was centered close to the center of the beam section. Strains were also very similar between the bare steel and composite specimens until yielding at the 2.4 in. load cycles, at which point the composite strains became much higher. Principal axis of strain angles once again hovered between 40 and 45 degrees until fracture or significant section yielding was experienced after which the bare steel specimens tended to have an increase in the angle of principal

axis (post fracture), while the composite specimens showed more variation in the readings both higher and lower.

Maximum shearing strain readings were slightly reduced at each cycle beyond reaching the yielding strains, signifying strain hardening in the panel zone regions. Inelastic panel zone deformations in the deflection calculations generally corresponded to yielding in the panel zone as determined by the strain rosette data.

3) Observations from Strain Gage Data

Several observations were made from strain gage data. It was found that the strains were much more uniform across the flange width at the critical section, (15 to 19 inches from the column face), than at the column face. At the column face the dogbone specimens had a parabolic distribution of strains across the flanges until first yielding while the haunch specimens had erratic distributions of strain across the flange widths. Indications of high residual stresses at the column face due to the welding processes were found. Panel zones in the slab area were found to remain elastic through testing, while the beam section panel zones yielded for all specimens. Haunch panel zones showed shearing strains of almost exactly half of those in the beam panel zone.

G) Summary of Detailed Analysis

Detailed analysis found that the actual yield strength of the beams was much higher than the 36 ksi steel that was ordered and assumed in design, on the order of 50 ksi. This is typical of modern steel sections, but may not be representative of older buildings. This overstrength meant that the achieved

moments were far beyond the nominal plastic moments of specimens, however the estimated plastic moments were only achieved in the haunch specimens.

Most deformations were concentrated in the beams of all specimens. Only the composite haunch specimens exhibited inelastic deformations throughout the beam depth for all connections. The energy dissipation capacity of the composite haunch specimens was excellent, while the bare steel haunch specimens were marginal, and the dogbone specimens dissipated almost no additional energy once the welds fractured and would contribute little to seismic resistance of a structure should these fractures occur.

The greatest influence of the composite slab was on the stability of the specimen. The restraining action of the slab to lateral torsional and top flange local buckling along with the reduction of strains at the top flange were factors which allowed the composite haunch specimens to reach a high performance level. The assumed compressive strength of the slab of $1.3F'_c$ over the column flange width was not attained in most cases, most likely due to the shear stud failures. It is tentatively recommended that the assumed compressive strength be reduced to $0.85F'_c$ for section strength calculations, and that the nominal capacity for shear stud capacity be reduced by a factor of approximately 0.65 in cases of cyclic design.

Chapter 6: Development of Design Model Concepts

The ultimate objective of this study is to develop a design methodology for the retrofit of existing pre-Northridge steel moment connections. In this chapter the basis for the retrofit procedures will be presented. Specific dogbone and haunch retrofit recommendations will be proposed in Chapter 7.

A) Objectives of Retrofit

In the design of a retrofit for an existing connection there are many issues to consider. Firstly, there is the issue of providing life safety in existing buildings. While there is some question as to the safety of existing pre-Northridge connections, it must be acknowledged that there were no building collapses due to the weld fractures which occurred in the Northridge Earthquake. Life safety was therefore not jeopardized in those cases. However, the repair and loss of service costs were tremendous, and the possibility of greater damage in future earthquakes is a very real concern. It must also be realized that the retrofit of existing buildings can be quite expensive. On the one hand, it is desirable to provide as high a level of safety as possible and reduce the risk and cost associated with damage in future earthquakes, however this must be balanced with the reality of the high cost of retrofitting a building.

In order for a connection to address safety concerns and minimize the extent of damage, one should avoid the brittle fractures which have been observed in the pre-Northridge connections. It is desirable for the connection to absorb

energy through ductile deformations concentrated in the beam and panel zone sections. A measure of the connection ductility would be the total plastic rotation of the connection. For these design methods, the minimum expected connection design criteria was established in Chapter 3 and is taken as 0.020 radian of total plastic rotation. It is likely that connections designed by these methods could greatly exceed this minimum criteria, as was indicated by specimens HCH2 and HCH4.

In an attempt to minimize costs, the two methods studied in this report (dogbone and haunch) require minimal modifications to the existing structure. The designs studied modify only the bottom beam flange (although it may also be necessary to provide some top beam flange weld improvements), therefore removal of existing concrete slabs would be minimized.

It is beneficial to allow for some degree of variation in the design procedure. This would provide for multiple solutions for a given connection, allowing for the handling of possible constraints in an existing connection which may preclude some options.

It should be understood that the primary concern in structure response to an earthquake is life safety. In a very strong earthquake some damage should be expected in any structure. In fact, connection design typically allows for the energy dissipation to take place through inelastic deformations in the beam sections. These localized deformations are expected to take place at the center of the dogbone or end of the haunch section in the retrofit connections, just as they were expected at the column face in the original connections. Modifying a connection simply provides the capacity to withstand a larger earthquake with less

damage.

B) Summary of Existing Design Approaches

There are currently several different approaches for the design of new or retrofit connections. These approaches all attempt to develop estimates of the forces applied, as well as the forces which can be safely withstood, at the weld locations at the face of the column as well as at any critical locations (center of reduced flanges, end of haunch locations, etc.) Approaches can be divided into three major categories.

There are simplified models which base their designs on overall section properties, such as elastic or plastic section moduli, to calculate average stresses across sections. The underlying principle of this approach to design is that there are numerous factors and associated uncertainties involved with any design. By picking a simplified model, and then calibrating test results to this model it is possible to develop overall criteria which incorporate numerous factors, and can even account for factors which are not completely understood, or which would be otherwise difficult to include. Therefore, even though a design which is based on

$$\sigma = \frac{Mc}{I} \qquad (6\text{-}1)$$

where:

σ= elastic stress at the section at a distance c from the elastic neutral axis

M= applied moment

c= distance from elastic neutral axis

I= Moment of inertia of the cross section

would not directly model stress concentrations, triaxial forces, and other factors, it could provide a safe design so long as the calibration incorporates these factors. The goal, then, is to restrict the maximum σ values to safe limits which are developed from calibrations. These calibrations are only valid when used in the design of connections which are similar to the calibrated specimens. Extrapolation to other design details is difficult, since the method does not provide insight into the influence of individual factors. However, the method is a reasonable basis for design. In fact, its simplicity lends itself quite well to design.

Another approach would be to develop truss models, or strut and tie models, to determine the forces in the connection. Several of these have been developed with regard to the Northridge connections (46), and attempt to provide a more realistic model of the flow of forces than the simplified procedure of equation 6-1. These models are also simplified methods, as they do not look at the effects of individual factors, but deal only in overall average stress distributions. While there appears to be much promise in such design models, their main emphasis is on developing a model of stress distributions and then providing reinforcements to carry these distributions. For example, in Ref. 46 the model showed tension and shear at the beam flange welds, and ribs were then designed to carry these forces. This model would be much more difficult to apply to the case of a bottom flange only retrofit, as the method does not attempt to account for the combined state of stress applied at the top weld.

Finally, design can be accomplished through a rigorous modeling of the connection. This would include the many finite element models which have been

developed to address the Northridge connection fractures. While this type of modeling can often provide insight into the significance of individual factors, it must be recognized that these models are only as accurate as the assumptions which they are based on. In the case of a full connection model, a model would need to incorporate numerous factors into the design, such as typical acceptable weld defects which may exist, slip of the shear connection, continuity between the steel beam and composite slab (including slip of the slab), etc. The models must then be calibrated against test data to calibrate the modeling assumptions made with respect to these factors. Once developed, these models can be extremely valuable in extrapolating test results to other situations, but as a design model they may be overly tedious to employ. With the large number of factors involved in the flange groove weld stresses and weld capacities (see Chapter 2), and high degree of uncertainty of in situ weld properties, a simplified design method may be more appropriate.

C) Overall Approach to Retrofit Design

It is felt that the simplified procedure of equation 6-1 is a reasonable basis for design, and will be used as the basis for the retrofit design methods developed in Chapter 7.

The connection failures associated with the Northridge Earthquake were significant because they consisted of brittle fractures of the weld material or heat affected zone with negligible plastic deformations in the connection. The goal of this retrofit design method is to provide for energy dissipation in the beam section through inelastic deformations while precluding brittle fractures.

The two approaches studied in this research (dogbone and haunch) attempt to meet this goal by providing a "fuse" in the beam section. This is either done by weakening the beam cross section at a given location away from the column face (dogbone), or by strengthening the section at the column face and thereby also forcing the plastic hinge to form at a given location away from the column face (haunch). Through the design of these two "fuses" one can effectively limit the stresses on the flange groove welds at the column face. From data collected in these tests as well as results of previous research, a better understanding of a lower bound on the weld stresses which would preclude brittle fractures, (allowable average weld stresses), was obtained.

For the design methods presented, critical stresses will be determined both for the existing welds, and for several levels of modifications to these welds. The sizing of the haunch section or dogbone cutout determines the applied stresses on the welds at the column face. A designer is therefore able to alter the degree of weld modifications as well as the haunch size or extent of dogbone flange reduction in order to arrive at an acceptable design. This allows for multiple solutions to a given retrofit and thereby freedom to adapt to in-situ constraints.

D) Factors Affecting Maximum Moments Developed at Connection

There are many factors that affect the demand side of a connection retrofit equation. These must be taken into account such that the stresses applied to the flange groove welds can be estimated.

1) Material Properties

The maximum moment developed at the connection is greatly influenced

by the material properties of the steel used in both the beam and column sections. Typically in existing buildings, the beam sections will be of grade A36 steel while the column will be of Grade 50 steel. As was seen in this study, A36 steel can have actual yield and ultimate stresses well beyond the assumed 36 ksi. This overstrength of the beam material directly influences the actual moment capacity of the beam which in turn affects the overall behavior of the structure.

The amount of material overstrength can be found directly from tension coupons taken from the building to be retrofit. When tension coupons are taken, it should be noted that material removed from the beam web normally results in capacities on the order of 5 percent higher than those from the flange material (75). Yield strengths based on material removed from the web could therefore be multiplied by 0.95 since most all of the moment capacity is provided by the flange material. Sufficient samples should be taken to produce meaningful results. In general, the dynamic yield point will be applicable to a seismic design, and should be used when available.

One should use caution when using yield strength values as reported on the mill reports as these values often are based on the upper yield point tested at a very high load rate and may not provide realistic estimates of material properties suitable for design purposes. These factors often produce mill test data which exceeds the actual flange material design yield strengths.

When neither in situ or mill tests are available, the material overstrength may also be approximated by the following method. The AISC Seismic Provisions (76) define the expected yield strength F_{ye} as

$$F_{ye}=R_yF_{yn} \qquad (6\text{-}2)$$

where

R_y= material overstrength multiplier

F_{yn}= minimum specified yield stress

In the AISC Seismic Provisions (76) R_y is recommended as 1.5 for ASTM A36 steel, and 1.1 for other grades of steel. The factor for A36 steel is based on the current distribution of yield strengths (including the relatively new "multi-grade certified" steel sections) and is not necessarily applicable to sections produced prior to the 1994 Northridge Earthquake. For older sections of A36 material, it would therefore be applicable to utilize a lower value of R_y, such as a value of 1.3 as recommended in Ref. 77.

2) Strain Hardening

As the section is strained beyond its yield moment, the yielded materials will begin to strain harden. It has been reported that an expected increase in material strength due to strain hardening is on the order of ten percent (77). The estimated strength of material at the section plastic moment capacity would then be

$$F_{ysh}=1.1F_{ye} \qquad (6\text{-}3)$$

where

F_{ysh}= expected strength after strain hardening

F_{ye}= expected yield strength as defined in section 6.D.1

In the case of composite connections, the slab capacity has been backed out of test results based on the actual measured dimensions and properties of the

section, but not including strain hardening. Therefore, when a composite slab is considered for positive moments, strain hardening would already be included in the composite specimen strength estimates. However, the design methods presented in Chapter 7 will assume elastic behavior at the column face and strain hardened capacities at the critical section (end of haunch or center of dogbone). Since the same concrete compressive force will be assumed at each location, it would be appropriate to assume strain hardening in the steel at the critical section (F_{ysh}), and not at the face of the column (F_{ye}).

The design methods presented in Chapter 7 and App. F and G will therefore include strain hardening in all cases, (Eqn. 6-3), for the sake of clarity and consistency in calculations.

3) Slab Effects

The effects of the composite slab on the section moment capacity at the connection location are a function of the compressive force developed in the concrete slab. This force is dependant on the degree of composite action provided by the shear connectors, the strength of concrete, the depth of slab, amount of longitudinal slab reinforcement, orientation of the slab decking, and width of the column flange that the concrete bears against.

As was reported in section 5.E.3.c, for cases where the minimum attainable section capacity is desired, the value for the compressive force in the slab (C_c) of a partially composite section is recommended to be taken as

$$C_c=0.85F'_c t_s b_{cf} \qquad (6\text{-}4)$$

where

F'_c= compressive strength of concrete

t_s= effective thickness of slab

b_{cf}= width of the column flange

provided that the composite section neutral axis is in the steel beam and that the shear studs provided have the capacity to resist the associated shear.

The shear stud capacity should be calculated in accordance with the AISC LRFD code requirements (equation I5-1), although a reduction factor of 0.65 should be applied to the nominal capacity, (as discussed in Chapter 5), until further testing is completed to evaluate the strength of shear studs subjected to cyclic loads.

The effective depth of the slab should be considered only the portion of the slab above the decking flutes when the decking runs perpendicular to the beam, and should account for the concrete in flutes which directly intersect the column flange when the decking runs parallel to the beam.

It should also be noted that previous research (61) has shown that the expected maximum concrete compressive stress at the connection location for a fully composite section can be taken as 1.3F'c, indicating that this value can replace $0.85F'_c$ in the above calculation.

For the design of a retrofit section, one should utilized values which would provide the maximum strains on the connection welds. Therefore, calculations provided in this report use the higher composite value of $1.3F'_c$, although designers should keep in mind that the actual attained concrete compressive force may be much lower. This would be especially critical when evaluating the load carrying capacity of the section.

Therefore, for purposes of retrofit design method calculations:

$$C_c = 1.3F'_c t_s b_{cf} \qquad (6\text{-}5)$$

where

F'_c= compressive strength of concrete

t_s= effective thickness of slab

b_{cf}= width of the column flange

The total compressive force in the concrete slab will be similar at the face of the column and at the dogbone or end of haunch location, although the concrete stresses will be reduced due to the distribution of the compressive force into a wider cross section of the slab away from the column face. The change in moment capacity due to the retrofit design should be accounted for in evaluating the overall increase or decrease in demand on the connection welds when the slab is present.

It is assumed that the slab section does not develop any appreciable tension capacity in negative moment bending of the composite section. There was actually some indications that the slab did contribute to negative bending capacity in the test specimens, however, this increased capacity was not realized in all of the specimens and should not be counted on. In the case of a slab with a large amount of longitudinal reinforcement there may actually be some contribution in the negative moments, but this has been neglected. Therefore, in the negative bending direction a zero tensile force in the slab will be assumed in design.

It has been shown (54) that isolating the slab from the column face results

in moments at the connection similar to those obtained in the bare steel specimens. When this isolation is provided the composite action provisions of Chapter 7 should be neglected.

4) Gravity Load Effects

The moment at the connection location will also be affected by the gravity loads on the beam span. Moments produced by gravity loads may be directly superimposed on the design moment diagram utilized to size the dogbone or haunch retrofit. The design methods will include equations to account for a uniformly distributed gravity load on the span. Other specific loadings can be similarly handled.

5) Other Factors

Other factors which may affect the maximum moment demand at the connection include the actual seismic load on the structure, drift requirements, presence of lateral bracing, details of the retrofit, and the strength of the column and panel zone.

It is obvious that the demand on the structure is directly dependant on the expected seismic activity in the area, and as such, it is possible that a detailed evaluation of a structure would show the actual expected strength and/or rotational demands on specific connections to be less than those recommended for typical design. Similarly, since the stiffness of a structure will often control the sizing of members to meet drift requirements, members are often overdesigned from a strength perspective. Extreme caution should be used in devaluing the need for ductility of any critical connections, as the possibility of seismic forces in a major event exceeding known records is a distinct possibility. It is also

important to realize that resistance to seismic forces in design is typically reliant on the energy dissipation of the beam members, which can only be accomplished if the connection behaves in a ductile manner. In the case of a highly redundant structure, or one which is highly overdesigned from a strength point of view due to severe drift requirements, one may be able to isolate specific critical connections for retrofit and revise the expected demand on the remaining connections.

It is also possible that the removal of material in a dogbone retrofit may allow earlier or more severe lateral torsional buckling of the beam section, thereby limiting the maximum attained moment. For practically all expected applications of the dogbone retrofit, the full plastic moment would be attainable and should be designed for in all cases, as there is always the possibility of lateral bracing from the floor system and other elements.

The details of the retrofit will have a direct influence on the expected moment at the column face as will be accounted for in the design methodology. This will include such factors as the amount of material removed from the beam flanges in a dogbone retrofit, as well as the length and sizing of a haunch.

It is possible that an existing building will have a column or panel zone section which limits the maximum moment that can be attained at the connection. The design of a retrofit connection will generally attempt to provide strong column, weak beam behavior, and therefore the plastic moment of the retrofitted beam section would be attained. A weak panel zone should typically be strengthened in a retrofit design due to relatively little data on the effects of a weak panel zone in conjunction with a composite floor or with the retrofit

methods considered.

E) Factors Affecting Maximum Allowable Stresses

There are many factors that affect the capacity side of a connection retrofit equation. These must be considered when determining the stresses which one can safely apply to the connection flange groove welds.

1) Weld Metal Toughness

The weld metal toughness has been shown to have been a significant factor in the Northridge Earthquake failures (see Chapter 2). Toughness is a measure of a material's ability to absorb energy without brittle fracture and is therefore directly related to its ability to restrict both the initiation and unstable propagation of cracks in the material. Fracture mechanics could be applied to determine the allowable stresses for a weld of specific toughness, but there are many variables involved in the fracture process which complicate the problem. For instance, it is difficult to assess in situ weld toughness, states of stress, and typical sizes and types of defects which would exist in typical welds. The E70T-4 electrode which was commonly utilized in pre-Northridge connections provides a very low toughness. The in place toughness of this electrode has been reported to be less than 10 ft-lbs at 70^{o} F (12). A recommendation for minimum weld toughness of all new welds provided in the retrofit of a connection can be found in Ref. 77, which requires a minimum tensile strength of 70 ksi and a minimum specified Charpy V-Notch value of 20 ft-lbs at -20^{o} F. Care should be taken to substantially reduce the demand on any existing low toughness welds, or the weld materials should be replaced with a higher toughness material as part of the

retrofit.

2) Backing Bars and Weld Tabs

The backing bars and weld tabs have also been shown to be a source of crack initiation (see Chapter 2). As such, any time that the stresses and/or strains on the existing welds are not sufficiently restricted by the retrofit detailing, the welds should be modified by removing the backing bars and weld tabs.

All new flange groove welds or re-welding of existing flange groove welds should conform to the recommendations of Ref. 77. This would typically include the removal of weld tabs and grinding the ends of the groove welds smooth to remove any possible notches and discontinuities in the weld metals at the run-off regions. This procedure should also be followed any time that the existing backing bars are removed.

The more critical bottom flange groove weld should ideally have its steel backing removed, the exposed area ground to remove any inclusions or discontinuities in the bottom of the weld, and then a reinforcing fillet placed at the base of the groove weld. This is intended to eliminate the notch effect which can be induced by the backing bar as well as improve the inspection and ultrasonic testing procedures. In the case of the haunch retrofit, the stresses on the bottom flange groove weld are significantly reduced and the bottom flange welds in this case may often be left as is, with no modifications.

The top flange is felt to have a less critical notch effect due to the backing bar. Therefore, retrofit requirements for the top flange weld does not need to be as stringent as that at the bottom flange weld. As a minimum, the top flange groove weld should have the backing bar welded to the face of the column using a

fillet weld in the case where the expected stresses on the weld are not significantly reduced by the retrofit. This additional fillet has been shown to further reduce the notch effect (45). The presence of a composite slab was shown to reduce the stresses and local buckling distortions on the top flange welds, and so the top welds in this case may be left as is, with no modifications.

3) Beam Web Connection Details

The beam web connection details can also affect the moment capacity at the connection location. Previous research has shown that the moment transfer of the commonly utilized bolted web connection does not effectively transfer moment in the web region of the beam cross section due to slip of the bolts (22,26). This essentially increases the stresses on the flange groove welds due to the entire plastic moment of the beam cross section being transferred at the beam flange locations only. A fully welded web connection has been shown to be much more effective in transferring the full plastic moment of the beam cross section to the column (20,21,22,35,37).

The 1988 UBC code adopted the requirement of supplemental welds at the shear tab location when the plastic moment capacity of the beam flanges is less than 70 percent of the plastic moment capacity of the entire beam section. This intended to provide some moment capacity in the beam web area of the connection assuming that bolt slip precludes moment transfer in this area. These supplemental shear tab welds may be provided if the retrofit is felt to require the additional moment transfer in the beam web section of the connection. If it is felt that a fully welded connection is required, this can be accomplished by several means. The beam web can be welded directly to the column with a complete joint

penetration groove weld, or the use of a web doubler plate as reported in repair of damaged Northridge connections (78) can be employed.

In the design method presented in Chapter 7, weld stresses are limited to allowable stresses based on the moment of inertia of the entire cross section. This is consistent with the method of determining the allowable stresses developed in Section 6.F. The critical values cited are for cases with bolted web connections. The design method would therefore have a higher factor of safety associated with it when additional moment capacity is transferred through the beam web.

4) Continuity Plate Details

The presence of a continuity plate at the connection has been shown to reduce the stresses on the center of the flange groove welds by restricting the bending of the column flange (27). The stresses induced by the flange bending can be significant, although in the case of very thick column flanges the flange stiffness may be sufficient to control this action. The 1988 UBC code adopted continuity plate requirements for special moment resisting frames based on the bending capacity of the column flange. In the Interim Guidelines and Advisory No.1 (68), continuity plates were required in all new construction of welded moment connections. In this study, none of the connections contained continuity plates, as none were required per the codes which were in place at the time of the Northridge Earthquake.

The requirements for continuity plates in all new construction appears to be overly restrictive given the excellent performance of the composite haunch specimens in this study along with the borderline performance of the composite dogbone specimen, none of which contained continuity plates. It should also be

noted that the addition of continuity plates in existing buildings could prove to be very expensive as it could require the removal of slab material as well as the modification of connections framing into the column in the transverse direction.

It is felt that in the course of a retrofit, judgement is required as to the potential benefit of continuity plates versus the associated costs. Reference 77 recommends that, as a general minimum requirement for the potential need of continuity plates, the 1988 UBC provisions should be consulted. Guidelines for the sizing and welding of continuity plates can be found in the Seismic Provisions for Structural Steel Buildings (76).

5) Panel Zone Strength

In the 1988 UBC code, the dissipation of energy in the shear panel zone was allowed. It has been shown in previous research that shear panel zone deformations can result in an increase in stresses developed in the beam flange groove welds (24,26,38,50). While the overall connection plastic rotation capacity can be increased by allowing for the panel zone deformations, the beam plastic rotation capacity and energy dissipation of the connection may end up being limited by weld fractures due to these additional stresses. Reference 77 recommends that panel zone deformations be limited in the design of a connection retrofit. Per Ref. 77, the panel zone capacities should be checked as per the UBC code requirements. Further recommendations regarding panel zone required strengths can be found in Refs. 67 and 68. The connections tested in this project were designed to have minimal panel zone shear deformations and all results are therefore applicable to this condition only.

Panel zones in the beam region when a composite slab is provided have

been estimated to extend into the center of the slab cross section (64), and this additional capacity may be used in evaluating the panel zone strength. The results of this project support this. The haunch panel zones consist of "dual" panel zones in the beam and haunch areas which appear to act as one larger panel zone extending from the bottom of the haunch section to the top of the beam section (or center of slab). The haunch panel zones tested in this study were found to have almost exactly one half of the shearing strains associated with the beam section panel zone.

Should the panel zone strength be inadequate, it can be increased through the addition of a welded doubler plate in accordance with the provisions of the UBC code.

6) Slab Effects

The presence of a composite slab tends to reduce the strains on the top flange of the beam and increase the strains on the bottom beam flange as compared to a bare steel specimen. This is accomplished by the migration of the neutral axis towards the top of the beam section when the composite section is considered in conjunction with the increased composite moment capacity as compared to the bare steel section capacity.

In addition, the presence of the composite slab was shown to greatly limit the lateral torsional and local buckling of the top flange of the beam. This is felt to benefit the capacity of the weld materials by preventing the huge differential strains and deformations which can otherwise occur at the top flange groove weld during load reversals.

7) Other Factors

Extreme local buckling can place severe strain deformations on the weld material. The load reversals can produce extreme differential strains. These localized strain requirements can lead to crack propagation and early weld fractures.

Triaxial states of stress at the weld material may exist due to the detailing of the connection, and restraint from thick column sections may cause these to be quite severe. These triaxial states of stress can result in brittle modes of failure. The dogbone and haunch retrofit attempt to concentrate inelastic actions at a distance from the column face (center of flange reduction, end of haunch), and therefore minimize the effects from the triaxial forces.

As a general practice in retrofit, attention should be paid to the detailing of the weld access holes. Any sharp discontinuities between the access hole and inside face of the beam flanges can act as stress risers and initiate fractures. Details for the preparation and concerns thereof are addressed in Ref. 77. Reference 72 contains requirements pertaining to the geometry of the access hole with regard to proper shape, sizing, and finishing.

All other possible stress risers in the beam and column sections should likewise be corrected. These could include damage incurred during the repair process (accidental gauging during removal of original weld material, fireproofing, etc.), existing discontinuities or stress risers in the connection, or those introduced during the provision of the retrofit (smooth transition and surface of dogbone flange cutouts, etc.) Many of these are addressed in Ref. 77.

All welding processes not in accordance with the AWS code, such as running the weld “hot”, inadequate surface preparation, use of “end dams”, etc.

can affect the allowable stresses of the weld material. Therefore all welds should be made in strict accordance with the AWS code (72) and inspected to ensure compliance. Existing welds which are still critical after a retrofit design should undergo 100 percent inspection in order to check for general weld quality. It may be difficult to obtain reliable inspection readings at the top flange welds when the backing bar is left in place and a slab is present. Depending on the level of stresses expected on these welds, the removal of the backing bar to aid inspection may be necessary.

The change in base metal properties in the heat affected zone of the welds can reduce the ductility of these sections. This problem can be severe if proper pre-heat is not employed during welding.

Welding in an existing building as part of a retrofit can be much more difficult and expensive than welds made during new construction. Factors such as access for the welder and inspector, restraint of the connection, fire danger, and control of fumes from welding and cutting should be considered when evaluating the need for additional welding and/or improvements to existing welds as other methods may prove to be as effective and much easier to accomplish in the field.

F) Estimate of Safe Limiting Stresses

As mentioned in Section 6.B and 6.C, an estimate of allowable stresses for the weld materials can be reported as an average stress value across the flange in order to incorporate the factors affecting allowable weld stresses into one overall value. Safe limiting stresses or moments in our specimens can be estimated by studying the load histories of the specimens. These weld stresses will be based on

a simple calculation assuming the full section participating in moment transfer, plane sections remaining plane, etc.

Therefore in the case of a non-yielded section:

$$F_w = \frac{M}{S_x} \qquad (6\text{-}6)$$

where:

F_w= reference weld stress

M= applied moment

S_x= the elastic section modulus of the gross section

For our composite haunch specimens, there were no failures and the welds could withstand the entire applied stresses. In the case of the dogbone and bare steel haunch specimens it was noted at which stress levels the specimen's welds failed and, more importantly, the previous cycled force levels at which there was no failure.

The bare steel dogbone specimen (DB1) sustained a moment at the column face on the order of 12250 kip-in. This would correspond to a weld stress on the order of 46 ksi when the entire cross section was assumed effective in providing moment capacity, (based on Eq. 6-6). This magnitude of stress is within the elastic range of the tested beam steel, however it would not be in the elastic range of beams where actual material yield stress is closer to the specified yield values. Many Northridge connection weld fractures occurred with very little apparent inelastic deformation in specimens where the yield strength was likely below 45 ksi. Therefore, while a value of 46 ksi calculated on the gross section

properties appeared to be safe for our specimen DB1, it was felt that a lower limiting stress was warranted based on the field fractures in Northridge.

In the composite dogbone specimen (DB2) it was found that tears formed in the beam k-region from the cope hole outward into the beam span, effectively de-coupling the beam flanges prior to the weld fractures. This failure mechanism in conjunction with the previously discussed difficulties in obtaining the section neutral axis at the column face (see Chapter 5), made it impossible to predict the weld stresses that were reached prior to fracture.

The final fractures were obtained in the top flange welds of the bare steel haunch specimens (HCH1 and HCH3). All but one of these fractures occurred in a later cycle of loading during which there was a high degree of inelastic action. The load capacity was already diminished in these cases by the local and lateral torsional buckling of the sections. All of these reached ultimate moments in excess of the moment which caused earliest weld fracture in the south beam of HCH1. At the time of weld fracture in the south beam of specimen HCH1 local top beam flange buckling was visible. All of the failures appeared to initiate at the edge of the specimen flange near the runoff tabs. It was felt that it was the localized distortions associated with the flange buckling, as opposed to the average flange stress level, which were the major contributors to these fractures. Of the four haunch specimens, the earliest weld fracture (south beam of HCH1), occurred at a moment in excess of 17,500 kip-in. at the column face. Based on the full cross section properties at the column face, this translated to approximately 43 ksi on the top weld (based on Eqn. 6-6).

Seventy specimens from studies on pre-Northridge connections were

referenced, and the apparent average attained weld stresses, (based on Eqn. 6-6), are listed in Table 6.1. Assumed and measured yield stresses are also noted. Reported elastic weld stresses in excess of the actual F_{yf} indicates that the yield of the base material was attainable, not that the elastic weld stress was realized in the welds.

From Table 6.1, the lowest attained stresses on the welds based on gross section properties were 32.9 ksi (Popov et al. specimen 5), 34.6 ksi (SAC specimen 7), and 36.2 ksi (Tsai and Popov specimen 15). A safe estimate for allowable stress on the welds could therefore be assumed at approximately 30 ksi, for an original E70T-4 electrode weld with the backing bars and end tabs left in place for bare steel specimens. When the backing bars were removed from these original welds, only one specimen appeared to fracture prior to reaching the yield stress of the base material, and the elastic stress at fracture was 33.6 ksi (Popov et al specimen 3). All other specimens with backing bars removed achieved the yield stresses of the base materials, although a large number of cycles at these stresses was not generally possible. There are relatively few of the tests in Table 6.1 which include removal of backing bars. It would therefore be advisable to limit the working stresses to a fraction of the nominal yield of a beam section, say a maximum value of 32 ksi ($0.9F_y$).

When new welds are provided utilizing E71T-8 or other moderate toughness electrodes with a full weld inspection and removal of backup bars and end tabs, there is relatively little data on the allowable stresses. However, when dogbones were tested for new construction, and the dogbone “fuse” designed to limit the moment at the face of the column to 0.85 to 0.95 M_p the connections

have performed very well. This was very close to the ratio of M_y to M_p for these specimens. It is therefore assumed that one can safely reach the yield moment and stress with these welds, (extreme fiber of weld at yield of base material). This value will be used as a limiting stress in the design methods which follow.

For the case where the flange is restrained against inelastic deformations in the weld area, (as in the case of the top flange in our composite specimens), it appeared as though even the original E70T-4 welds with backing bars and runoff tabs left in place had no trouble withstanding full inelastic action through the flange thickness. Based on these findings, it is recommended that any weld that connects members which are restrained against local buckling in the region of the weld be designed for stresses up to the full yield capacity of the welded sections. Further research should be performed to verify this assumption.

In addition to the criteria mentioned above regarding allowable stresses on the flange groove welds, design guidelines in Advisory No.1 (68) recommend that an absolute limit on the stress at the face of the column not exceed 90 percent of the minimum specified yield stress of the column. This stress limit appears to have been chosen somewhat arbitrarily, and future research may indicate that this limit can be increased. For the time being, one should use this value as a cap on the allowable stress at the weld area.

Recommended values of safe limiting (allowable) stresses at the welds are compiled in Table 6.2.

Chapter 7: Design Methods for Retrofit of Existing Structures

In this chapter design methods will be described for both the dogbone and haunch retrofit of existing structures. The guidelines could also be applied to new construction, but are not specifically derived as such.

A connection retrofit according to the guidelines of this report provides a connection which meets a much higher performance level than the typical existing pre-Northridge connection. Retrofit of structures which provide additional measures to improve performance would reduce the expected repairs required after a major seismic event and should therefore be considered by owners and engineers. Several modifications which may increase the performance level are mentioned.

A) Design of Dogbone Retrofit

1) Choice of Shape and Size of Dogbone

There are several methods which have been studied for reducing the beam flanges in dogbone specimens. All previous studies have used flange reductions in both the top and bottom flanges as opposed to only the bottom flange as was studied in this project. Shapes of the dogbone cutouts have been of three types to date, constant cut, tapered cut, and radius cut (see Fig.7.1). The tapered cut attempts to maintain a constant stress over the reduced flange section by reducing the moment capacity at the same rate as the moment gradient of the section. This may not be fully effective, as the design assumes a point of inflection along the

beam which would be in a state of flux during a seismic event. The radius cut attempts to minimize sharp changes in flange section. Previous testing of constant and tapered cut sections has occasionally resulted in fractures at these points in the later stages of loading (17,19). It is felt by the author that this benefit of the radius cut is more desirable than the possible advantages of the tapered cut sections, and the radius cut will therefore be the focus of the design method presented.

The dimensions of the dogbone are somewhat arbitrary, with recommendations presented here based on previous designs which have worked well, and the recommendations of Ref. 77. Other variations are most likely possible. See Figure 7.2 for dimension definitions.

Two conflicting goals come into play when designing the dogbone section. It is desirable to place the weakened section far from the column face in order to limit distortions at the column face from inelastic deformations and to allow the redistribution of stresses over the full beam flange width at the column face location. On the other hand, the required section reduction to maintain a similar applied moment at the column face would increase as the weakened cross section is moved away from the column face, due to the moment gradient. As a compromise between these two goals, it has been recommended (77) that the dimension a be taken as

$$a = (0.5 \text{ to } 0.75)b_f \qquad (7\text{-}1)$$

where b_f= beam flange width

In addition, the total length of the dogbone cutout is required to be long enough to provide a gradual change in cross section. It has been recommended

(77) that this dimension b be taken as

b=(0.65 to 0.85)d (7-2)

where d= beam depth

The depth of cut, c, is determined by calculation and will be discussed in the design method section (7.B.5).

The radius of cut can be determined from the other dimensions chosen, and is given by

$$R=\frac{4c^2+b^2}{8c} \quad (7\text{-}3)$$

Thermal cutting is typically used for the dogbone flange reduction. The surface should be as smooth as possible, avoiding nicks, gouges, and other discontinuities. The surface should then be ground smooth, with grinding done in the direction parallel to the beam flange to avoid grind marks perpendicular to the beam flange which may act as stress risers.

2) Welding Modifications and Details

As a minimum, existing welds at the bottom flange should be inspected using non-destructive testing methods. Should the welds be free of rejectable defects per the AWS (72) code, the maximum weld stress as determined from design of the dogbone cutout should be F_{cr}=30 ksi, as was developed in Section 6.F. It is recommended that welds left in this condition have an additional fillet weld provided to weld the steel backing bar to the face of the column unless the applied stresses are very low. With the removal of the backing bar and runoff tabs, cleanup of the weld, and additional fillet the maximum stress at the location can be increased to F_{cr}=32 ksi, as was recommended in Section 6.F. While this is

not a huge jump in capacity, it is recommended that this procedure be performed when possible as better performance and improved ability to inspect welds are achieved. This would provide higher confidence in the future performance of the connection. The full replacement of weld material with a moderate toughness weld material (minimum CVN value of 20 ft-lb at -20^{o} F) with removal of backing bars, runoff tabs, cleanup of the weld, and additional fillet can increase the allowable maximum stress to $F_{cr}= F_{ye}$ of the base material at the extreme fiber of the weld, as was recommended in Section 6.F.

At the top flange, the amount of repair depends on the applied stresses as well as on whether a composite slab is provided. When a composite, or partially composite slab is present, no alterations are required for the existing welds, ($F_{cr}=F_{ye}$ of base metal, see Section 6.F), unless there is reason to believe that the original weld quality was sub-standard. For a bare steel section, it is recommended that an additional fillet be provided to weld the top flange steel backing bar to the face of the column. This minimal retrofit, the removal of backing bar and runoff tabs, or the replacement with higher toughness weld material would result in allowable stresses similar to those reported for the bottom flange.

While the changes in allowable stresses may appear to be minimal for the different weld modifications, in a dogbone design even a slight decrease in weld capacity can result in a significant change in the amount of material to be removed from the beam flange. This is especially true in the case of a retrofit where it is likely that only the bottom beam flange would be reduced.

In addition to the criteria mentioned above regarding allowable stresses on

the flange groove welds, design guidelines in Advisory No.1 (68) recommend that an absolute limit on the stress at the face of the column not exceed ninety percent of the minimum specified yield stress of the column. This stress limit appears to have been chosen somewhat arbitrarily, and future research may indicate that this limit can be increased. For the time being, one should use this value as a cap on the allowable stress in the weld area.

For the replacement of existing welds the following recommendations were developed in Ref. 77. The replacement weld metal provide a minimum specified tensile strength of 70 ksi and a minimum specified CVN value of 20 ft-lb at -20^{o} F. Removal of the existing weld metal is usually accomplished by air carbon arc cutting (arc gouging), or by grinding. One should take care to remove all of the weld metal, while avoiding the removal of excessive base metal from the beam or column, and avoid damaging the column or beam. If the welds are removed by gouging, the gouged surface should be ground to remove any surface material adversely affected by the heat of the gouging operation.

Prior to re-welding, the groove weld joint dimensions should conform to the requirements or be qualified by test as per AWS D1.1-96 (72). The access holes should also be modified prior to welding as needed. The proper size, geometry, and finish of the access holes as required by AWS D1.1-96 (72) will optimize the connection performance through allowing proper access by the welder, minimizing access hole stress concentrations, and minimizing triaxial states of stress.

3) Slab Effects

The presence of the slab affects several aspects of the dogbone design,

namely the capacity of the section (applied stresses) at both the reduced section and at the column face, as well as the allowable stresses on the welds. It was found that for a partially composite specimen which had a shear stud capacity in excess of

$$Q_s \geq 1.3F'_c t_s b_{fc} \qquad (7\text{-}4)$$

where

Q_s= shear stud capacity

F'_c= compressive strength of concrete slab

t_s= effective thickness of concrete slab

b_{fc}= width of column flange

the expected concrete compressive force was not achieved when Q_s was based on the AISC LRFD code. The shear stud capacity as defined by the AISC LRFD code should be reduced by a factor of 0.65, (see Chapter 5), when designing for cyclic loads in an attempt to prevent the early shear stud fractures which were experienced in this study. This was a tentative recommendation until further research can determine the actual capacity of shear studs. The compressive force in the concrete slab is felt to approach $1.3F'_c t_s b_{fc}$ (61) when the slab becomes fully composite as defined by the AISC LRFD code. In this study, the minimum estimated compressive force in the concrete slab was approximately $0.85F'_c t_s b_{fc}$. These two values are therefore used as boundary compressive forces for calculations, with the most critical results on applied stresses used in design (0.85 factor for design capacity of the section, 1.3 factor for retrofit design evaluation of weld stresses). If the level of composite action is not known, it may be advisable

to design the retrofit as both bare steel and composite and provide for the most critical cases.

When accounting for the composite slab in design, the sections must be checked for both composite and bare steel behavior, as the slab would not be effective in the negative bending capacity. Top flange stresses are generally not critical since the presence of the composite slab would allow full capacity of the beam flange for both the composite and bare steel cases.

The slab effects on allowable weld stresses were discussed in the previous section.

4) Other Factors

Once a dogbone retrofit design is completed, one must ensure that the retrofitted structure still meets all appropriate code requirements for strength and stiffness. The strength of the beam at the minimum section of a dogbone cutout must satisfy code requirements under all applicable load combinations including gravity, wind, and any other loads appropriate for the structure under consideration. This would include checks on the panel zone strength capacity compared to applied forces, checks on strong column-weak beam behavior, requirements on continuity and doubler plates, and supplemental web weld requirements. These checks would be required even though the dogbone retrofit does not provide an increase in beam section strength capacity. They are needed since the original structure may not conform to current code requirements which in turn could override the benefits of the applied retrofit.

The dogbone retrofit will also reduce the elastic stiffness of the structure. Several studies have been done to investigate the influence of the stiffness

reduction (13,14,79) and found that the reduction in stiffness is generally insignificant. For reductions in both the top and bottom flanges of 50 percent, elastic frame stiffness reductions were found to be in the range of 5 to 7 percent. It would follow that a reduction of 50 percent or less in only the bottom flange should affect the overall stiffness by less than 5 percent. The reduction in stiffness, and therefore increase in drift, should be evaluated against the structure drift criteria. A refined structural model which includes the reduced cross section properties can be constructed for individual structures if deemed necessary.

5) Overall Design Method

The design method presented first determines an allowable moment at the column face of the connection based on the level of modification to existing welds. The corresponding moment at the center of the dogbone reduced section is then determined. A flange reduction can then be designed to limit the capacity of the section at the center of the dogbone to this value.

To start the design process, an initial choice for the dogbone length and location (a and b in Fig 7.2) should be made in accordance with section 7.A.1. The amount of welding modifications should then be decided upon, which will lead one to the allowable weld stresses as determined in section 7.A.2. Two factors must then be determined, the expected gravity load conditions and the amount of composite action provided by any existing slab.

The following calculations are based on an assumed uniform beam loading w, and a bottom dogbone flange reduction only. Modifications to these calculations for a dogbone cutout in both the top and bottom flanges will be discussed later in this section.

The maximum moment to be allowed at the column face may first be assessed.

For a bare steel section,

$$M_c = S_b F_{cr} \qquad (7\text{-}5)$$

where:

M_c= critical moment at the column face

S_b= elastic section modulus at the column face

F_{cr}= critical stress as defined in section 7.A.2

When considering a composite connection, the following modification should be made. Due to the lack of data on slab effects the higher slab capacity multiplier of 1.3 will be used in design. The compressive force in the slab should be taken as $(1.3)F'_c t_s b_{fc}$. Next, a strain diagram as indicated in Fig. 7.3 should be chosen, with the bottom or top strain equal to

$$\varepsilon_{bot\ or\ top} = \frac{F_{cr}}{E_s} \qquad (7\text{-}6)$$

where:

$\varepsilon_{bot\ or\ top}$= attainable strain at the bottom or top extreme fiber of the section

F_{cr}= critical stress at weld section (see section 7.A.2)

E_s= Modulus of Elasticity of Steel

The choice of setting the bottom or top weld stress at this critical value will depend on which location would become critical first. For a given concrete slab, the bottom flange would yield first for a smaller beam section since the

concrete will have more influence and reduce the top flange strains by a greater amount.

One must then balance forces to get zero axial force in the section and thereby arrive at a strain diagram for the steel section. This is a trial and error procedure, however it can be accomplished quickly through a spreadsheet calculation. If the stress at the opposite extreme fiber from that assumed to be critical is larger than its critical value, an incorrect assumption as to the first yielding extreme fiber was used. The calculation must be repeated with the other assumption taken.

In order to reach the assumed compressive strains in the concrete, strains at the top of the slab are required to reach values of 0.001 in/in or greater (corresponds to approximately $0.85F'_c$ per Ref. 80). Therefore a check must be made to ensure that $\varepsilon_{top} \geq 0.001$ in/in. The equations shown in Fig. 7.3 were based on a neutral axis located in the web of the beam, so a quick check should be made to ensure that this is the case. In the case of a dogbone retrofit this should invariably be true.

It may not be possible to accommodate the slab compression without exceeding the weld allowable stresses. A higher level of weld improvements would then be required at the flange welds. If the allowable stress of the base material, (associated with replacement of entire weld with higher toughness material), is not sufficient, it is possible to further improve the capacity of the bottom flange with a cover plate, although one may then be advised to consider the haunch retrofit. It is also possible to isolate the composite slab from the column face, as this has been shown to produce behavior corresponding to that of

a bare steel specimen (54).

Once it has been determined that the desired weld improvements will provide the capacity of the section at the column face, this moment capacity of the section can then be calculated by summing the moments of all of the section forces, in accordance with Fig. 7.3.

The maximum moment developed at the center of the dogbone, M_{pd} is found from the following equation.

$$M_{pd}=Z_{RBS}F_{ysh} \qquad (7\text{-}7)$$

where:

M_{pd}= design moment at the center of the dogbone cutout

Z_{RBS}= plastic section modulus at minimum section of the dogbone cutout

F_{ysh}= expected strain hardened stress of beam flange as defined in 6.D.2

For the case of a bottom flange dogbone, the computation of Z_{RBS} can be accomplished with the following equation (see Fig. 7.4)

$$Z_{RBS}=Z_b-\frac{(ct_f)^2}{t_w}-ct_f(d-t_f) \qquad (7\text{-}8)$$

where:

Z_b= Plastic section modulus for full beam cross section (without dogbone reduction)

c= depth of dogbone cutout

t_f= thickness of top beam flange

t_w= thickness of beam web

d= depth of beam

Note that for a composite section, the previous equation should be modified as per Fig. 7.5, whereby the composite slab force is included in the calculations. For the neutral axis location as shown in the figure

$$Z_{RBS(composite)}=Z_b-\left(\frac{\left(C_c+2F_{ysh}ct_f\right)}{2F_{ysh}t_w}\right)^2 t_w - ct_f\left(d-t_f\right)+\frac{C_c\left(d/2+g+t_s/2\right)}{F_{ysh}} \quad (7\text{-}9)$$

where:

Z_b= Plastic section modulus for full beam cross section (without dogbone reduction)

c= depth of dogbone cutout

t_f= thickness of top beam flange

t_w= thickness of beam web

d= depth of beam

t_s= effective slab thickness

g= gap between beam and effective slab

C_c= compressive force in slab

Assuming a uniform beam loading w (see Fig. 7.6), the moment at the face of the column would be

$$M_f=\left[1+\frac{2s_c}{L'}\right]M_{pd}+\frac{wLs_c}{2} \quad (7\text{-}10)$$

where:

M_f= maximum applied moment at face of column

M_{pd}= design moment at center of dogbone cutout, defined in Eqn. 7-7.

s_c= distance from face of column to center of dogbone cutout

L'= clear beam span minus $2s_c$

L= beam span

w= uniformly distributed gravity load on beam

Note that the gravity load portion of the previous equation is slightly conservative as it assumes all load between the column face and center of dogbone to be acting at the center of dogbone. Loading conditions other than uniformly distributed load can be handled according to the specific load distributions.

One can now work backwards, filling in all known values in the previous equation, setting it equal to the allowable moment at the column face (M_c defined earlier) and solving for M_{pd}. One can then refer to the defined values for M_{pd} for either bare steel or composite connections and solve for the value of c, or the required flange reduction to limit the stresses at the column face to the allowed values. It is advantageous to set the value of c for the flange reduction at a larger value than the minimum value calculated if possible. This would provide an extra margin of safety against attaining the critical weld stresses.

To date, there have been no dogbone designs tested with flange cutouts greater than 55 percent of the flange area (corresponding to $c=0.27b_f$). There have been concerns over the stability of the beam should larger flange reductions be provided. It is therefore recommended that this percentage of reduction not be exceeded until further testing can quantify the performance of such connections.

Therefore, at this time, if the required reduction is greater than 55 percent the dogbone retrofit is not an acceptable design for the given weld modifications. The design may need to be altered to provide both top and bottom flange cutouts.

Design examples are included in App. F. It can be seen from the examples that it may not be possible to design a bottom flange only dogbone with less than 55 percent flange reduction. Sections with larger flange widths and greater depths would have a greater chance of working than others, and only a limited number of sections would be able to be designed by this method. Therefore, in order for this to be a viable retrofit method further testing would be required to determine the validity of this assumed maximum reduction percentage.

With top and bottom flange reductions (described in Section 7.A.6), designs in App. F were successfully designed as acceptable retrofits according to these guidelines. Composite designs which are unsuccessful may be rectified by isolating of the slab from the column to induce bare connection behavior. This could be easily accomplished in the case of top and bottom flange cutouts as portions of the slab would most likely need to be removed to make the top flange dogbone. Unfortunately, this slab removal may make the retrofit quite expensive.

In Tables 7.1 and 7.2 the design method is used to assess the design of dogbone specimens tested to date in this and other studies. Only specimens which were attached to the strong axis of an I shaped column are included, as the allowable weld stresses were calibrated to this type of connection. Table 7.1 provides information on the specimen properties, while Table 7.2 applies the design method to these sections. It can be seen in Table 7.1 that most of the tests were designed as new construction, and so dogbone cutouts were provided in both

flanges, and moderate toughness weld materials were utilized. As part of this project, allowable stresses on higher toughness weld materials with backing bars left in place, or similar top welds with a sealer weld attaching the backing bar to the column face were not estimated. It appears as though these higher toughness welds are capable of attaining stresses on the order of the yield stress of the base material, (as assumed in Table 7.2). Designs were based on nominal section properties and assumed F_y values based on the approximate method of Equation 6-2. Ribs were included in the analysis of Ref. 19 specimens, (handled similarly to haunch analysis of Section 7.B), and top and bottom flange reductions were handled as per Section 7.A.6.

The design method shows several specimens which exhibited acceptable behavior to be slightly overstressed (Ref. 16 and 17). These specimens have 38 to 45 percent flange reductions, and retrofits with a greater flange reduction which meet these design guidelines could be provided. As was mentioned previously, these specimens were tested as new construction details and were therefore welded initially with the moderate toughness electrode. Removal of existing welds prior to re-welding with a moderate toughness electrode, (as would likely be the case in an existing building to provide a comparable section), has the potential of altering the base metal properties. In addition, the new construction designs provided continuity plates which may not be provided in a retrofit. As was mentioned in section 6.E.4, continuity plates can improve the behavior at the welds. The specimens from Ref. 17 also had the beam webs fully welded to the column flange which would likely improve the behavior as was discussed in section 6.E.3. Therefore, the apparent conservatism of the design guideline would

be warranted.

The specimens of the NIST studies are shown to be highly overstressed at the welds for all specimens which failed to meet the acceptable total plastic rotation requirement of 0.020 radian. The two specimens (UCSD4 and DB2) which met the design criteria were shown to have moderately overstressed welds. These specimens did not significantly exceed the acceptance criteria, and did not exhibit ideal overall performance (see descriptions of DB2 performance in Chapters 4 and 5). Composite capacities of these specimens were also inadequate.

It can be seen in Table 7.2 that the column through thickness requirements of Ref. 68 were exceeded in practically all specimens, with only one divot fracture reported. This fracture (Ref. 16 specimen DBT2B) occurred beyond the acceptance criteria rotation and at a much higher assumed stress than the allowable value. For specimens with beam yield stresses approaching those of the columns the designs can be significantly affected by this criteria which does not appear to correlate with test data. The through thickness guidelines therefore appear overly restrictive and should be modified.

It should also be noted that while this design method was presented to be equally applicable to bottom flange only cutouts as well as top and bottom flange cutouts, most bottom flange only specimens tested to date have failed prematurely. Those which did not were of composite design and although they met the acceptance criteria of 0.020 radian of total plastic rotation, they did not exceed this by a large margin and did not exhibit ideal behavior. This was expected based on this design method. However, testing of specimens which

conform with this design method should be performed in order to verify the method. This should be accomplished prior to their use in an actual retrofit.

6) Techniques to Further Enhance Connection Performance

Should the dogbone retrofit prove to be insufficient as determined by calculations, it may be desirable to provide dogbone cutouts at both the top and bottom beam flanges. This may also improve the overall performance by maximizing the section's resistance to lateral torsional buckling at the dogbone location. The removal of material from the top beam flange, however, would most likely necessitate the removal of the concrete slab at this location, which could prove both costly and time consuming.

If both the top and bottom flanges are reduced, the previous design method would still be applicable, however the equations for M_{pd} would need to be revised as follows.

For the case of the bare steel specimen, the value of Z_{RBS} utilized in the calculation of M_{pd} would need to be changed to

$$Z_{RBS}=Z_b-2ct_f(d-t_f) \qquad (7\text{-}11)$$

For the case of the composite specimen, the values of $\bar{y}$ and M_{pd} as calculated from Fig. 7.5 would be changed to account for the similar flange widths.

As was detailed in section 6.E, several other factors may improve the overall performance of the connection, such as the beam web connection details, continuity plate details, and panel zone strength. The existing connection details should be considered along with any improvements to these details when assessing the best retrofit solution.

B) Design of Haunch Retrofit

1) Sizing Haunch

The section shape to be used for haunch material, depth, and length of a triangular haunch section have not been fully investigated. The recommendations presented here are based on previous designs which have worked well, but other variations are most likely possible.

In choosing haunch dimensions there are several factors to consider. The length of haunch directly influences the moment which is applied to the column face, with a longer haunch dimension increasing this moment (all other variables remaining constant). At the same time, the length of haunch needs to extend far enough from the column face to limit the distortions at the column face from inelastic deformations and to allow the stresses to effectively distribute into the haunch section by limiting the maximum haunch angle. An increase in only the depth of the haunch would reduce the stresses on the welds at the column face, but this must be weighed against the additional interference to clear height between the stories of the building, and the increase in haunch angle.

Typical recommended haunch dimensions based on previous testing and Ref. 77 are as follows, (see Fig 7.7).

$$a=(0.5 \text{ to } 0.6)d \qquad (7\text{-}12)$$

where

a= length of haunch

d= beam depth

and

θ_{hch}= 25 to 35 degrees

Therefore b, the depth of haunch, can be calculated from the given dimensions and assumed angle.

The initial choice for the haunch material to be used is left to the judgement of the designing engineer although there are some general guidelines. First, the flange width must not exceed a dimension which could be easily welded to the column face (the column flange width minus approximately one inch), the minimum web thickness should be on the order of the beam web thickness, and the flange thickness should be larger than the existing beam flange thickness (successful haunches have had flange thickness of about 1.2 to 1.8 times the beam flange thickness, and generally had a flange load capacity component in the horizontal direction in excess of the entire beam flange capacity). Once a spreadsheet is set up for the design method calculations, one can quickly investigate several haunch sections until an appropriate shape is found.

2) Welding Modifications and Details

The addition of the haunch material in a retrofit will significantly reduce stresses at the bottom beam flange. The existing weld can therefore typically be left as is. If expected stresses on the bottom flange weld appears to be high (above 20 ksi), existing welds at the bottom flange should be inspected using non-destructive testing methods. Should the welds be free of rejectable defects per the AWS code (72), the maximum weld stress as determined from the haunch design should be F_{cr}=30 ksi as was developed in Section 6.F. It is recommended that welds left in this condition have an additional fillet weld provided to weld the

steel backing bar to the face of the column unless the applied stresses are very low. With the removal of the backing bar and runoff tabs, cleanup of the weld, and additional fillet the maximum stress at the location can be increased to F_{cr}=32 ksi, as recommended in Section 6.F. The full replacement of weld material with a moderate toughness weld material (minimum CVN value of 20 ft-lb at -20^{o} F) with removal of backing bars, runoff tabs, cleanup of the weld, and additional fillet can increase the allowable maximum stress to $F_{cr}=F_{ye}$ of the base material at the extreme fiber of the weld (see Section 6.F).

At the top flange, the amount of repair depends on the applied stresses as well as on whether a composite slab is provided. When a composite, or partially composite slab is present, no alterations are required for the existing welds ($F_{cr}=F_{ye}$ of base metal), unless there is reason to believe that the original weld quality was sub-standard. For a bare steel section, it is recommended that an additional fillet be provided to weld the top flange steel backing bar to the face of the column if the estimated stresses become large (greater than 20 ksi). This minimal retrofit, the removal of backing bar and runoff tabs, or the replacement with higher toughness weld material would result in allowable stresses similar to those reported for the bottom flange.

In addition to the criteria mentioned above regarding allowable stresses on the flange groove welds, design guidelines in Advisory No.1 (68) recommend that an absolute limit on the stress at the face of the column not exceed ninety percent of the minimum specified yield stress of the column. This stress limit appears to have been chosen somewhat arbitrarily, and future research may indicate that this limit can be increased. For the time being, one should use this value as a cap on

the allowable stress in the weld area.

For the replacement of existing welds the following recommendations were developed in Ref. 77. The replacement weld metal provide a minimum specified tensile strength of 70 ksi and a minimum specified CVN value of 20 ft-lb at -20^{o} F. Removal of the existing weld metal is usually accomplished by air carbon arc cutting (arc gouging), or by grinding. One should take care to remove all of the weld metal, while avoiding the removal of excessive base metal from the beam or column, and avoid damaging the column or beam. If the welds are removed by gouging, the gouged surface should be ground to remove any surface material adversely affected by the heat of the gouging operation.

Prior to re-welding, the groove weld joint dimensions should conform to the requirements or be qualified by test as per AWS D1.1-96 (72). The access holes should also be modified prior to welding as needed. The proper size, geometry, and finish of the access holes as required by AWS D1.1-96 (72) will optimize the connection performance through allowing proper access by the welder, minimizing access hole stress concentrations, and minimizing triaxial states of stress.

3) Slab Effects

The presence of the slab affects several aspects of the haunch design, namely the capacity of the section (applied stresses) at both the column face and haunch tip locations, as well as the allowable stresses on the welds. It was found that for a partially composite specimen which had a shear stud capacity in excess of :

$$Q_s \geq 1.3F'_c t_s b_{fc} \qquad (7\text{-}13)$$

where

Q_s= shear stud capacity as defined by the AISC LRFD code

F'_c= compressive strength of concrete slab

t_s= effective thickness of concrete slab

b_{fc}= width of column flange

the expected concrete compressive force was not achieved when Q_s was based on the AISC LRFD code. The shear stud capacity as defined by the AISC LRFD code should be reduced by a factor of 0.65, (see Chapter 5), when designing for cyclic loads in an attempt to prevent the early shear stud fractures which were experienced in this study. This was a tentative recommendation until further research can determine the actual capacity of shear studs. The compressive force in the concrete slab is felt to approach $1.3F'_c t_s b_{fc}$ (61) when the slab becomes fully composite as defined by the AISC LRFD code. In this study, the minimum estimated compressive force in the concrete slab was approximately $0.85F'_c t_s b_{fc}$. These two values are therefore used as boundary compressive forces for calculations, with the most critical results on applied stresses used in design (0.85 factor for design capacity of the section, 1.3 factor for retrofit design evaluation of weld stresses). If the level of composite action is not known, it may be advisable to design the retrofit as both bare steel and composite and provide for the most critical cases.

When accounting for the composite slab in design, the sections must be checked for both composite and bare steel behavior, as the slab would not be effective in the negative bending capacity. Top flange stresses are generally not

critical since the presence of the composite slab would allow full capacity of the beam flange for both the composite and bare steel cases.

The slab effects on allowable weld stresses were discussed in the previous section.

4) Other Factors

A haunch retrofitted structure must meet all appropriate code requirements for strength and stiffness. The strength and stiffness of the beam is increased by a haunch retrofit, so satisfying code requirements under all applicable load combinations including gravity, wind, and any other loads appropriate should not be affected by the retrofit. Overall drift of the structure should also be reduced by the retrofit. However, a haunch retrofitted beam must be checked to ensure that the increase in strength does not change the overall behavior of the structure. This would include checks on the panel zone strength capacity compared to applied forces, checks on strong column-weak beam behavior, requirements on continuity and doubler plates, and supplemental web weld requirements. In addition, it must be checked that the original strength and drift requirements were adequate.

5) Overall Design Method

The design method presented first determines the maximum moment which can be developed at the end of the haunch location. The corresponding moment at the column face is then determined. The haunch section capacity at the column face of the connection can then be determined based on the level of modification to existing welds and haunch dimensions. This capacity must be higher than the applied load.

To start the design process, initial choices for the haunch dimensions should be made in accordance with section 7.B.1. The amount of welding modifications should then be decided upon, which will lead one to allowable weld stresses as determined in section 7.B.2. As a general rule, bottom flange welds can be left in their original state, with backing bars and runoff tabs intact. The same can be said for the top flange welds when a partially composite slab is present which provides the minimal composite action as described in section 7.B.3. A bare steel haunch connection's required top flange modifications will be influenced by the haunch dimensions chosen and subsequent weld stresses. The expected gravity load conditions and the amount of composite action provided by any existing slab should then be evaluated for inclusion in the design calculations.

The following calculations are based on an assumed uniform beam loading w, and a bottom flange haunch only. Calculations for a haunch provided in both the top and bottom flanges would be very similar, and are not specifically covered in this report. Dual haunch retrofits are generally only practical in cases where no composite slab is present, or when severe restrictions on floor clearances limit the dimensions of a bottom flange haunch. It should be mentioned that providing a haunch at the top flange for retrofit construction would require removal of a large portion of the concrete slab around the column, and possibly extend above this slab. It is therefore seen as a very large expense for relatively little benefit as a bottom flange haunch was shown to exhibit excellent behavior in this study when a partially composite slab was present.

The maximum moment developed at the end of the haunch, M_{pd} is found from the following equation.

$$M_{pd}=Z_b F_{ysh} \qquad (7\text{-}14)$$

where:

M_{pd}= design moment at the end of the haunch

Z_b= plastic section modulus of beam section

F_{ysh}= expected strain hardened stress of beam flange as defined in 6.D.2

Note that for a composite section, the previous equation should be modified as per Fig. 7.8, whereby the composite slab force is included in the calculations. For the neutral axis location as shown in the figure

$$Z_{b(composite)}=Z_b-\left(\frac{C_c}{2F_{ysh}t_w}\right)^2 t_w+\frac{C_c\left(d/2+g+t_s/2\right)}{F_{ysh}} \qquad (7\text{-}15)$$

where:

Z_b= Plastic section modulus for full beam cross section (without dogbone reduction)

t_w= thickness of beam web

d= depth of beam

t_s= effective slab thickness

g= gap between beam and effective slab

C_c= compressive force in slab

Assuming a uniform beam loading w (see Fig. 7.6), the moment at the face of the column would be

$$M_f=\left[1+\frac{2a}{L'}\right]M_{pd}+\frac{wLa}{2} \qquad (7\text{-}16)$$

where:

M_f= maximum applied moment at face of column

M_{pd}= design moment at the end of the haunch as defined in Eqn. 7-14

a= distance from face of column to end of haunch

L'= clear beam span minus 2a

L= beam span

w= uniformly distributed gravity load on beam

Note that the gravity load portion of the previous equation is slightly conservative as it assumes all load between the column face and end of the haunch to be acting at the end of the haunch. Loading conditions other than uniformly distributed load can be handled according to the specific load distributions.

The maximum moment to be allowed at the column face may then be assessed.

$$M_c=S_hF_{cr} \qquad (7\text{-}17)$$

where:

M_c= critical moment at the column face

S_h= elastic section modulus of the haunch section at the column face

F_{cr}= critical stress as defined in section 7.B.2

The evaluation of S_h is demonstrated in Fig 7.9. The moment of inertia is calculated in a straightforward manner, although there is some question as to the thickness of the haunch flange in the two dimensional cross section to be

evaluated. The actual projected section on the column face is equal to the thickness of the angle divided by the cosine of the haunch angle, a value in excess of the flange thickness. However, the maximum stress possible in the flange would be limited by the flow of force in the flange longitudinal direction which would correspond to the thickness of the flange. Finally, it could be argued that the maximum stress into the column face is therefore limited by the flange thickness times the cosine of the haunch angle. To simplify the calculation procedure, the nominal flange thickness is used. A separate value of S_h should be calculated for the three weld locations (top beam flange, bottom beam flange, and haunch flange).

When considering a composite connection, the following modification should be made. Due to the lack of data on slab effects the higher slab capacity multiplier of 1.3 will be used in design. The compressive force in the slab should then be taken as $(1.3)F'_c t_s b_{fc}$. Next, a strain diagram as indicated in Fig. 7.10 should be calculated, with the bottom or top strain equal to

$$\varepsilon_{bot\ or\ top} = \frac{F_{cr}}{E_s} \qquad (7\text{-}18)$$

where:

$\varepsilon_{bot\ or\ top}$= attainable strain at the bottom or top extreme fiber of the section

F_{cr}= critical stress at weld section (see section 7.B.2)

E_s= modulus of elasticity of steel

The choice of setting the bottom or top weld stress at this critical value will depend on which location would become critical first. For a given concrete

slab, the bottom fiber would yield first for a smaller beam section since the concrete will have more influence and reduce the top flange strains by a greater amount.

One must then balance forces to get zero axial force in the section and thereby arrive at a strain diagram for the steel section. This is a trial and error procedure, however it can be accomplished quickly through a spreadsheet calculation. If the stress at the opposite extreme fiber from that assumed to be critical is larger than it's critical value, an incorrect assumption as to the first yielding extreme fiber was used. The calculation must be repeated with the other assumption taken.

In order to reach the assumed compressive strains in the concrete, strains at the top of the slab are required to reach values of 0.001 in/in or greater (corresponds to approximately $0.85F'_c$ per Ref. 80). Therefore a check must be made to ensure that $\varepsilon_{top} \geq 0.001$ in/in. Also, a check must be done to ensure that the allowable stresses within the extreme fibers of the section are not exceeded (bottom flange of bottom haunch, both flanges on dual haunch). The equations shown in Fig. 7.10 were based on a neutral axis located in the web of the beam, so a quick check should be made to ensure that this is the case.

It may not be possible to accommodate the slab compression without exceeding the weld allowable stresses. A higher level of weld improvements would then be required at the flange welds. If the allowable stress of the base material (associated with replacement of entire weld with higher toughness material) is not sufficient, it is possible to further improve the capacity through providing a deeper or heavier haunch section. It is also possible to isolate the

composite slab from the column face, as this has been shown to produce behavior corresponding to that of a bare steel specimen (54).

Once it has been determined that the desired weld improvements will provide the capacity of the section at the column face, this moment capacity of the section can then be calculated by summing the moments of all of the section forces, in accordance with Fig. 7.10.

One can then take these defined values for M_c for either a bare steel or composite connection and design a haunch section which will provide a moment capacity of at least M_f while limiting the stresses on the welds to acceptable values. If the welds are overstressed, changes to the haunch dimensions, shape, and weld modifications, or the provision of a top and bottom flange haunch may be used to remedy the situation.

As was detailed in section 6.E, several other factors may improve the overall performance of the connection, such as the beam web connection details, continuity plate details, and panel zone strength. The existing connection details should be considered along with any improvements to these details when assessing the best retrofit solution.

Design examples are included in App. G. The design procedures presented in this section are compared to previous test results in Tables 7.3 and 7.4. Table 7.3 provides information on the specimen properties, while Table 7.4 applies the design method to these sections. All specimens with weld failures are shown to have overstressed welds at those locations and all specimens which failed to reach 0.020 radian of plastic rotation are shown to be inadequate. Successful specimen were shown to be adequate by the design method when

allowable weld stresses were considered, however the restrictions of Ref. 68 would indicate the designs to be inadequate due to overstressing the column in the through thickness direction. For specimens with beam yield stresses approaching those of the columns the designs can be significantly affected by this criteria which does not appear to correlate with test data. In addition, composite specimens which exhibited ideal behavior, (UCSD-NIST2C, HCH2, HCH4), would also have inadequate composite moment capacities at the column face when the through thickness provisions are enforced. The through thickness guidelines therefore appear overly restrictive and should be modified.

C) Limitations of Design Procedures

The design procedures have been developed based on the current testing and previous test data. Unfortunately, the results to date are rather limited, and the majority of tested connections have been designed as new construction. As such, very few incorporate dogbone cutouts in only the bottom flange. There are also very few tests which incorporate a composite or partially composite slab. The allowance of full capacity of top flange welds in a composite design appears to be valid based on these tests, however further testing needs to be done to validate this hypothesis and to obtain a better understanding of the degree of composite action's influence.

As previous testing for new construction indicated, a wide variation in weld modifications may be utilized. This design method has estimated allowable stresses in the cases of several states of modification that were felt to be applicable to repair. Other modifications are still possible (such as high

toughness electrodes with backing bars left in place), but were not covered in this report.

This design method was also predominantly based on specimens made up of very deep steel W shape beams, and jumbo steel W shape columns with strong panel zones. It is felt that the method would be conservative when applied to smaller beam sections, but this should be verified through further testing. The design method is not directly applicable to specimens with weak panel zones. Such candidates for retrofit should be provided with doubler plates to provide strong panel zones if these design methods are to be followed until further research is performed to investigate the influence of a weak panel zone.

D) Other Retrofit Design Approaches

This report and design method has focused on two retrofit methods, the dogbone (or reduced beam section) and haunch. Both of these rely on creating a "fuse" in the beam section which is used to both limit the applied stresses at the column face and to force beam plastic hinging to occur at a point away from the column face and welds.

In addition to these methods, there are many other approaches for addressing the Northridge connection problems.

1) Local Connection Modifications

Several retrofit procedures focus on improving the performance of the individual moment frame connections. In addition to the dogbone or haunch, some have proposed simpler methods, such as simply improving the weld quality through replacing welds with high toughness weld metals with improvements to

the welds (9), or adding weld overlays to minimize the stresses on the original weld (81). These methods have had marginal success, and should be used with caution. They should be avoided in cases where the connection is likely to reach its plastic capacity in a seismic event, or in a structure without a high degree of redundancy.

A more promising method which has had some success in new construction strengthens the beam flanges at the column location through the addition of cover plates. In essence, this is the same concept as the haunch retrofit. However, the haunch is felt to be more applicable to a retrofit design due to its ability to greatly reduce the flange stresses when applied to the bottom flange only. With the increased capacity of the top flange welds when a composite slab is present, it may be possible to provide a reliable retrofit with only the addition of a bottom flange cover plate, but this has not been tested.

Finally, a few more unusual retrofit and new construction designs exist. Some research has attempted to accomplish the same results as a dogbone design by drilling a number of holes in the beam flanges (19), however this appears to lead to stress concentrations that are avoided with a radius cut dogbone design. In addition, the processes of adding side plates, slots in the beam and column webs to "soften" the connection, fin plates, cover plates, or using a fully bolted design have been studied (9,51,52,53).

2) Global Frame Modifications

Another approach to the prevention of the Northridge connection failures would be to reduce the demand on the connections by providing another means of seismic force resistance. This could be accomplished through the addition of

concentric or eccentric bracing, shear walls, or additional moment frame connections. In addition, methods of reducing the seismic load transferred to the structure through such means as base isolation or damping systems may be utilized. All of these approaches would modify the overall structure behavior, and require a complete analysis to evaluate the risk to existing connections.

Chapter 8: Summary and Conclusions

Damage to steel moment resisting frames in the Northridge Earthquake has spurred tremendous interest in a variety of topics related to beam-column connection design and construction. Results of previous tests of pre-Northridge connections, as well as designs to improve these connections for both new and retrofit construction were examined to provided insight into typical steel moment connection problems and possible causes of failures. The major factors involved in the Northridge failures were the use of low toughness welding electrodes, the stress concentrations and general flange overstress present in a typical connection, the influence of leaving steel backing bars in place (leading to stress concentrations, possible weld inclusions, and added difficulty in inspection of welds), and the presence of a composite slab.

Previous studies have led to estimates of compressive forces in a composite slab equal to $1.3F'_c$ times the effective slab area. Testing conducted as part of the SAC initiative (71) could be used as a benchmark of pre-Northridge connection performance. Specimens of similar size were used in the test program reported here.

A) Experimental Program

From the background information, a program consisting of six test specimens was formulated. Dogbone (reduced beam section) and haunch retrofit methods were tested. The effects of a composite slab were also studied. The

performance of the six specimens was discussed in terms of overall behavior and a more detailed analysis of the results.

1) Dogbone

The dogbone design chosen did not perform well in the bare steel specimen. The composite specimen with weld improvements met the project acceptance criteria for total plastic rotation, however there was concern regarding fractures in the welds and the lack of energy dissipation thereafter. In addition, variations in slab details, (such as higher strength concrete, larger percentage of reinforcing steel, change in steel decking orientation, etc.) could result in early weld fractures. Both dogbone specimens failed when beam bottom flange welds fractured. The test program results for the dogbone specimens were inconclusive in the sense that a successful design was not achieved.

2) Haunch

The bare steel haunch sections typically failed by fractures at the top flange welds. With the addition of the composite slab, the haunch retrofitted connections exhibited excellent behavior in all respects. Composite haunch specimen connections formed a plastic hinge at the end of the haunch location, and continued to dissipate large amounts of energy through extensive local and lateral torsional buckling of the beam elements up to the point where the tests were stopped at total plastic rotations exceeding 0.03 radian. Load capacities were diminished at these later stages of loading. For total plastic rotations of 0.02 radian, beam moments exceeded 80 percent of the peak values achieved in the tests. Variations in slab details, (such as higher strength concrete, larger percentage of reinforcing steel, change in steel decking orientation, etc.), would

likely further reduce the top weld stresses and prevent weld fractures.

It was found that the panel zone of haunch specimens acted as a single panel zone with a depth extending from the top beam flange to the haunch flange in the bare steel specimens.

3) Slab Effects

A composite slab was found to influence the behavior of the specimens when shear studs were designed for the expected capacity of the slab, however some questions were raised over the adequacy of the AISC shear stud capacity provisions for purposes of cyclic loads. A tentative reduction factor of 0.65 was recommended for shear stud capacities subjected to cyclic loads. It was found that the slab restricted lateral torsional buckling as well as local buckling at the top flange weld location. This greatly improved the performance of these top welds even when no weld modifications were provided. In addition, a lower bound estimate for the compressive force in the composite slab was obtained which was lower than previously reported values. This lower value should be used when assessing the strength capacity of the section, although a higher value should be used in a retrofit design. The slab also extended the effective panel zone depths.

B) Design Methods

Complete design methods based on previous research as well as the findings of this experimental program were developed for the design of both dogbone and haunch retrofits. Design methods were based on limiting applied stresses at the column face to critical weld stress values which vary depending on

the degree of weld modifications. Allowable weld stresses were based on a survey of 70 previously tested connections of pre-Northridge design.

The design methods for both the dogbone and haunch retrofits were similar. Plastic moment capacities including strain hardening were calculated at the critical section, (center of dogbone or end of haunch). These moments were projected to the column face based on an assumed moment gradient and gravity loading. Stresses applied to the beam flange welds were then calculated based on a simplified elastic analysis and compared with allowable values. Composite slab effects were included in the design methods.

The dogbone design method was evaluated by checking the conformance of 26 previously tested specimens. The design method showed welds to be overstressed for specimens with early weld fractures. Specimens conforming to the design method exhibited acceptable behavior. Some specimens with acceptable behavior required greater flange reductions per the design method. All such specimens were developed and detailed as new construction designs. The conservatism of the design method was felt to be warranted due to detailing of specimens which may not be provided in a retrofit. From the dogbone design method it was ascertained that a bottom flange only dogbone would be expected to perform adequately for only a select number of beam shapes unless a flange reduction greater than 50 percent was provided. Top and bottom flange reductions would generally be much more effective, although this may be an expensive process in the case of a retrofit. The presence of a composite slab can greatly influence the amount of flange reduction required and should be considered in both retrofit and new designs.

The haunch design method was evaluated by checking the conformance of 19 previously tested specimens. The design method accurately predicted experimental performance.

In cases where the beam yield stress approached that of the column, column through thickness requirements (from Ref. 68) would limit the range of acceptable designs. From all referenced experimental data, these provisions appear to be overly restrictive and should be re-evaluated.

It is felt that the design model is an effective tool for retrofitting existing connections and could also be applied to the design of new connections. The straightforward technique relies on standard design equations, is easy to apply, and was shown to match existing test data. The methods have the capability to account for a composite slab.

C) Final Remarks and Future Research Needs

Through this experimental test program, analytical interpretation of the results, and development of design procedures, an advancement in the understanding of steel moment frame connections was obtained. It is hoped that knowledge acquired from this and related projects will provide a means of ensuring the safety of existing as well as new buildings in seismically active areas. A better understanding of steel moment resisting frames is needed to restore the confidence of engineers and the general public in such structures.

Several aspects of connection behavior need further investigation. The capacity of shear studs under cyclic loads should be re-evaluated in light of the shear stud failures experienced in this program. In addition, there is still

uncertainty regarding the compressive capacity of the composite slab, and how slab continuity in an actual building would affect this capacity. In order for a bottom flange only dogbone design to be effective, the effects of flange reductions exceeding 50 percent need to be evaluated. A successful design of a bottom flange dogbone has not been tested to date. Prior to the use of this retrofit technique in an actual building, such “proof-of-design” is needed.

Appendix A: Weld Procedures and Fabrication Sequence

This appendix provides detailed information on the fabrication procedure used for specimens tested in this study. General procedures followed were developed in Ref. 10 as part of the SAC initiative. Details of the Pre-Northridge connection, dogbone retrofits, and haunch retrofits are found in Figures 3.3, 3.4, and 3.5 respectively. Ultrasonic test reports for the specimens are presented in Appendix D.

A) SPECIFIED FABRICATION DETAILS

General Notes:

1. All steel A36, unless noted otherwise.
2. All welding shall be in conformance with AWS D.1.1-94.
3. Web bolts shall be installed in conformance with "Specification for Structural Joints Using ASTM A325 or A490 Bolts." Bolts shall be tightened using the turn-of-nut method.
4. All "field" welds shall be made with the specimen in an upright position to simulate field welding positions.
5. Beam flange groove welds shall be made using backup bars and weld tabs. The backup bars and weld tabs shall extend 2 inches beyond the edge of the beam flange. Tack welds for the backup bars shall be made inside the groove only. Backup bars and weld tabs shall not be removed after welding, unless specified.
6. All welders, welding operators, and tack welders shall be qualified by test for the types of welds they will be required to make, including the process, position, and thickness of material used, per AWS D1.1-94.

Connection Fabrication Sequence for Pre-Northridge Connections (see Fig. A.1)

1. Weld shear tab to column (by fabricator).
2. Attach beam to shear tab with bolts. Fully tension all web bolts using turn-of-nut method.
3. Weld the beam top flange to the column flange.
4. Weld the beam bottom flange to the column flange. Alternate weld layers from one side of the web to the other until the weld is complete.

Connection Fabrication Sequence for Haunch Retrofit (See Fig. A.2)

1) Prepare haunch per drawing (Fig. A.3)
2) Install haunch, and tack weld in place. Install weld tabs.
3) Weld the haunch in the following sequence:
    a. Weld haunch flange to column flange.
    b. Weld haunch flange to beam flange.
    c. Fillet weld haunch web to column flange.
    d. Fillet weld haunch web to beam flange.
    e. Remove weld tabs and grind surface smooth. Inspect ground surfaces for discontinuities. Inclusions 1/16" or less in depth shall be removed by grinding. Deeper indications shall be removed and repaired by welding.
4) Install long vertical stiffeners in beam. The corners of the stiffeners should contain a snipe to eliminate welding in the K region.
5) Weld stiffeners to beam. Weld stiffeners to bottom beam flange first, then make longitudinal welds.

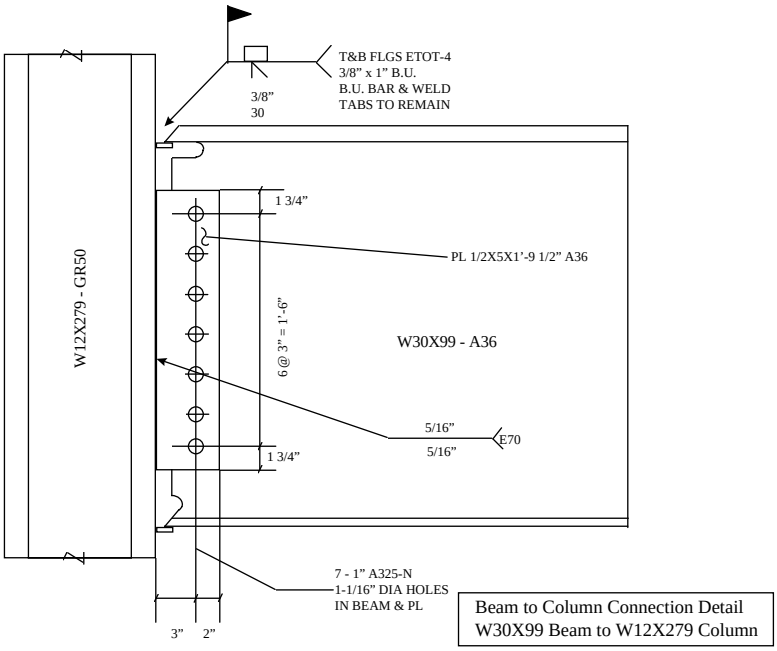

Figure A.1 - Beam to Column Weld Details

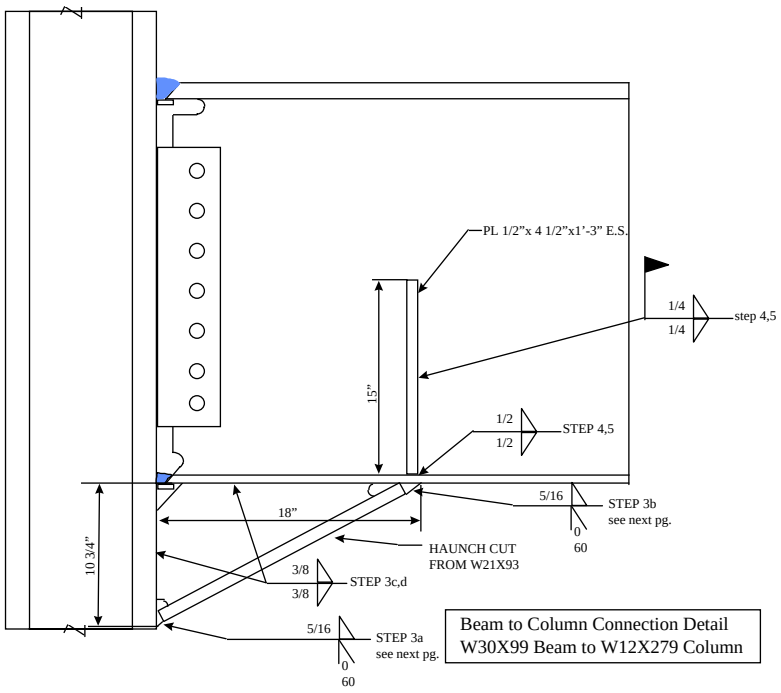

Figure A.2 - Haunch Weld Details

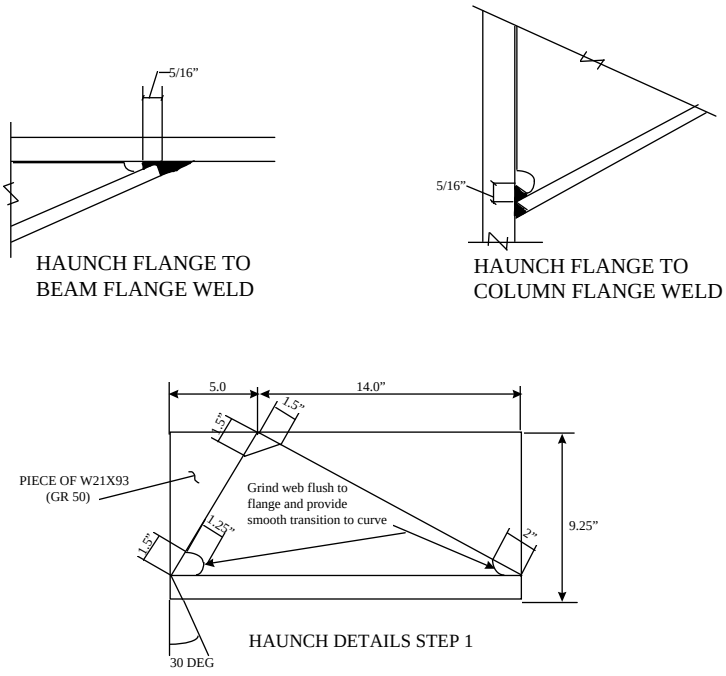

Figure A.3- Haunch Details

Appendix B: Connection Design Calculation

This appendix includes the calculations which were completed to size the specimens and design the pre-Northridge, unretrofitted connection.

A) Beam Capacity

The overall specimen layout can be seen in Fig. B.1. Beam capacity was based on both nominal strengths as well as estimated actual strengths. Beams were selected as W30X99 Gr. A36 material.

Nominal properties:

F_y= 36 ksi

$M_p = Z_x(F_y) = 312(36) = 11232$ kip-in

Estimated properties:

Assume strain hardening factor of 1.1.

F_{ye}= 50 ksi

$M_p = 1.1Z_x(F_y) = 1.1(312)(50) = 17160$ kip-in

Composite capacity in positive moment:

Assume $M_{pCe} = 1.3M_{pe} = 1.3(17160) = 22308$ kip-in

Composite capacity in negative moment:

Assume equal to M_{pe} (no tensile slab contribution)

From Fig. B.2, assume values for L_1

Nominal section: take $L_1 = d_c/2$

Haunch section: take $L_1 = (d_c/2)+a$

where a= Length of haunch

Dogbone section: take $L_1=(d_c/2)+s_c$

where s_c= Distance from face of column to center of dogbone

Then, $L_2=144-L_1$

From virtual work:

$W_{int}= M_{p+}(\theta(1+L_1/L_2)) +M_{p-}(\theta(1+L_1/L_2))$

$W_{ext}= F\theta(144)$

therefore:

$F\theta(144)= (M_{p+}+M_{p-})(\theta(1+L_1/L_2))$

$F=(M_{p+}+M_{p-})(1+L_1/L_2)/144$

Maximum column tip force will be for the composite haunch specimen,

Here:

M_{pe+}= 17160 kip-in

M_{pe-}= 22308 kip-in

L_1= 28 in

L_2= 116 in

then F= 340 kip

B) Column Design

Provide $\Sigma Z_{col} > \Sigma Z_{beam}$ $\therefore$ $Z_{col} > 312in3$

Panel Zone

$$V_{max}= \frac{\Sigma M_{pbeam}}{.95d_b} - \frac{\Sigma M_{pbeam}}{H} = \frac{M}{d} - \frac{M}{H} = V_{beam} - V_{col}$$

$$= \left[\frac{17160}{.95(29.65)} - \frac{17160}{144} \right] 2 = 980 \text{ kips estimated for bare steel sections}$$

$$980\left(\frac{11232}{17160}\right) = 642\text{K nominal}$$

Provide:

$.55F_y d_c t_w > V_{max}$(nominal)

then:

$$d_c t_w > \frac{642}{.55(50)} = 23.3 \text{ in2}$$

try W12x279

$d_c t_w = 15.85(1.530) = 24.25 > 23.3$ OK

note that actual F= $\frac{980}{.55(50)} = 35.6 \text{in}^2$

yield probable with expected overstrength in beams

Check strong column/weak beam

$$\Sigma M_f = (22308+17160)\left(\frac{144-8}{144-8-20}\right) = 46{,}273\text{K”}$$

ΣM_{pcol}= 2(481) 50= 48,100K” > 46,273K” OK

C) Connection Design

Beam = W30x99 (A36)

Column = W12x279 (A572 GR50)

Assumptions

$M_{max}= M_p(beam) = Z_b(36)$

$V_{max}= \frac{2M_p}{L}$ use L= 288 in

$M_p= 312(36)= 11{,}232K"$

$V_{max}= \frac{2M_p}{L} = \frac{2(11{,}232)}{12(24)} =78K$

Web Bolts

Use 1"-A325-N with 3"c-c

Assume bolts carry all shear

From Table 1-D V_{bolt}= 16.5 k/bolt (AISC 8th ed.)

From Table I-E $V_{bearing}$ =36.3k/bolt w/1/2"+ shear tab (AISC 8th ed.)

Base bolt strength on 1.7 f_{allow}

bolts= $\frac{78}{1.7(16.5)}$ = 3 bolts

Use more typical 7-1" A325-N 3" c-c

Shear Tab

Use A36

From Table 1.16.5.1 min edge d=1.75" (AISC 8th ed.)

total h= 6(3) +2(1.75)= 21.5"

Assume w= 5" >1.75" each side, OK

Use 0.5" minimum thickness (bearing calculations based on this)

F_v(gross)= .4(36)21.5(t)= 155K >78K

F_v(net)= .4(58)(21.5-7(1.0625))t= 163K >78K

Use plate ½" x 5" x 21.5" A36 material

Shear tab - Column weld

V= 78K M= 78(3)= 234K"

From table XIX $\ell = 21.5"$ P = 78K $a\ell = 3" \therefore a = 0.14$ and k = 0

C_1=1.0 C=1.53

$$\therefore D = \frac{P}{CC_1\ell} = \frac{78}{1.53(1)21.5} = 2.37$$

3/16"weld required

Minimum weld size= 5/16"

Use 5/16" fillet welds

Continuity Plates

$$A_{st} = \frac{Pb_f - F_{yc}t(t_b + 5K)}{F_{yst}} \quad (1.15\text{-}1)$$

F_{yc}= 50 F_{yst}= 36 K=3.1875" P_{bf}= 5/3(10.45).67(36)=420.1K

t= 1.530" t_b=.670"

$A_{st}=\frac{420.1-50(1.530)(.670+5(3.1875))}{36}=$ -23.6 None req'd.

d_c=15.85-2(2.470)=10.91"

Per (1.15-2) $\frac{4100t^3\sqrt{F_{yc}}}{P_{bf}}=\frac{4100(1.530)^3\sqrt{50}}{420.1}=$ 247" >10.91 None req'd.

Per (1.15-3) $\frac{.4\sqrt{P_{bf}}}{F_{yc}}=.4\sqrt{\frac{420.1}{50}}=$ 1.16" < t_f= 2.470 None req'd.

No continuity plates required.

D) Shear Stud Design

Base shear stud design on composite section requirements of AISC LRFD code, Chapter I. Assume the use of 3/4" by 5-1/4" long shear studs.

Stud Capacity:

$Q_n= R_{md}(.5)\ A_{sc}\sqrt{F'_cE_c}\ \leq A_{sc}F_y$

where:

$R_{md}=\frac{.85}{\sqrt{N_r}}\left(\frac{w_r}{h_r}\right)\left[\left(\frac{H_s}{h_r}\right)-1\right]\leq 1$

and N_r=1, $W_r\approx$4.75", h_r= 3", H_s =5 1/2"

then:

$R_{md}= .85\left(\frac{4.75}{3}\right)\left[\frac{51/2}{3}-1\right]=1.12$

therefore:

Q_n= 21.9 K from table 5-1, 4 ksi concrete, w=115 lbs/ft3

Shear Forces:

F_{studs}= smaller of F_yA_s or $.85F'_ct_sb_{eff}$

$F_y A_s$= 29.1(36)= 1048K

F_{stud}=.85F'$_c t_s b_{eff}$= .85(4) 3.25 (72)= 796K

where b_{eff}= smaller of:

2 (24/8) = 6 feet - controls

24/2=12 feet

8 feet

Number Required

For fully composite design,

studs= F_{stud}/Q_n

=796/21.9= 37

37 shear studs required for fully composite gravity load

However, this was based on the gravity load requirements, with a six foot wide composite slab. Actually, the slab forces expected due to lateral loads are much smaller. The slab could be considered fully composite for lateral loads when studs are provided to resist the following:

P_{slab}= 1.3F'$_c(t_s)b_{cf}$=1.3(4)3.25(13.14)= 222K

$\frac{222\text{kips}}{21.9\text{kips/stud}}$ = 11 required for lateral loads

12 shear studs provided

$\frac{12(21.9)}{796}$ = 33 percent composite

Appendix C: Dogbone Design Calculation

The calculations which were performed to size the dogbone flange reduction cutouts in this project are provided here. These were based on new construction design methods which were being developed at the time. *These do not represent a successful design, do not follow the design methods of Chapter 7, and are not recommended for use.* They are provided for reference only. See Chapter 7 and the definitions of symbols list for further information.

First pick dogbone dimensions:

Suggested values:

$a = \frac{b_f}{2}$ to $\frac{3b_f}{4}$ = 5.2" to 7.8"

$b = \frac{2d}{3}$ to $\frac{3d}{4}$ = 19.8" to 22.2"

Assume a= 5" b=20"

Then s_c=15"

From these dimensions, and the dimension L_b=136"

$$M_f = \left(1+\frac{2a}{L'}\right)M_{pd} = \left(1+\frac{2(15)}{242}\right)M_{pd} = 1.12M_{pd}$$

Next, calculate M_{pd}

Assume $M_{pd} = 1.1Z_{RBS}F_y$ (including strain hardening)

$M_f = 1.1(1.12)Z_{RBS}Fy = 1.232Z_{RBS}F_y$

Limit M_f to M_c

Previously, M_c (limiting moment at the column face) was based on a fraction of M_p of the section at the column face. Previous designs for new construction had been successful limiting M_c to about $0.85M_p$. It was unknown whether higher allowable values could be utilized.

therefore:

$$\frac{Z_b}{Z_{RBS}} > 1.228 \text{ since } M_c < Z_b F_y$$

Note: $M_y = 269F_y$

$M_p = 312F_y$

$M_y/M_p = 0.86$

A decision was made that a bottom flange only reduction of no more than 50 percent would be used. Based on this criteria,

$$Z_{RBS} = Z_b - \frac{(ct_f)^2}{t_w} - ct_f(d-t_f)$$

$$= 312 - \frac{(2.6875(.670))^2}{.520} - 2.6875(.670)(29.65 - .670) = 254 \text{ in}^3$$

Then:

$$\frac{Z_b}{Z_{RBS}} = \frac{312}{254} = 1.23$$

This ratio just barely exceeded the required ratio of 1.228 and was deemed acceptable. It was thought that it might be possible to prevent weld fractures by merely preventing the moment from exceeding M_p at the column face while allowing the dogbone section to strain harden.

Cutout dimension c=2.6875 was used for design.

Appendix D: Ultrasonic Testing Reports

This appendix provides copies of all reports for ultrasonic testing conducted on the specimens. The flange groove welds of the 6 Pre-Northridge specimens were ultrasonically tested by a certified non-destructive testing company. The acceptance criteria was based on Table 8.2 of AWS d1.1-94. All ultrasonic testing and reports were completed by ASNT Level II qualified inspectors. The tests were conducted at the Ferguson Structural Engineering Laboratory at the University of Texas at Austin.

A) Interpreting the Ultrasonic Test Reports

The interpretation of the ultrasonic test reports requires the location of the defined "X" and "Y" lines and the location of the "A" surface. For this report:

- The "X" line runs parallel to the weld axes, and falls on the outside face of the column flange.
- The "Y" line runs perpendicular to the weld axes, and falls on the left hand edge of the beam flange when facing the column.
- The "A" surface is the top face of the beam flange under consideration.

The important/relevant rows in these test reports are (from top to bottom)

- Weld Identification: what specimen is being tested
- Weld number and location: weld location and indication number (1,2,3...)

- Length: length of discontinuity
- Depth “A” Surface: depth of discontinuity from the “A” surface
- Distance from “X”: location of discontinuity with respect to “X” line
- Distance from “Y”: location of discontinuity with respect to “Y” line
- Discontinuity Evaluation: discontinuity severity class based on ASW D1.1-94 Table 8.2 These are:

  Class A - large discontinuities- all rejectable

  Class B - medium discontinuities - rejectable based on length and location

  Class C - small discontinuities - rejectable based on length and location

  Class D - minor discontinuities - all acceptable regardless of length or location
- Remarks: classification as a rejectable or acceptable discontinuity

B) Comments on Results

Dogbone specimens had their top and bottom beam flange to column flange groove welds tested. Specimen DB2 had the original E70T-4 welds removed and replaced with E71T-8 welds (see Chapter 3), and inspections were only conducted on the final welds. It can be seen that all welds were acceptable on specimen DB1. Two reports are included for specimen DB2 are included, as welds were repaired until inspections showed there to be no remaining rejectable flaws. The first inspection (3-17-97) contained 3 rejectable flaws in the south beam bottom flange weld and one in the north beam bottom flange weld. These were repaired and a second inspection (4-11-97) showed that one of the flaws was

not completely repaired. After a second repair a third ultrasonic test showed the welds to be acceptable (no weld inspection provided).

Although specimens HCH1 and HCH2 contained rejectable flaws, the connections were left as is. It was felt that repairs of the welds could significantly alter the material properties at the weld areas, and it was desired to keep the connection as close as possible to that which would be found in an existing building. It was also felt that an existing building may include weld flaws.

Specimen HCH1 (8-30-96) was reported to have five rejectable flaws in its north beam bottom flange weld, two in its south beam top flange weld, and four in its south beam bottom flange weld. A follow up test was conducted after the welding of the haunch (9-12-96), which reported one new additional flaw in the south beam bottom beam flange weld. In addition, due to the weld process, the haunch flange welds were shown to have defects running the length of the weld. It was realized that these were just indications of the discontinuity between the two welds made at each location, which would be expected from the weld detail. This was acceptable, and later haunch welds were not tested.

Specimen HCH2 was only tested after the haunches were welded in place (10-3-96). The north beam bottom flange, south beam top flange, and south beam bottom flange welds each were reported to contain one rejectable flaw.

Several weld inspection reports are shown for each of specimens HCH3 and HCH4. These specimen's top flange welds were repaired and re-tested until the welds were acceptable. Bottom flange welds were presumed to be protected against fracture by the addition of the haunches, and were therefore left as is. Specimen HCH3 therefore contained four rejectable flaws in its north beam

bottom weld and one in its south beam bottom weld (6-17-97). Specimen HCH4 was reported to contain two rejectable flaws in the north beam bottom flange (9-4-97).

Appendix E: Data Reduction Procedures for Calculation of Specimen Deformations

Data reduction procedures are included in this section. First, the overall rotations of Chapter 4 are discussed. Then the decomposition of data is performed to provide the results presented in Chapter 5.

A list of symbols is presented in the glossary.

A) Chapter 4 Calculations

Total rotations as reported in Chapter 4 consist of taking the measured column tip deflection, and dividing by the column height H (144 in.). This measurement is actually a measure of drift ratio, except that it is not multiplied by 100. This is a generally accepted definition of total rotation which has been used as a comparison with other studies as well as a measure for general acceptance criteria.

Calculations of total plastic rotations referenced to the north and south beams were found by plotting the total plastic rotations versus the reaction at the end of the north or south beam respectively. The elastic portion of these plots are then subtracted from the plot

$\theta_{totp}=\theta_{tot}-\theta_{tote}$ where $\theta_{tote}=M/k_e$

k_e= slope of elastic portion of the Moment-θ_{tot} plot

These rotations still correspond to column tip displacements divided by the story height.

B) Chapter 5 Calculations

The calculations in Chapter 5 are based on a more detailed analysis of measured deformations. These results are decomposed into deformations taking place in the panel zone, column, and beams.

Panel Zone Deformations

Panel zone deformations were measured with potentiometers which measured changes in lengths of the panel zone diagonals. These are represented by δ_3 and δ_4. From the geometry shown in Fig. E.1, the following calculations can be derived.

Let $d_1=\sqrt{a^2+b^2}+\delta_4$ where δ_4= negative value

Let $d_2=\sqrt{a^2+b^2}+\delta_3$ where δ_3= positive value

Where $d_1=\sqrt{a^2+b^2-2ab(\cos\phi)}$

$d_2=\sqrt{a^2+b^2+2ab(\cos\phi)}$

a= lateral distance between measurement points for δ_3

b= vertical (undeformed section) distance between measurement points for δ_3

Define $\tan\gamma=\cos\phi$

for small angles of rotation, $\tan\gamma=\gamma$

Then: δ_4= 2 in. potentiometer reading= $\sqrt{a^2+b^2-2ab\gamma}-\sqrt{a^2+b^2}$

$$\sqrt{a^2+b^2}+\delta_4=\sqrt{a^2+b^2-2ab\gamma}$$

Square both sides

$$a^2+b^2+2\delta_4\sqrt{a^2+b^2}+\delta_4{}^2=a^2+b^2-2ab\gamma$$

$$\gamma = \frac{\delta_4{}^2 + 2\delta_4\sqrt{a^2 + b^2}}{-2ab}$$

Similarly: δ_3= 2 in. potentiometer reading= $\sqrt{a^2 + b^2 + 2ab\gamma} - \sqrt{a^2 + b^2}$

$$\sqrt{a^2 + b^2} + \delta_3 = \sqrt{a^2 + b^2 + 2ab\gamma}$$

Square both sides

$$a^2 + b^2 + 2\delta_3\sqrt{a^2 + b^2} + \delta_3{}^2 = a^2 + b^2 + 2ab\gamma$$

$$\gamma = \frac{\delta_3{}^2 + 2\delta_3\sqrt{a^2 + b^2}}{2ab}$$

Average the two values, then:

$$\gamma = \frac{\delta_3{}^2 - \delta_4{}^2 + 2\sqrt{a^2 + b^2}(\delta_3 - \delta_4)}{4ab} = \frac{\delta_3{}^2 - \delta_4{}^2}{4ab} + \frac{\sqrt{a^2 + b^2}(\delta_3 - \delta_4)}{2ab}$$

Influence of Panel Zone Deformation on Specimen Displacements and Rotations

Once the panel zone deformation, γ, has been calculated, its effect on total connection rotation and column tip deflection can be determined.

First, were there no restraints on the specimen, the panel zone deformations would deform the overall specimen as in Fig. E.2. Here:

L_b=distance from end of beam to column face

d_b= panel zone depth

d_c= column depth

H= story height

Beam end restraints require the vertical displacements at the ends of the beams to be equal to zero (δ_b tip= 0).

Therefore, rotate entire system by $\frac{\gamma L_b}{L_b + d_c/2} = \tan\alpha$ as shown in Fig. E.3.

Check Beam end vertical displacement = $\gamma d_b - (\frac{\gamma L_b}{L_b + d_c/2}(L_b + d_c/2)) = 0 \leftarrow$yes

As indicated in Fig. E.3, the column tip lateral displacement due to shear deformations is therefore the sum of the panel zone deformations acting over the depth of the panel zone plus the overall specimen rotation to meet end conditions multiplied times the column height, or:

$$\delta_{cpz} = \gamma d_b - \frac{\gamma L_b}{L_b + d_c/2}(H)$$

The rotation of the connection due to the panel zone deformations was indicated in Fig. E.3, and is equal to the rotation required to meet the end constraints:

$$\text{Rotation } \theta_{pz} = \text{Tan}^{-1}\left[\frac{\gamma L_b}{L_b + d_c/2}\right]$$

Beam Deformations

Beam deformations are indicated in Fig. E.4. Here:

H= story height

θ_b= connection rotations due to beam deformations =

δ_{cb}= column tip lateral displacement due to beam deformations = $\theta_b H$

Column Deformations

Column deformations are indicated in Fig. E.5. Here:

δ_{cc}= Tip of column lateral displacement

Note that connection rotations due to column deformations are equal to zero.

Total Rotations

Rotational components for the connection (θ_{con}= total rotation of the connection) can then be calculated as follows:

$$\Sigma\theta_{con} = \theta_{pz}+\theta_b = -\mathrm{Tan}^{-1}\left[\frac{\gamma L_b}{L_b + d_c/2}\right] + \theta_b$$

Solve for θ_b (use average of all rotation gage readings= θ_{con})

$$\theta_b = \left[\theta_{con} + \mathrm{Tan}^{-1}\left(\frac{\gamma L_b}{L_b + d_c/2}\right)\right]\frac{\pi}{180} \text{ radian}$$

θ_b= connection rotation due to beam deformations

Total Column Tip Displacement

Next, components of the column tip deflection (δ_{ctot}) due to the panel zone, beam, and column deformations can be calculated.

$\delta_{ctot}=\delta_{cb}+\delta_{pz}+\delta_{cc}$

$$= \gamma d_b - \left(\frac{\gamma L_b}{L_b + d_c/2}\right)H + \theta_c H + \delta_c$$

set δ_{ctot}= average of 25 in. displacement transducer readings at column tip, then:

$$\delta_{cc} = d_{ctot} - \gamma d_b + \left(\frac{\gamma L_b}{L_b + d_c/2}\right)H - \theta_c H$$

δ_{cc}= column tip deflection due to column deformations

Plastic Rotations

To obtain plastic deformations utilize:

Panel Zone:

$\gamma_p=\gamma-\gamma_e$ where $\gamma_e=M/k_e$

k_e= slope of elastic portion of the Moment-γ plot

$$\theta_\gamma = -\mathrm{Tan}^{-1}\left(\frac{\gamma L_b}{L_b + d_c/2}\right)$$

$\theta_{\gamma p}=\theta_\gamma-\theta_{\gamma e}$ where $\theta_{\gamma e}=M/k_e$

k_e= slope of elastic portion of the Moment-θ_γ plot

Beam:

θ_b

$\theta_{bp}=\theta_b-\theta_{be}$ where $\theta_{be}=M/k_e$

k_e= slope of elastic portion of the Moment-θ_b plot

Note that one can calculate a "column rotation" θ_c by dividing the column deformation contribution of column tip displacement by the column height H, but this would not be a component of the connection rotation as has been defined here, and these have not been reported.

Then:

$$\theta_c = \frac{\delta_c}{H - d_b}$$

$\theta_{cp}=\theta_c-\theta_{ce}$ where $\theta_{ce}=M/k_e$

k_e= slope of elastic portion of the Force-θ_c plot

Similarly, total specimen rotations of Chapter 4 (θ_{tot}) can be broken into components due to the beam, column, and panel zone and are sometimes reported. These are no different than the components of column tip deflection of Chapter 5 (δ_{cc}, δ_{db}, δ_{cpz}) divided by the story height. In general, these are not felt by the

author to be as informative as the connection rotations reported in Chapter 5 in regards to demand on the connection (Note that the beam contribution would be similar in both instances). Due to the concentration of inelastic deformations in the beam sections of the specimens in this study, the differences between the two methods of referencing rotations are minimal for this study.

Haunch Calculations:

When determining the deflections and rotations for the haunch specimens, calculation would be identical to those shown, but would utilize the average of the 2 panel zones (beam and haunch) i.e.:

Calculate panel zone strain angles individually for the individually instrumented beam panel zone(γ_b) and haunch panel zone (γ_h), using the individual panel zone depths for d_b.

Then:

$$\gamma_{Avg} = \frac{\gamma_b d + \gamma_h d_h}{d + d_h}$$

Replace all γ in the above calculations with γ_{Avg}, and note that d_b is now equal to the total panel zone depth ($d+d_h$)

Appendix F: Dogbone Design Calculation Examples

A dogbone design will be carried out for both bare steel, and composite sections. These will include both bottom flange only reductions as well as top and bottom flange reductions. Results were consolidated in Table 7.1.

A) Example 1 - Bare Steel, Bottom Flange Dogbone

Beam = W30X99 (A36) Column = W12X279 (A572 Gr50)

Bare Steel Specimen

Pick the dogbone a and b dimensions

a= (0.5 to 0.75)b_f = 5.22 to 7.84 in. Use a= 5.25 in.

b= (0.65 to 0.85)d= 19.27 to 25.20 in. Use b=19.50 in.

Therefore s_c= 5.25+19.50/2= 15 in. (Similar to tested specimens)

Assume measured F_{yb}=45.0 ksi, F_{yc}=52.0 ksi

F_{ye}= F_{yb}= 45.0 ksi

F_{ysh}= 1.1F_{ye}= 49.5 ksi

Assume full weld replacement with moderate toughness material, therefore allowable weld stresses are

F_{cr}= F_{ye}= 45.0 ksi

Column limiting stress =0.9F_{yc} = 0.9(52)= 46.8 ksi>45.0 ksi

Determine yield capacity at column face

M_c= $S_b F_{cr}$= 269(45.0)= 12105 kip-in.

Assume L=288 in.

L'= L-d_c-2s_c= 288-15.85-2(15)= 242 in.

Assume no gravity loading

Therefore

$$M_f=\left[1+\frac{2s_c}{L'}\right]M_{pd}+\frac{wLs_c}{2}=\left[1+\frac{2(15)}{242}\right]M_{pd}+0$$

M_f= 1.12M_{pd}

Since M_f must be limited to M_c, set these values equal to each other.

$$M_{pd}=\frac{M_c}{1.12}=\frac{12105}{1.12}=10800 \text{ kip-in.}$$

For a bottom flange only dogbone

$$M_{pd}=Z_{RBS}F_{ysh}=\left[Z_B-\frac{(ct_f)^2}{t_w}-ct_f(d-t_f)\right]F_{ysh}<10800$$

$$=\left[312-\frac{(0.670c)^2}{0.520}-0.670(29.65-0.670)c\right]49.5<10800$$

Solving for the minimum value of c

c= 4.09 in., or a 78 percent flange reduction.

This percentage reduction is in excess of the 55 percent which has been tested to date, therefore it is not an acceptable design. Since the maximum allowable weld stresses were allowed (assumed full weld replacements), a bottom flange reduction only would not be acceptable.

B) Example 2 - Bare Steel, Top and Bottom Flange Dogbone

Beam = W30X99 (A36) Column = W12X279 (A572 Gr50)

Bare Steel Specimen

Pick the dogbone a and b dimensions

a= (0.5 to 0.75)b_f = 5.22 to 7.84 in. Use a= 5.25 in.

b= (0.65 to 0.85)d= 19.27 to 25.20 in. Use b=19.50 in.

Therefore s_c= 5.25+19.50/2= 15 in. (Similar to tested specimens)

Assume measured F_{yb}=45.0 ksi, F_{yc}=52.0 ksi

F_{ye}= F_{yb}= 45.0 ksi

F_{ysh}= 1.1F_{ye}= 49.5 ksi

Assume removal of backing bar at bottom flange, no modification to top flange, therefore allowable weld stresses are

Top flange F_{cr}= 30.0 ksi

Bottom flange F_{cr}= 32.0 ksi

Note that the bottom weld modification does not affect the capacity as the top weld critical stress will be reached first.

Column limiting stress =0.9F_{yc} = 0.9(52)= 46.8 ksi>30.0 ksi

Determine yield capacity at column face

M_c= $S_b F_{cr}$= 269(30.0)= 8070 kip-in.

Assume L=288 in.

L'= L-d_c-2s_c= 288-15.85-2(15)= 242 in.

Assume no gravity loading

Therefore

$$M_f=\left[1+\frac{2s_c}{L'}\right]M_{pd}+\frac{wLs_c}{2}=\left[1+\frac{2(15)}{242}\right]M_{pd}+0$$

M_f= 1.12M_{pd}

Since M_f must be limited to M_c, set these values equal to each other.

$$M_{pd}=\frac{M_c}{1.12}=\frac{8070}{1.12}=7205 \text{ kip-in.}$$

For a top and bottom flange dogbone

$M_{pd}= Z_{RBS}F_{ysh}= Z_B-2ct_f(d-t_f)< 7205$

$= (312-2(0.670)c(29.65-0.670))49.5< 7205$

Solving for the minimum value of c

c= 4.29 in., or a 82 percent flange reduction.

This percentage reduction is in excess of the 55 percent which has been tested to date, therefore it is not an acceptable design. This value of c would be reduced to 2.41 inches, (46 percent flange reduction), if maximum allowable weld stresses were allowed, (full weld replacements). Therefore, an acceptable design is possible when greater modifications to the welds are performed.

C) Example 3 - Composite, Bottom Flange Dogbone

Beam = W30X191 (A36) Column = W14X311 (A572 Gr50)

Composite Specimen

Assume slab similar to those tested

t_s= 3.25 inches g= 3 in. F'_c= 4000 psi

Then, $C_c=1.3F'_cb_{fc}t_s=1.3(4)16.23(3.25)=274$ kip

Pick the dogbone a and b dimensions

a= (0.5 to 0.75)b_f = 7.52 to 11.28 in. Use a= 8 in.

b= (0.65 to 0.85)d= 19.94 to 26.08 in. Use b= 22 in.

Therefore s_c= 8+22/2= 19 in.

Assume measured F_{yb}=45.0 ksi, F_{yc}=52.0 ksi

$F_{ye}= F_{yb}$= 45.0 ksi

F_{ysh}= 1.1F_{ye}= 49.5 ksi

Assume full weld replacement with moderate toughness material at bottom flange, no weld modification at top flange, therefore allowable weld stresses are

Top F_{cr}= F_{ye}= 45.0 ksi (slab presence allows full base metal capacity)

Bottom F_{cr}= F_{ye}= 45.0 ksi

Column limiting stress =0.9F_{yc} = 0.9(52)= 46.8 ksi>45.0 ksi

Determine capacity at column face

First, assume that the top flange is critical.

F_{top}= 45.0 ksi and ε_{top}=0.00155

Then, balancing forces,

F_{bot}= 54.8 ksi and ε_{bot}=0.00191

This value of F_{bot} exceeds the allowable stress of 45.0 ksi, so the wrong assumption was made.

Assume that the bottom flange is critical.

F_{bot}= 45.0 ksi and ε_{bot}=0.00155

Then, balancing forces,

F_{top}= 35.1 ksi and ε_{top}=0.00121

The associated moment capacity with this strain distribution is

M_c= 29240 kip in.

Assume L=288 in.

L'= L-d_c-2s_c= 288-17.12-2(19)= 233 in.

Assume no gravity loading

Therefore

$$M_f=\left[1+\frac{2s_c}{L'}\right]M_{pd}+\frac{wLs_c}{2}=\left[1+\frac{2(19)}{233}\right]M_{pd}+0$$

$M_f= 1.16M_{pd}$

Since M_f must be limited to M_c, set these values equal to each other.

$$M_{pd}=\frac{M_c}{1.16}=\frac{29240}{1.16}=25210 \text{ kip-in.}$$

For a bottom flange only dogbone

$$Z_{RBS(composite)}= Z_b-\left(\frac{\left(C_c+2F_{ysh}ct_f\right)}{2F_{ysh}t_w}\right)^2 t_w - ct_f\left(d-t_f\right)+\frac{C_c\left(d/2+g+t_s/2\right)}{F_{ysh}}$$

$$= 673-\left(\frac{\left(274+2(49.5)c(1.185)\right)}{2(49.5)0.71}\right)^2 0.710 -$$

$$1.185c\left(30.68-1.185\right)+\frac{274\left(15.37+3+1.625\right)}{49.5}$$

$M_{pd}= Z_{RBS(composite)}F_{ysh}= <25210$

$$= \left[673-\frac{(274+117.3c)^2}{6959}-34.0c+110.7\right]49.5 <25210$$

Solving for the minimum value of c

c= 4.97 in., or a 66 percent flange reduction.

This percentage reduction is in excess of the 55 percent which has been tested to date, therefore it is not an acceptable design. Since the maximum allowable weld stresses were allowed (assumed full weld replacement at bottom flange), a bottom flange reduction only would not be acceptable.

D) Example 4 - Composite, Top and Bottom Flange Dogbone

Beam = W30X191 (A36) Column = W14X311 (A572 Gr50)

Composite Specimen

Assume slab similar to those tested

t_s= 3.25 inches g= 3 in. F'_c= 4000 psi

Then, $C_c=1.3F'_c b_{fc} t_s=1.3(4)16.23(3.25)=274$ kip

Pick the dogbone a and b dimensions

a= (0.5 to 0.75)b_f = 7.52 to 11.28 in. Use a= 8 in.

b= (0.65 to 0.85)d= 19.94 to 26.08 in. Use b= 22 in.

Therefore s_c= 8+22/2= 19 in.

Assume measured F_{yb}=45.0 ksi, F_{yc}=52.0 ksi

$F_{ye}= F_{yb}$= 45.0 ksi

$F_{ysh}= 1.1F_{ye}$= 49.5 ksi

Assume full weld replacement with moderate toughness material at bottom flange, no weld modification at top flange, therefore allowable weld stresses are

Top $F_{cr}= F_{ye}$= 45.0 ksi (slab presence allows full base metal capacity)

Bottom $F_{cr}= F_{ye}$= 45.0 ksi

Column limiting stress =$0.9F_{yc}$ = 0.9(52)= 46.8 ksi>45.0 ksi

Capacity at column face is identical to Example 3, or

M_c= 29240 kip in.

Assume L=288 in.

L'= L-d_c-2s_c= 288-17.12-2(19)= 233 in.

Assume no gravity loading

Therefore

$$M_f=\left[1+\frac{2s_c}{L'}\right]M_{pd}+\frac{wLs_c}{2}=\left[1+\frac{2(19)}{233}\right]M_{pd}+0$$

$M_f = 1.16M_{pd}$

Since M_f must be limited to M_c, set these values equal to each other.

$$M_{pd} = \frac{M_c}{1.16} = \frac{29240}{1.16} = 25206 \text{ kip-in.}$$

For a top and bottom flange dogbone

$$Z_{RBS(composite)} = Z_b - \left(\frac{(C_c)}{2F_{ysh}t_w} \right)^2 t_w - 2ct_f(d - t_f) + \frac{C_c(d/2 + g + t_s/2)}{F_{ysh}}$$

$$= 673 - \left(\frac{(274)}{2(49.5)0.71} \right)^2 0.710 -$$

$$2(1.185)c(30.68 - 1.185) + \frac{274(15.37 + 3 + 1.625)}{49.5}$$

$$M_{pd} = Z_{RBS(composite)}F_{ysh} = <25206$$

$$= [673 - 10.79 - 69.9c + 110.7]49.5 < 25206$$

Solving for the minimum value of c

c= 3.77 in., or a 50 percent flange reduction.

This percentage reduction is below 55 percent and would be an acceptable design for positive moment.

Next, the bare steel section would need to be checked for the case of negative bending moments.

Allowable weld stresses are

Top $F_{cr} = F_{ye} = 45.0$ ksi (slab presence allows full base metal capacity)

Bottom $F_{cr} = F_{ye} = 45.0$ ksi

Column limiting stress $= 0.9F_{yc} = 0.9(52) = 46.8$ ksi>45.0 ksi

Determine yield capacity at column face

$M_c = S_bF_{cr} = 598(45.0) = 26910$ kip-in.

Since M_f must be limited to M_c, similar to positive moment calculations

$$M_{pd}= \frac{M_c}{1.16} = \frac{26910}{1.16} = 23200 \text{ kip-in.}$$

For a top and bottom flange dogbone

$$M_{pd}= Z_{RBS}F_{ysh}= Z_B-2ct_f(d-t_f)< 23200$$

$$= (673-2(1.185)3.20(30.68-1.185))49.5= 22240 \text{ kip in.}$$

This value is less than the critical moment M_{pd} of 23200 kip in, and is an acceptable design.

Appendix G: Haunch Design Calculation Examples

A Haunch design will be carried out for both bare steel, and composite sections. Beam, column, and haunch sizes will be similar to those tested.

A) Example 1 - Bare Steel Haunch

Beam = W30X99 (A36) Column = W12X279 (A572 Gr50)

Haunch = W21X93 (A572 Gr50)

Bare Steel Specimen

Pick the haunch a and b dimensions

a= (0.50 to 0.75)d = 14.82 to 22.24 in. Use a=18 in.

θ=25 to 35 degrees

therefore

b= 8.39 to 12.6 in. Use b= 10.75 in.

(Similar to tested specimens)

Assume measured F_{yb}=45.0 ksi, F_{yc}=52.0 ksi

$F_{ye}= F_{yb}$= 45.0 ksi

$F_{ysh}= 1.1F_{ye}$= 49.5 ksi

Assume removal of backing bar at top weld, no modification to bottom weld, and moderate toughness material with backup bar removal at haunch welds, therefore allowable weld stresses are

F_{top}= 32.0 ksi

F_{bot}= 30.0 ksi

$F_{hch}= F_{ye}= 45.0$ ksi

Column limiting stress $=0.9F_{yc} = 0.9(52)= 46.8$ ksi>45.0 ksi

At the end of the haunch

$M_{pd}= Z_B F_{ysh}= 312(49.5) =15444$ kip-in

Assume L=288 in.

$L'= L-d_c-2a= 288-15.85-2(18)= 236$ in.

Assume no gravity loading

Therefore

$$M_f=\left[1+\frac{2a}{L'}\right]M_{pd}+\frac{wLa}{2}=\left[1+\frac{2(18)}{236}\right]M_{pd}+0$$

$M_f= 1.15M_{pd}=1.15(15444)=17761$ kip-in

Determine M_c which must be greater than the applied M_f

For the assumed section, it is found that $\bar{y}=7.32$ in.

the moment of inertia, $I_x=8865$ in^4

Therefore:

$S_{top}= 400.4$ in^3

$S_{bot}= 1180.4$ in^3

$S_{hch}= 485.4$ in^3

$M_c= S_{top}F_{cr}= 400.4(32.0)= 12810$ kip-in. ←controls

$M_c= S_{bot}F_{cr}= 1180.4(30.0)= 35410$ kip-in.

$M_c= S_{hch}F_{cr}= 485.4(45.0)= 21843$ kip-in.

This haunch is expected to fail at the top flange. Either a new haunch shape could be selected, or a deeper section used, or greater improvements could be applied to

the top weld. Assume full replacement of top weld with moderate toughness weld material and removal of backing bar

Then

$M_c = S_{top}F_{cr} = 400.4(45.0) = 18020$ kip-in. ←controls

This critical capacity value is greater than the applied moment of 17761 kip-in, so the design is acceptable.

B) Example 2 - Composite Haunch

Beam = W30X99 (A36) Column = W12X279 (A572 Gr50)

Composite Specimen

Assume slab similar to those tested

$t_s = 3.25$ inches $g = 3$ in. $F'_c = 4000$ psi

Then, $C_c = 1.3F'_c b_{fc} t_s = 1.3(4)13.14(3.25) = 222$ kip

Pick the haunch a and b dimensions

$a = (0.50 \text{ to } 0.75)d = 14.82$ to 22.24 in. Use a=18 in.

$\theta = 25$ to 35 degrees

therefore

b= 8.39 to 12.6 in. Use b= 10.75 in.

(Similar to tested specimens)

Assume measured $F_{yb} = 45.0$ ksi, $F_{yc} = 52.0$ ksi

$F_{ye} = F_{yb} = 45.0$ ksi

$F_{ysh} = 1.1F_{ye} = 49.5$ ksi

Assume no modification to top or bottom welds, and moderate toughness material with backup bar removal at haunch welds, therefore allowable weld stresses are

F_{top}= 45.0 ksi (slab is present)

F_{bot}= 30.0 ksi

F_{hch}= F_{ye}= 45.0 ksi

Column limiting stress =0.9F_{yc} = 0.9(52)= 46.8 ksi>45.0 ksi

At the end of the haunch

$$Z_{b(composite)}= Z_b-\left(\frac{C_c}{2F_{ysh}t_w}\right)^2 t_w + \frac{C_c\left(d/2+g+t_s/2\right)}{F_{ysh}}$$

$$= 312-\left(\frac{222}{2(49.5)0.520}\right)^2 (0.520) + \frac{222\left(14.825+3+1.625\right)}{49.5}$$

$$= 390 \text{ in}^3$$

M_{pd}= $Z_{B(composite)}F_{ysh}$= 390(49.5) = 19283 kip-in

Assume L=288 in.

L'= L-d_c-2a= 288-15.85-2(18)= 236 in.

Assume no gravity loading

Therefore

$$M_f=\left[1+\frac{2a}{L'}\right]M_{pd}+\frac{wLa}{2}=\left[1+\frac{2(18)}{236}\right]M_{pd}+0$$

M_f= 1.15M_{pd}=1.15(19283)= 22176 kip-in

Determine M_c which must be greater than the applied M_f

Determine capacity at column face M_c which must be greater than M_f

First, assume that the haunch flange is critical.

F_{hch}= 45.0 ksi and ε_{hch}=0.00155

Then, balancing forces,

F_{top}= 42.9 ksi and ε_{top}=0.00148

Check F_{bot}, ε_{bot}=0.00074, therefore F_{bot}= 21.5 ksi<30.0 ksi

The associated moment capacity with this strain distribution is

M_c= 25236 kip in.

This critical capacity value is greater than the applied moment of 22176 kip-in, so the design is acceptable for the positive moment. however, one must still check the negative moment capacity as a bare steel section. This would be similar to Example 1, with the top flange allowable stress of 45.0 ksi. The final design of Example 1 used this criteria and showed it to be acceptable. Note, however, that in Example 1 this weld capacity was provided through the replacement of the existing weld with moderate toughness weld material and removal of the backing bar whereas in Example 2 it is provided by the presence of the composite slab while leaving the existing welds as is.

Glossary

a= distance from column face to start of dogbone cutout, length of haunch (in)
b= length of dogbone cutout, depth of haunch (in)
b_{cf}= column flange width (in)
b_f= beam flange width (in)
c= depth of cut for dogbone reduced section, distance from neutral axis to the extreme fiber of a section (in)
d= overall depth of beam (in)
d_b= effective depth of panel zone (in)
d_c= overall depth of column (in)
d_1,d_2= dimension of panel zone along diagonals (in)
f_r= modulus of rupture of concrete (psi)
g= gap between beam and effective slab (in)
k_e= slope of elastic portion of a plot
s_c= distance from column face to critical section of beam (in)
t_{cf}= thickness of column flange (in)
t_{cw}= column web thickness (in)
t_f= thickness of beam flange (in)
t_s= effective thickness of concrete slab (in)
t_w= thickness of beam web (in)
w= uniformly distributed gravity load
$\bar{y}$ = distance from centroid of original section to neutral axis (elastic or plastic) (in)
A= cross sectional area (in^2)
C_c= effective compressive force of concrete slab (kip)
C_s= seismic design coefficient
E_c= modulus of elasticity of concrete (ksi)
E_s= modulus of elasticity of steel (29000 ksi)
F= applied force
F'_c= compressive strength of concrete (ksi)
F_{cr}= critical weld stress (ksi)
F_w= reference weld stress (ksi)
F_u= minimum specified tensile strength of the specimen (ksi)
F_y= minimum specified yield stress of the specimen (ksi)
F_{yc}= yield stress of the column (ksi)
F_{ycw}= yield stress of the column web (ksi)
F_{ye}= expected or measured yield strength (ksi)
F_{yf}= measured beam flange yield strength (ksi)

F_{ysh}= expected strength after strain hardening (ksi)
F_{yw}= reference weld stress (ksi)
H= story height (in)
I= modulus of inertia (in^4)
L= beam span (in)
L_1= distance from center of column to critical section (in)
L_2= distance from critical section to reaction (in)
L_b= length of beam from point of load application to column face (in)
L'= length of beam between critical sections (in)
M= applied moment (kip-in)
$M+_{max}$= maximum positive moment measured in test (kip-in)
$M-_{max}$= maximum negative moment measured in test (kip-in)
M_c= maximum moment allowed at the column face (kip-in)
M_f= maximum moment applied at the column face (kip-in)
M_{nb}= maximum beam moment developed at the face of the column in the north beam
M_{pd}= design moment at the center of the dogbone cutout (kip-in)
M_{nHCH}= nominal plastic moment of haunch section at column face (kip-in)
M_{nRBS}= nominal plastic moment at center of dogbone cutout (kip-in)
M_p= plastic moment of a section (kip-in)
M_{pd}= design moment at the critical section (kip-in)
M_{pe}= estimated actual plastic moment (kip-in)
M_{pn}= nominal plastic moment (kip-in)
M_{pCe}= estimated actual moment of a composite section for the full beam cross section (kip-in)
M_{pCn}= nominal plastic moment of a composite section for the full beam cross section (kip-in)
M_{pCnHCH}= nominal plastic moment of a composite section for the full haunch section at the column face (kip-in)
M_{pCnRBS}= nominal plastic moment of a composite section at the center of dogbone cutout (kip-in)
M_{pCHCH}= estimated actual plastic moment of a composite section for the haunch section at the column face (kip-in)
M_{pCRBS}= estimated actual plastic moment of a composite section at the center of dogbone cutout (kip-in)
M_{pHCH}= estimated actual plastic moment if haunch section at the column face (kip-in)
M_{pRBS}= estimated actual plastic moment at center of dogbone cutout (kip-in)
M_{sb}= maximum beam moment developed at the face of the column in the south beam (kip-in)

M_{ye}= estimated yield moment of full cross section (kip-in)
M_{yHCH}= estimated actual yield moment of the haunch section at the column face (kip-in)
P_{max}= maximum load attained (kip)
P_{sus}= maximum load sustained (kip)
Q_s= shear stud capacity as defined by AISC LRFD code (kip)
R= radius of dogbone cutout (in)
R_y= material overstrength multiplier
S_b= elastic section modulus of the full beam section (in^3)
S_h= elastic section modulus of the haunch section at the column face (in^3)
S_x= elastic section modulus of the section cross section (in^3)
V_{beam}= column shear force from beam moments (kip)
V_{col}= column shear force outside panel zone area (kip)
V_{max}= maximum shear force developed in the column panel zone (kip)
V_n= panel zone strength based on equation 11-1 of the 1997 UBC (kip)
V_p= plastic shear capacity of the column web (kip)
W_{int}= internal work in the system
W_{ext}= external work in the system
Z= plastic section modulus (in^3)
Z_b= plastic section modulus of full beam cross section (in^3)
$Z_{b(composite)}$= plastic section modulus of full beam cross section for a composite section (in^3)
Z_{beam}= plastic section modulus of beam section (in^3)
Z_{col}= plastic section modulus of column section (in^3)
$Z_{fillets}$= plastic section modulus component from beam fillets (in^3)
Z_{flange}= plastic section modulus component from beam flange (in^3)
Z_{web}= plastic section modulus component from beam web (in^3)
Z_{HCH}= plastic section modulus of haunch section at column face (in^3)
Z_{RBS}= plastic section modulus at the minimum section of the dogbone cutout (in^3)
$Z_{RBS(composite)}$= plastic section modulus at the minimum section of the dogbone cutout for a composite section (in^3)
$Z_{RBSfillets}$= plastic section modulus (in^3)
$Z_{RBSflange}$= plastic section modulus (in^3)
Z_{RBSweb}= plastic section modulus (in^3)
δ_3, δ_4= measured change in length of panel zone dimension along diagonals (in)
δ= displacement (in)
δ_b= vertical displacement at end of beams (in)
δ_{cb}= lateral column tip displacement due to beam deformations (in)
δ_{cc}= lateral column tip displacement due to column deformations (in)

δ_{cpz}= lateral column tip displacement due to panel zone deformations (in)
δ_{ctot}= total lateral column tip displacement (in)
δ_y= lateral column tip displacement causing first beam yield, based on nominal section properties and full beam cross section (in)
ε= strain (in/in)
ε_{bot}= attainable strain at bottom extreme fiber (in/in)
ε_r= concrete strain at rupture (in/in)
ε_{top}= attainable strain at top extreme fiber (in/in)
ϕ= angle
γ= panel zone strain angle (radian)
γ_{avg}= haunch panel zone strain angle (radian)
γ_e= elastic panel zone strain angle (radian)
γ_p= inelastic panel zone strain angle (radian)
θ= rotation (radian)
θ_b= connection rotation due to beam deformations (radian)
θ_{be}= elastic connection rotation due to beam deformations (radian)
θ_{bp}= inelastic connection rotation due to beam deformations (radian)
θ_c= column rotation (radian)
θ_{con}= connection rotation (radian)
θ_{ce}= elastic column rotation (radian)
θ_{cp}= plastic column rotation (radian)
θ_{hch}= haunch angle
θ_{pz}= connection rotation due to panel zone deformations (radian)
θ_{pze}= elastic connection rotation due to panel zone deformations (radian)
θ_{pzp}= inelastic connection rotation due to panel zone deformations (radian)
θ_{tot}= total specimen rotation based on column tip deflection divided by the story height (radian)
θ_{totp}= inelastic portion of θ_{tot} (radian)
θ_{totpn}= total inelastic rotation referenced to north beam (radian)
θ_{totps}= total inelastic rotation referenced to south beam (radian)
σ= stress (ksi)

References

1) Northridge Earthquake Reconnaissance Report, Volume 2. *Earthquake Spectra*. Supplement C to Volume 11. January 1996.

2) *Proceedings of AISC Special Task Committee on the Northridge Earthquake Meeting*. American Institute of Steel Construction. March 14-15 1994.

3) Youssef, N. F. G., Bonowitz, D., and Gross, J. L. *A Survey of Steel Moment-Resisting Frame Buildings Affected by the 1994 Northridge Earthquake*. National Institute of Standards and Technology, Report NISTR 5625. 1995.

4) Kaufmann, E. J., Fisher, J. W., Di Julio, R. M., and Gross, J. L. *Failure Analysis of Welded Steel Moment Frames Damaged in the Northridge Earthquake*. National Institute of Standards and Technology, Report NISTIR 5944. 1997

5) Paret, T. F. and Freeman, S. A. "Is Steel Frame Damage Being Diagnosed Correctly?" *Building to Last*. Proceedings of Structures Congress XV. ASCE. 1997. pp. 261-266.

6) Gates, W. E. and Morden, M. "Professional Structural Engineering Experience Related to Welded Steel Moment Frames Following the Northridge Earthquake." *The Structural Design of Tall Buildings*. Volume 5. 1996. pp. 29-44.

7) Sabol, T. A. and Engelhardt, M. D. *Welded Steel Moment Frame Joint Testing Programs*. Los Angeles: Englekirk & Sabol, Inc.

8) Miller, D. K. "Lessons Learned from the Northridge Earthquake." *Welding in the World/Le Soudage dans le Monde*. Volume 38. November 1996. pp. 257-276.

9) Maranian, P. "Vulnerability of Existing Steel Framed Buildings following the 1994 Northridge (California, USA) Earthquake: Considerations for Their Repair and Strengthening." *The Structural Engineer*. Volume 75, No. 10. May 1997. pp. 165-172.

10) Shuey, B. and Engelhardt, M. D. *Testing of Repair Concepts for Damaged Steel Moment Connections*. SAC Report. 1996.

11) Uang, C. M., and Bondad, D. *Static Cyclic Testing of Pre-Northridge and Haunch Repaired Steel Moment Connections*. SAC Report. 1996

12) Xue, M., Kaufmann, E. J., Lu, L. W., and Fisher, J. W. "Fracture and Ductility of Welded Moment Connections under Dynamic Loading." *Building to Last*. Proceedings of Structures Congress XV. ASCE. 1997. pp. 607-613.

13) Plumier, A. *Summary of Technical Data on Beams Using Reduced Sections as Dissipative Zones*. Liege, Belgium: University of Liege-Belgium. May 1995.

14) Chen, S. J. and Yeh, C. H. "Enhancement of Ductility of Steel Beam-to-Column Connections for Seismic Resistance." *Paper presented at SSRC Task Group Meeting & Technical Session*, Lehigh University, Pennsylvania. 1994.

15) Uang, C. M., and Noel, S. *Brief Summary on Cyclic Response of Specimen COH-1*. San Diego: University of California. 1995.

16) Iwankiw, N. R. and Carter, C. J. "The Dogbone: A New Idea to Chew On." *Modern Steel Construction*. April 1996. pp. 18-23.

17) Engelhardt, M. D., Winneberger, T., Zekany, A. J. and Potyraj, T. J. "The Dogbone Connection: Part II." *Modern Steel Construction*. August 1996. pp. 46-55.

18) Iwankiw, N. "Ultimate Strength Considerations for Seismic Design of the Reduced Beam Section (Internal Plastic Hinge)." *AISC Engineering Journal*. First Quarter. 1997. pp. 3-16.

19) Uang, C. M. and Noel, S. *Testing of Steel Moment Connections for the City of Hope National Medical Center*, Report No. TR-96/05, University of California, San Diego. La Jolla, CA. 1996.

20) *Preliminary Reports: Earthquake Response of Steel Frames*. Presentation of the 1965 Annual Meeting of the Structural Engineers' Association of California. American Iron and Steel Institute. 1966.

21) Popov, E. P. and Pinkney, R. B. “Cyclic Yield Reversal in Steel Building Connections.” *Journal of the Structural Division*. Proceedings of the American Society of Civil Engineers. Volume 95, No. ST3. March 1969. pp. 327-351.

22) Popov, E. PP. and Stephen, R. M. *Cyclic Loading of Full-Size Steel Connections*. American Iron and Steel Institute Bulletin. Number 21. 1970.

23) Popov, E. P. and Bertero, V. V. “Cyclic Loading of Steel Beams and Connections.” *Journal of the Structural Division*. Proceedings of the American Society of Civil Engineers. Volume 99, No. ST6. June 1973. pp. 1189-1204.

24) Bertero, V. V., Popov, E. P., and Krawinkler, H. “Beam-Column Subassemblages under Repeated Loading.” *Journal of the Structural Division*. Proceedings of the American Society of Civil Engineers. Volume 98, No. ST5. May 1972. pp. 1137-1159.

25) Krawinkler, H., Bertero, V. V. and Popov, E. P. “Shear Behavior of Steel Moment Frames.” *Journal of the Structural Division.* Proceedings of the American Society of Civil Engineers. Volume 101, No. ST11. November 1975. pp. 2317-2336.

26) Krawinkler, H. and Popov, E. P. “Seismic Behavior of Moment Connections and Joints.” *Journal of the Structural Division*. . Proceedings of the American Society of Civil Engineers. Volume 108, No. ST2. February 1982. pp. 373-391.

27) Popov, E. P., Amin, N. R., Louie, J. J. C., and Stephen, R. M. “Cyclic Behavior of Large Beam-Column Assemblies.” *Engineering Journal-American Institute of Steel Construction*. Volume 23, No. 1. First Quarter. 1986. pp. 9-23.

28) Popov, E. P. “On California Structural Steel Seismic Design.” *Earthquake Spectra*. Volume 2, No. 4. October 1986. pp. 703-727.

29) Popov, E. P. “Panel Zone Flexibility in Seismic Moment Joints.” *Journal of Constructional Steel Research*. 1987. pp. 91-117.

30) Fielding, D. J. and Huang, J. S. “Shear in Steel Beam-to-Column Connections.” *Welding Research Supplement*. July 1971. pp. 313S-326S.

31) Krawinkler, H. “Shear in Beam-Column Joints in Seismic Design of Steel Frames.” *Engineering Journal*. American Institute of Steel Construction. Third Quarter. 1978. pp. 82-91.

32) Leger, P., Paultre, P. and Nuggihalli, R. “Elastic Analysis of Frames Considering Panel Zones Deformations.” *Computers & Structures*. Volume 39, No. 6. 1991. pp. 689-697.

33) Tsai, K. C. and Popov, E. P. “Beam-Column Panel Zone Deformations in Steel Moment Resisting Frames.” Paper submitted for publication to *Journal of Structural Engineering.* American Society of Civil Engineers. 1989.

34) Krawinkler, H. “Performance Assessment of Structural Components.” *Proceedings: Pacific Structural Steel Conference*, Auckland, New Zealand. 1986.

35) Popov, E. P. and Tsai, K. C. “Performance of Large Seismic Steel Moment Connections Under Cyclic Loads.” *Engineering Journal*. American Institute of Steel Construction. Second Quarter. 1989. pp. 51-60.

36) Anderson, J. C. and Linderman, R. R. *Post Earthquake Repair of Welded Moment Connections*. University of Southern California, Department of Civil Engineering, Report No. CE 91-04. 1991

37) Engelhardt, M. D. and Husain, A. S. “Cyclic-Loading Performance of Welded Flange-Bolted Web Connections.” *Journal of Structural Engineering*. Volume 119, No. 12. December 1993. pp. 3537-3550.

38) Tsai, K. C., Wu, S., and Popov, E.P. “Experimental Performance of Seismic Steel Beam-Column Moment Joints.” *Journal of Structural Engineering*. American Society of Civil Engineers. 1994.

39) Beedle, L. S. and Christopher, R. “Tests of Steel Moment Connections.” *AISC Engineering Journal*. Volume 1, No. 4. October 1964. pp. 116-125.

40) Graham, J. D., Sherbourne, A. N., Khabbaz, R. N., and Jensen, C. D. *Welded Interior Beam-to-Column Connections*. Chicago: American Institute of Steel Construction.

41) Huang, J. S., Chen, W. F., and Beedle, L. S. *Behavior and Design of Steel Beam-to-Column Moment Connections*. WRC Bulletin. No. 188. October 1973. pp. 1-23.

42) Chen, W. F. and Lui, E. M. "Steel Beam-to-Column Moment Connections-Part I." *SM Archives*. Volume 11, No. 4. 1986. pp. 257-316.

43) Popov, E. PP. 1988. "Seismic Moment Connections for MRF's." *Journal of Constructional Steel Research*. Number 10. 1988. pp. 163-198.

44) Tremblay, R. Timler, P. Bruneau, M. and Filiatrault, A. "Performance of Steel Structures During the 1994 Northridge Earthquake." *Canadian Journal of Civil Engineering*. Volume 22, No. 2. 1995. pp. 298-299.

45) Yang, T. S. and Popov, E. P. *Behavior of Pre-Northridge Moment Resisting Steel Connections*. Earthquake Engineering Research Center, University of California at Berkeley. Report No. UCB/EERC-95/08. 1995.

46) Goel, S. C. Stojadinovic, B. and Lee, K. H. "Truss Analogy for Steel Moment Connections." *Engineering Journal (AISC)*. Volume 34, No. 2. 1997. pp. 43-53.

47) "Problematic Connections." *The Construction Specifier*. Volume 48, No. 1. January 1995. pp. 65-71.

48) Engelhardt, M. D. and Sabol, T. A. *Testing of Welded Steel Moment Connections in Response to the Northridge Earthquake.* Progress Report to the AISC Advisory Subcommittee on Special Moment Resisting Frame Research. University of Texas at Austin. 1994.

49) Ojdrovic, R. P. and Zarghamee, M. S. "Fracture of Steel Moment Connections in the Northridge Earthquake." *Proceedings of the Institute of Civil Engineers-Structures & Buildings.* Volume 122, No. 2. May 1997. pp. 209-217.

50) Roeder, C. W. and Foutch, D. A. "Experimental Results for Seismic Resistant Steel Moment Frame Connections." *Journal of Structural Engineering*. Volume 122, No. 6. June 1996. pp. 581-588.

51) Fairweather, V. "Seismic Solutions for Steel Frame Buildings." *Civil Engineering.* March 1996, pp. 40-43.

52) Houghton, D. L. "MNH-SMRF™ Connection System: Solving Pre-Northridge Steel Frame Dilemmas Using Simple and Reliable Post-Northridge Innovation." *Building to Last*. Proceedings of Structures Congress XV. ASCE. 1997. pp. 105-113.

53) Kouyoumdjian, H. H. "High Rotational Capacity Moment Connections." *Building to Last*. Proceedings of Structures Congress XV. ASCE. 1997. pp. 119-123.

54) Tremblay, R., Tchebotarev, N. and Filiatrault, A. "Seismic Performance of RBS Connections for Steel Moment Resisting Frames: Influence of Loading Rate and Floor Slab." *Proceedings - STESSA 1997*, Kyoto, Japan. August, 1997. pp. 4-7.

55) Anderson, J. C. "Repair/Retrofit Schemes for Low Rise Steel Moment Frames." *Building to Last*. Proceedings of Structures Congress XV. ASCE. 1997. pp. 777-781.

56) Lee, C. H. and Uang, C. M. "Analytical Modeling of Dual Panel Zone in Haunch Repaired Steel MRF's." *Journal of Structural Engineering*. Volume 123, No. 1. January 1997. pp. 20-29.

57) Hart, G. H., Huang, S. C., Lobo, R. F., Jain, A., and Van Winkle, M. 1997. Earthquake Response of Strengthened Steel Special Moment Resisting Frames. The Structural Design of Tall Buildings, Volume 6, pp. 37-58.

58) Daniels, J. H. Kroll, G. D. and Fisher, J. W. "Behavior of Composite-Beam to Column Joints." *Journal of the Structural Division.* Proceedings of the American Society of Civil Engineers. Volume 96, No. ST3. March 1970. pp. 671-685.

59) Fahmy, E. H. and Robinson, H. "Analyses and Tests to Determine The Effective Widths Of Composite Beams In Unbraced Multistorey Frames." *Canadian Journal of Civil Engineering*. Volume 13. 1986. pp. 66-75.

60) Oehlers, D. J. "Deterioration in Strength of Stud Connectors in Composite Bridge Beams." *Journal of Structural Engineering*. Volume 116, No. 12. December 1990. pp. 3417-3431.

61) Du Plessis, D. P. and Daniels, J. H. *Strength of Composite Beam to Column Connections*. Report No. 374.3, Fritz Engineering Laboratory, Lehigh University, Bethlehem. PA, 1972

62) Kato, B., and Tagawa, Y. “Strength of Composite Beams under Seismic Loading.” *Composite and Mixed Construction*. ASCE. 1985. pp. 42-49

63) Tagawa, Y., Kato, B., and Aoki, H., “Behavior of Composite Beams in Steel Frame Under Hysteretic Loading.” *Journal of Structural Engineering.* ASCE. Vol. 115, No. 8. August 1989. pp. 2029-2045.

64) Lee, S. J. and Lu, L. W. “Cyclic Tests of Full-Scale Composite Joint Subassemblages.” *Journal of Structural Engineering*. ASCE. Vol. 115, No. 8. August 1989. pp. 1977-1998.

65) Hajjar, J. F., Leon, R. T., Gustafson, M. A. and Shield, C. K. *Full Scale Cyclic Experiments of Composite Moment-Resisting Frame Connections*. Report No. ST 98-02. University of Minnesota. 1998

66) *Analytical and Field Investigations of Buildings Affected by the Northridge Earthquake of January 17, 1994*. Technical Report SAC 95-04. SAC Joint Venture, Sacramento, CA. 1995.

67) *Interim Guidelines: Evaluation, Repair, modification and Design of Steel Moment Frames*. FEMA-267 (SAC-95-02). Federal Emergency Management Agency. Washington D. C. August 1995.

68) *Interim Guidelines Advisory No. 1*. FEMA-267A (SAC-96-03). Federal Emergency Management Agency. Washington D. C. March 1997.

69) *NEHRP Handbook for the Seismic Evaluation of Existing Buildings*. FEMA-178. Federal Emergency Management Agency. Washington D. C. June 1992.

70) NEHRP Recommended Provisions for the Development of Seismic Regulations for New Buildings. FEMA-223. Federal Emergency Management Agency. Washington D. C. January 1992.

71) *Connection Test Summaries*. FEMA-289. Federal Emergency Management Agency. Washington D. C. June 1997.

72) *Structural Welding Code - Steel*. AWS D1.1-94. American Welding Society. Miami, FL. 1996

73) "AISC Advisory Statement on Mechanical Properties Near the Fillet of Wide Flange Shapes and Interim Recommendations; January 10, 1997." *Modern Steel Construction*. Vol. 37, No. 2. February 1997. pp. 18.

74) "AISC Initiates Research into k Area Cracking." *Modern Steel Construction*. Vol. 37, No. 9. September 1997. pp. 23-24.

75) Galambos, T. V. and Ravinda, M. K. "Properties of Steel for use in LRFD." *Journal of Structural Division*. ASCE. Vol. 194, No. ST9. September 1978. pp. 1459-1469

76) *Seismic Provisions for Structural Steel Buildings*. American Institute of Steel Construction. Chicago. 1997.

77) *Modification of Existing Welded Steel Moment Frame Connections for Seismic Resistance*. Draft Document. National Institute of Standards and Technology. June 1998.

78) *Background Reports: Metallurgy, Fracture Mechanics, Welding, Moment Connections and Frame Systems Behavior*. FEMA-288, (SAC-95-09). Federal Emergency Management Agency. Washington D. C. March 1997.

79) Grubbs, K. V. *The Effect of the Dogbone Connection on the Elastic Stiffness of Steel Moment Frames*. Master's Thesis. The University of Texas at Austin. August 1997.

80) Wang, C. and Salmon, C. *Reinforced Concrete Design- 4th Edition*. Harper & Row. New York. 1985

81) "Economic Seismic Connection Repairs: Weld Overlays." *Modern Steel Construction*. January 1998. pp. 38-41.

82) Popov, E. P. *UCB Specimen DB1 Test Summary Memo*. University of California, Berkeley. February 1996.

83) Uang, C. M. and Bondad, D. *Dynamic Testing of Pre-Northridge and Haunch Repaired Steel Moment Connections*. Report No. SSRP 96/03. University of California, San Diego. La Jolla, CA. 1996.

84) Noel, S. and Uang, C. M. *Cyclic Testing of Steel Moment Connections for the San Francisco Civic Center Complex*. Report No. TR-96/07. University of California, San Diego. La Jolla, CA. 1996.

Vita

Scott Adam Civjan was born in Washington D.C. on May 10, 1967. His parents are Ralph Haime Civjan and Rebecca Swersky Civjan. He graduated from Enterprise High School, Enterprise, Alabama in 1985. He then attended Washington University in St. Louis, Missouri and received his Bachelor of Science in Civil Engineering in 1989. For the following four years he was employed at Black and Veatch Architects and Engineers in Overland Park, Kansas. In September of 1993 he entered the Graduate School of the University of Texas at Austin, where he received his Masters of Science in Civil Engineering in 1995. He then began his Doctoral work.

Permanent address: 205 North Maple, Florence, MA, 01062

This dissertation was typed by the author.

?) Regec, J. E., Huang, J. S., and Chen. W. F. 1973. Test of a Fully-Welded Beam-to-Column Connection. WRC Bulletin, Number 188, pp. 24-35.

?Englehardt, M. D. and Sabol, T. A. 1995. Lessons Learned from the Northridge Earthquake: Steel Moment Frame Performance. Paper presented at Symposium on a New Direction in Seismic Design, Architectural Institute of Japan, Tokyo.

?) Frank, K. H., 1995, "The Physical and Metallurgical Properties of Structural Steels", Background Reports: Metallurgy, Fracture Mechanics, Welding, Moment Connections and Frame Systems Behavior, FEMA-288, (SAC-95-09), Federal Emergency Management Agency, Washington D. C., March 1997.

?) Heidebrecht, A. C. 1995. Introduction to papers on the 1994 Northridge Earthquake. Canadian Journal of Civil Engineering. Volume 22, pp. 298-299.

Chen, W. F. and Lui, E. M. 1988. Static Flange Moment Connections. Journal of Constructional Steel Research. Volume 10, pp. 39-88.

Popov, E. P., Tsai, K. C., and Engelhardt, M. D. 1988. On Seismic Steel Joints and Connections. Paper presented at SEAOC Conference, Hawaii.

El-Ghazaly, H. A. and Sherbourne, A. N. 1987. Ultimate Strength of Stiffened Symmetrical Welded Steel Beam-to-Column Flange Connections. Computers & Structures. Volume 26, Number 5, pp. 749-760.

Kunnath, S. H. 1995. Enhancements to Program IDARC: Modeling Inelastic Behavior of Welded Connections in Steel Moment-Resisting Frames. National Institute of Standards and Technology, Report NIST GCR 95-673.

Popov, E. PP. and Tsai, K. C. 1989 Performance of Large Seismic Steel Moment Connections Under Cyclic Loads. Engineering Journal American Institute of Steel Construction. Volume 26, No. 2. pp. 51-60.

Johnson, R. PP. and Huang, D. 1995. Resistance to Longitudinal Shear of Composite Beams with Profiled Sheeting. Proceedings of the Institute of Civil Engineers- Structures & Buildings. Volume 110, NO. 2, pp. 204-215.

Redwood, R. G., Lefki, L. and Amar, G. 1990. Earthquake Resistant Design of Steel Moment Resisting Frames. Canadian Journal of Civil Engineering. Volume 17, pp. 659-667.

Popov, E. PP. 1990. U. S. Seismic Steel Codes. Paper presented at the Fourth Congress on Tall Buildings, Hong Kong.

Schneider, S. P., Roeder, C. W., and Carpenter, J. E. 1993. Seismic Behavior of Moment Resisting Steel Frames: Experimental Study. Journal of Structural Engineering. Volume 119, No. 6, pp. 1885-1903.

Schneider, S. P., Roeder, C. W., and Carpenter, J. E. 1993. Seismic Behavior of Moment Resisting Steel Frames: Analytical Study. Journal of Structural Engineering. Volume 119, No. 6, pp. 1866-1884.

Sabol, T. A. 1994. Steel Damage in L.A.: What Went Wrong. Modern Steel Construction. Volume 34, No. 6, pp. 18-24.

AISC Special Task Committee on the Northridge Earthquake. 1994. Assessing Steel Damage in the Northridge Earthquake. Modern Steel Construction. Volume 34, No. 5, pp. 14-18.

Lessons Learned from the Northridge Earthquake. 1994. Modern Steel Construction. Volume 34, No. 4, pp. 24-26.

Osman, A., Ghobarah, A. and Korol, R. M. 1995. Implications of Design Philosophies for Seismic Response of Steel Moment Frames. Earthquake Engineering and Structural Dynamics. Volume 24, No. 1, pp. 127-143.

SAC Joint Venture. 1997. Protocol for Fabrication, Inspection, Testing, and Documentation of Beam-Column Connection Tests and Other Experimental Specimens. Report No. SAC/BD-97/02. Sacramento: SAC Joint Venture.

De Pineres, O. G. 1995. A Safer Earthquake Design Code After Northridge. Civil Engineering. pp. 72-73.

Fairweather, V. 1994. Northridge: Questioning Our Codes. Civil Engineering. pp. 60-63.

Zarghamee, M. S. and Ojdrovic, R. PP. 1995. Northridge Postscript: Lessons on Steel Connections. Civil Engineering. pp. 68-71.

Chen, W. F. and Yamaguchi, E. 1996. Spotlight on Steel Moment Frames. Civil Engineering. p.. 44-45.

Lee, S. J. 1987. Seismic Behavior of Steel Building Structures with Composite Slabs. Doctoral Dissertation, Lehigh University, Bethlehem, PA.

Du Plessis, D. PP. 1974. The Interaction of Floors and Frames in Multistory Buildings. Doctoral Dissertation, , Lehigh University, Bethlehem, PA.

Uang, C. M. and Bondad, D. 1996. Static Cyclic Testing of Pre-Northridge and Haunch Repaired Steel Moment Connections. Final Report to SAC Joint Venture, Report No. SSRP-96/02.

Humar, J. L. 1979. Composite Beams Under Cyclic Loading. Journal of the Structural Division-Proceedings of the American Society of Civil Engineers. Volume 105, No. ST10, pp. 1949-1965

Rotter, J. M. and Ansourian, PP. 1979. Cross-Section Behavior and Ductility in Composite Beams. Proceedings of the Institution of Civil Engineers, Part 2. Volume 67, pp. 453-474.

Lu, L. W., Slutter, R. R., and Yen, B. T. Recent Research on Composite Structures for Building and Bridge Applications. Composite Structures Research. pp. 150-163.

Clifton, G. C. 1985. Composite Design. Bulletin of the New Zealand National Society for Earthquake Engineering. Volume 18, No. 4, pp. 381-396.

Iwankiw, N. 1995., Some Ultimate Strength Considerations for Reduced Beam Section (Internal Plastic Hinge). Chicago: American Institute of Steel Construction.

Partridge, J. E. 1995. Report of Test Number DBT-2A-150-257. Los Angeles: Smith-Emery Company.

Partridge, J. E. 1995. Report of Test Number DBT-1A-99-176. Los Angeles: Smith-Emery Company.

Engelhardt, M. D., Potyraj, T. and Shuey, B. D. 1995. Brief Report of Steel Moment Connection Test: Specimen DB2. Austin: University of Texas at Austin Ferguson Laboratory.

Engelhardt, M. D., Potyraj, T. and Shuey, B. D. 1995. Brief Report of Steel Moment Connection Test: Specimen DB1. Austin: University of Texas at Austin Ferguson Laboratory.

Earthquake Engineering Research Institute. 1996. New Madrid Zone Regional Seminar on Seismic Engineering Issues. Proceedings of the EERI Regional Seminar, Memphis, Tennessee.

Kasai, K. and Mao, C. 1997. Bolted Repair for Steel Moment Connection Damage from the Northridge Earthquake. Bethlehem, PA: Lehigh University ATLSS Center.

Engelhardt, M. D., Kim K, Uzarski, J., Husain, A., Sabol, T. A., Ho, L., and Kim, H. I. 1995. Parametric Studies on Inealstic Modelling of Steel Moment Frames. PFMSEL Report No. 95-4. Austin: Phil M. Ferguson Structural Engineering Laboratory, University of Texas at Austin.

Kim, K. and Engelhardt, M. D. 1995. Development of Analytical Models for Earthquake Analysis of Steel Moment Frames. PFMSEL Report No. 95-2. Austin: Phil M. Ferguson Structural Engineering Laboratory, University of Texas at Austin.

Engelhardt, M. D., Kim K, Sabol, T. A., Ho, L., Kim, H. I., Uzarski, J. and Husain, A. 1995. Analysis of a Six Story Steel Moment Frame Building in Santa Monica. PFMSEL Report No. 95-3. Austin: Phil M. Ferguson Structural Engineering Laboratory, University of Texas at Austin.

Engelhardt, M. D. and Sabol, T. A. 1994. Testing of Welded Steel Moment Connections in Response to the Northridge Earthquake. Progress Report to the AISC Advisory Subcommittee on Special M oment Resisting Frame Research. Austin: The University of Texas at Austin.

Leon, R., Hajjar, J. F., and Sheild, C. K. The Effect of Composite Floor Slabs on the Behavior of Steel Moment-Resisting Frames in the Northridge Earthquake.

Youssef, N. Retrofitting SMRF Connections: Lessons Learned. *Building to Last*. Proceedings of Structures Congress XV. ASCE. 1997., pp. 253-260.

Sabol, T. A. Design Methodologies to Retrofit Steel Moment Frame Connections. *Building to Last*. Proceedings of Structures Congress XV. ASCE. 1997., pp. 267-271.

Malley, J. O. SAC Phase 1 Experimental Investigations of Pre-Northridge and Repaired Beam-Column Connection Subassemblages. *Building to Last*. Proceedings of Structures Congress XV. ASCE. 1997., pp. 272-276.

Engelhardt, M. D., Shuey, B. D., and Sabol, T. A. Testing of Repaired Steel Moment Connections. *Building to Last*. Proceedings of Structures Congress XV. ASCE. 1997., pp. 408-412.

Kariotis, J. Evaluation of the Benefit of Strengthening Existing Beam-Column Welds. *Building to Last*. Proceedings of Structures Congress XV. ASCE. 1997., pp. 413-417.

Uang, C. M. and Noel, S. Testing of Retrofitted Steel Moment Connections. *Building to Last*. Proceedings of Structures Congress XV. ASCE. 1997., pp. 418-422.

Eberts, R. T. and Chen, T. A. Seismic Retrofit Alternatives for Steel Buildings. *Building to Last*. Proceedings of Structures Congress XV. ASCE. 1997., pp. 423-427.

Tide, R. H. R. Steel Moment Connection Detailing, Workmanship, Material Properties and Fractures. *Building to Last*. Proceedings of Structures Congress XV. ASCE. 1997., pp. 590-595.

Ojdrovic, R. P. and Zarghamee, M. S. A Repair Approach for Fractured Steel Moment Connections. *Building to Last*. Proceedings of Structures Congress XV. ASCE. 1997., pp. 596-601.

Iwankiw, N. R. and Carter, C. J. Reduced Beam Section Connections for Steel SMRF's. *Building to Last*. Proceedings of Structures Congress XV. ASCE. 1997., pp. 602-605.

Barker, D. D. Dynamic Material Behavior. *Building to Last*. Proceedings of Structures Congress XV. ASCE. 1997., pp. 614-623.

Leon, R. T. Contributions of Earthquake Reconnaissance to Experimental Research in Earthquake Engineering. *Building to Last*. Proceedings of Structures Congress XV. ASCE. 1997., pp. 652-657.

Roeder, C. W. An Evaluation of Cracking Observed in Steel Moment Frames. *Building to Last*. Proceedings of Structures Congress XV. ASCE. 1997., pp. 767-771.

Leon, R. T. and Hajjar, J. F. Effect of Floor Slabs on Behavior of Full Moment Steel Connections. *Building to Last*. Proceedings of Structures Congress XV. ASCE. 1997., pp. 772-776.

Hong, L. and Schiff, S. D. Seismic Damage Model for Moment Resisting Steel Connections. *Building to Last*. Proceedings of Structures Congress XV. ASCE. 1997., pp. 782-786.

Bertero, V. V. and Popov, E. P. 1965. Effect of Large Altrnating trains of Steel Beams. Journal of the Structural Division, Proceedings of the American Society of Civil Engineers, Volume 91, No. ST1, pp. 1-12.

Krawinkler, H. 1978. Shear in Beam-Column Joints in Seismic Design of Steel Frames. Engineering Journal, American Institute of Steel Construction, pp. 82-91.